University of Nottingham
UK | CHINA | MALAYSIA

Role of 8-Oxoguanine and its repair mechanisms in paediatric medulloblastoma

Katheeja Imani

Thesis submitted to the University of Nottingham for the degree of Master of Research

March 2023

Abstract

Medulloblastoma a malignant tumour of the cerebellum constitutes around 20% of the Central Nervous System tumours occurring in children. In a recent PhD thesis, a previous student characterised the role of a multifunctional protein YB-1 (Y-Box Binding Protein 1), in paediatric medulloblastoma. A part of this work aimed to identify the transcriptional targets regulated by YB-1 under acute and chronic treatment of cisplatin and vincristine in Group 3 Medulloblastoma by performing chromatin immunoprecipitation and DNA sequencing. However, this work presented with unexpected peak enrichment in the input samples caused by 8-oxoguanine. One of the most commonly oxidized bases in the nucleotide pool, DNA and RNA is guanine and this oxidation is mutagenic as it can pair to either cytosine(C) or adenine(A). In the nucleotide pool, 8-oxoguanine can be repaired by NUDT1(Nudix Hydrolase 1) and in the DNA it is repaired by OGG1 (8-Oxoguanine DNA Glycosylase) and MUTYH (MutY DNA Glycosylase). The 8-oxoguanine in the RNA is assumed to be repaired by YB-1. 8-oxoguanine lesions detected in the ChIP sequencing data of the Group 3 medulloblastoma cell lines could have either been detected because they were already present naturally in these cell lines or they could have occurred artefactually during the ChIP sequencing assay. This study aimed to determine if the 8-oxoguanine lesions were natural or artefactual by employing immunofluorescence. With western blot analysis and immunofluorescence, single and dual staining assays the expression levels of the repair mechanisms of 8-oxoguanine, their role in regulating 8-oxoguanine levels and the extent of colocalization of YB-1 and 8-oxoguanine in group 3 primary tumour cell lines and their corresponding metastatic cell lines were analysed. Through these assays, we conclude that 8-oxoguanine lesions are naturally occurring in group 3 medulloblastomas despite the repair mechanisms being active. We provide evidence that YB-1 is involved in regulating the levels of 8-oxoguanine as well as shows a possibility of colocalization with 8-oxoguanine in the group 3 primary tumour cell lines and their corresponding metastatic cell lines. Thus, this study has shown that YB-1 has the ability to interact with 8-oxoguanine and further study will help establish the relationship

between YB-1 and 8-oxoguanine and their involvement in paediatric medulloblastoma.

Acknowledgement

It is only right for this thesis to start with a note of gratitude for all the people who have been a part of this one-year journey because this work wouldn't have existed without them.

Starting with the very first person who was the reason why I wanted to do my MRes at the University of Nottingham, my supervisor Dr Ian Kerr. He has been very encouraging and supportive from the time I got in touch with him. From making sure I settled comfortably at Nottingham to making sure the thesis writing was going well he has been really supportive. To my supervisor Dr Beth Coyle for all the encouragement and guidance. The two of you were very kind and friendly and I couldn't ask for better.

I also want to thank Deb Briggs for helping me and being patient with me while teaching new techniques. Dr Alistair Hume for helping me with the fluorescence microscope.

I am thankful to my fellow lab members Dr James Mitchell-White, Asmahan, Pippa and Susie for helping me around the lab and giving me advice when running my experiments.

Lastly, I would like to thank the ones most dear to me. My friends Simheca and Praveena, my grandparents Nayaki, Devaki and Asha and my aunts Suparna and Lakshmi for always making sure that I was doing fine in a new country and for showing their love through all the small gestures. A big thanks to my Mum and Dad, for all the love, support, encouragement and whatnot. Without them, I wouldn't be here. You guys are my strongest support system and I am beyond grateful to you guys for everything you have done for me. Thank you for being there for me always and thanks to the almighty for blessing me with all these kind and beautiful souls.

Declaration

This thesis, “Role of 8-oxoguanine and its repair mechanisms in paediatric medulloblastoma”, is the result of my own work undertaken during my period of registration at the University of Nottingham under the supervision of Dr Ian Kerr and Dr Beth Coyle.

Katheeja Imani
Student ID: 20303701
March 2023

Table of Contents

List of Figures

List of Table

Abbreviation

A	Adenine
A/P	Alanine/proline-rich N-terminal domain
APC	Adenomatous Polyposis Coli
APS	Ammonium Persulphate
ATP	Adenosine triphosphate
BER	Base excision repair
bFGF	basic Fibroblast growth factor
BSA	Bovine serum albumin
C	Cytosine
CD	Circular dichroism
ChIP	Chromatin immunoprecipitation
CircRNA	Circular RNA
CIS	Cisplatin
CNS	Central nervous system
CRS	Cytoplasmic Retention Site
CSD	Cold Shock Domain (CSD)
CSF	Cerebrospinal fluid
CTC	Circulating Tumour Cells
CTD	C-terminal Domain
CXCR-4	C-X-C chemokine receptor type 4
DAPI	4',6-diamidino-2-phenylindole
dGTP	deoxyguanosine triphosphate
DMEM	Dulbecco's Modified Eagle Serum
DMF	Dimethylformamide
DMSO	Dimethyl sulfoxide
DNA	Deoxyribonucleic acid
DT	Drug-tolerant
ECL	Enhanced chemiluminescence
ECM	Extracellular Matrix
EGF	Epidermal growth factor
EGFR	Epidermal Growth Factor Receptor
EMT	Epithelial-Mesenchymal Transition
FCS	Foetal calf serum
GAPDH	*Glyceraldehyde 3-phosphate dehydrogenase*
IF	Immunofluorescence
$KBrO_3$	*Potassium Bromate*
KD	Knockdown
LC/A	Large cell/anaplastic
LMD	Leptomeningeal dissemination
LncRNA	Long noncoding RNAs
MB	Medulloblastoma
MBEN	Medulloblastoma with extensive nodularity
MDR	Multi-drug resistance
MHC	Major histocompatibility complex
miRNA	microRNA
MMP	Matrix Metalloproteinase
mRNA	messenger RNA

mRNPs	messenger ribonuclear protein particles
MTH1	human MutT homolog 1
MUTYH	mutY DNA glycosylase
ncRNA	Non-coding RNA
NLS	Nuclear Localisation Signals
NUDT1	Nudix Hydrolase 1
OGG1	8-Oxoguanine glycosylase
PBS	Phosphate buffered saline
RNA	Ribonucleic acid
ROI	Region of Interest
ROS	Reactive oxygen species
RPMI 1640	Roswell Park Memorial Institute 1640
rRNA	ribosomal RNA
SDS	*Sodium dodecyl sulfate*
SDS-PAGE	Sodium dodecyl sulphate–polyacrylamide gel electrophoresis
SG	Stress granule
SHH	Sonic Hedgehog
SNAI1	zinc-finger Snail Family Transcriptional Repressor 1 SNAI1
SNV	Single Nucleotide Variation
TEMED	Tetramethyl ethylenediamine
TGF-β	Transforming Growth Factor Beta
tRNA	transfer RNA
TWIST1	Twist-related protein 1
UTR	Untranslated region
Vm	Vimentin
WHO	World health organisation
WNT	Wingless-related integration site
YB-1	Y-Box Binding Protein 1
Zeb-1	Zinc-finger E-box-binding homeobox 1

Chapter 1. INTRODUCTION

Cancer in children is rare, it constitutes less than 1% of all the new cancer cases in the UK. The annual number of paediatric cancer cases recorded in the UK is around 1800 with leukaemia (31% cases) being the most common followed by the Central Nervous System (CNS) tumours (25% cases) (Cancer Research, UK). Around 250 paediatric cancer deaths are recorded in the UK annually with brain and other CNS tumours being the major contributors (Table 1.1).

Table 1.1 Children's Cancers, UK, 2016-2018 (Cancer Research, UK)

	Children (0-14)	
Cancer Site	Average number of deaths	Average percentage of all cancer deaths
Malignant Brain, Other CNS and Intracranial Tumours	86	35%
Leukaemia	52	21%
Other cancers	106	44%
Total	244	100%

Over 130 types of tumours can originate in the brain and CNS, of which astrocytoma (low- and high-grade gliomas), medulloblastoma and ependymoma are the most common in children (Cancer Research, UK) with medulloblastoma being the focus of this thesis.

1.1 Medulloblastoma

Medulloblastoma, a malignant tumour seen in the cerebellum, constitutes around 20% of the CNS tumours occurring in children (Taillandier *et al.,* 2011; Ostrom *et al.,* 2014), and 70% of paediatric medulloblastoma cases are found in children below the age of 10 (Juraschka and Taylor, 2019). The incidence of medulloblastoma in males is 1.7 times more than that in females (Kaatsch *et al.,* 2017; Ostrom *et al.,* 2018). The symptoms exhibited by medulloblastoma

patients initially are non-specific, including headaches, clumsiness, nausea or morning vomiting, fatigue, or poor school performance, which can potentially be due to hydrocephalus-related increased intracranial pressure or a direct effect of the tumour. More specific symptoms in later stages include ataxia, vision problems, and difficulties with writing or other motor skills. Patients with spinal metastasis exhibit back pain, gait difficulties, and rarely, neurogenic bladder and bowel dysfunction (Wilne *et al.,* 2007). Diagnosis of medulloblastoma is based on the clinical symptoms presented, magnetic resonance imaging (MRI) of the brain and total spine (to screen for macroscopic metastases and assess primary tumours), cerebrospinal fluid (CSF) cytology (to identify microscopic metastases), and integrated histopathology and molecular analysis (Northcott *et al.,* 2019).

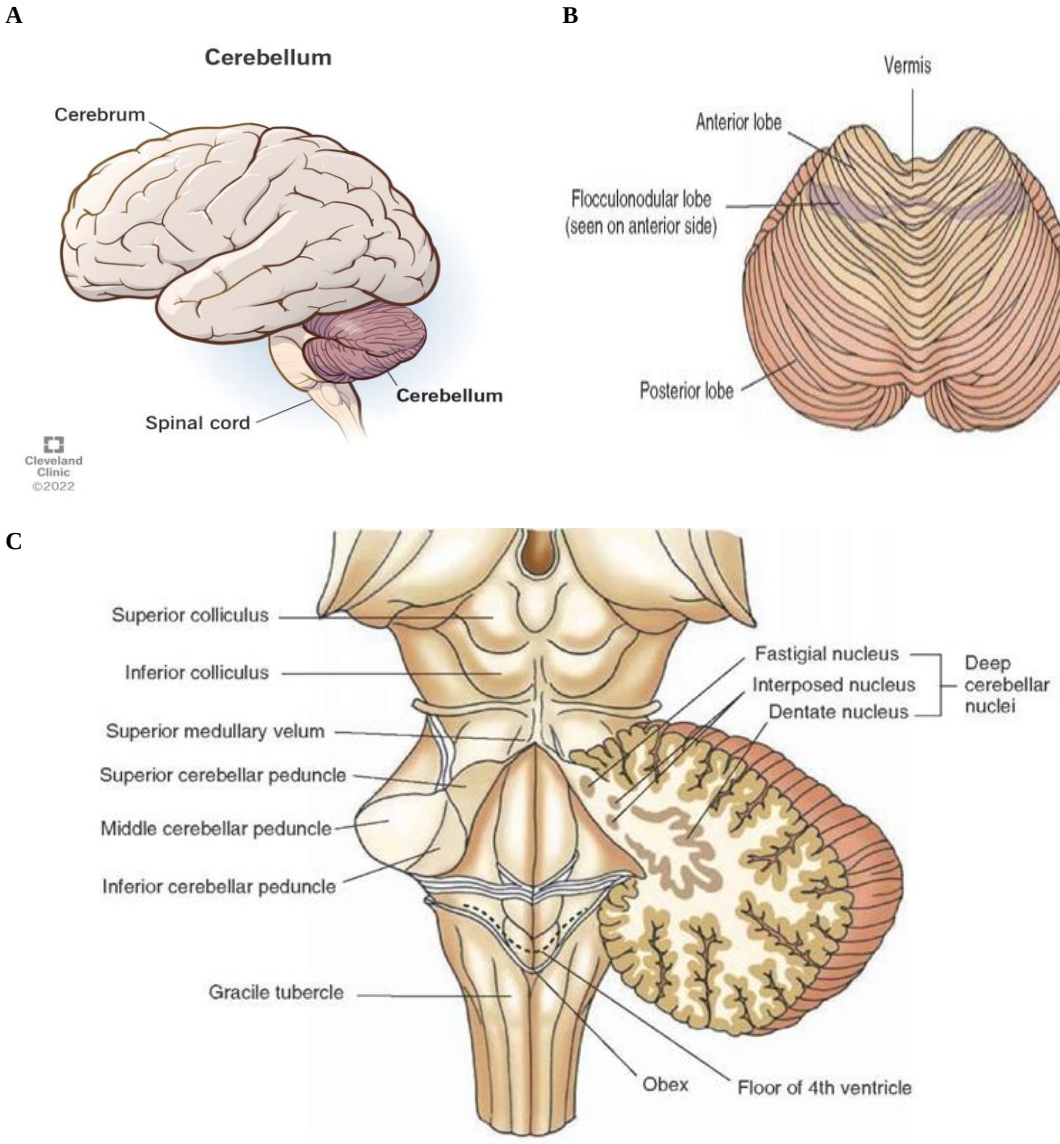

Figure1.1 Cerebellum and brainstem

A) Location of cerebellum B) Dorsal view of the cerebellum indicating the positions of the anterior, posterior, and flocculonodular lobes and the midline region called the vermis. C) Dorsal view of the brainstem with part of the cerebellum cut away for clarity. The connections of the cerebellum to the brainstem are indicated by the presence of the inferior, middle, and superior cerebellar peduncles (when-where-how.com/Neuroscience).

1.1.1 Medulloblastoma Classification

The 2007 World Health Organisation (WHO) CNS tumour classification initially aimed at classifying tumours based solely on their histology (Louis *et al.,* 2007). Recent advancements in biology led to the incorporation of molecular parameters with histology in the 2016 WHO CNS classification. This integration helps determine better the prognosis and treatment options (Louis *et al.,* 2016).

1.1.1.1 Histological classification of Medulloblastoma

The 2007 WHO CNS Tumour classification divided Medulloblastoma into four different histological variants: classical, desmoplastic, medulloblastoma with extensive nodularity (MBEN) and large cell/ anaplastic (LC/A) (Figure 1.2) (Louis *et al.,* 2007).

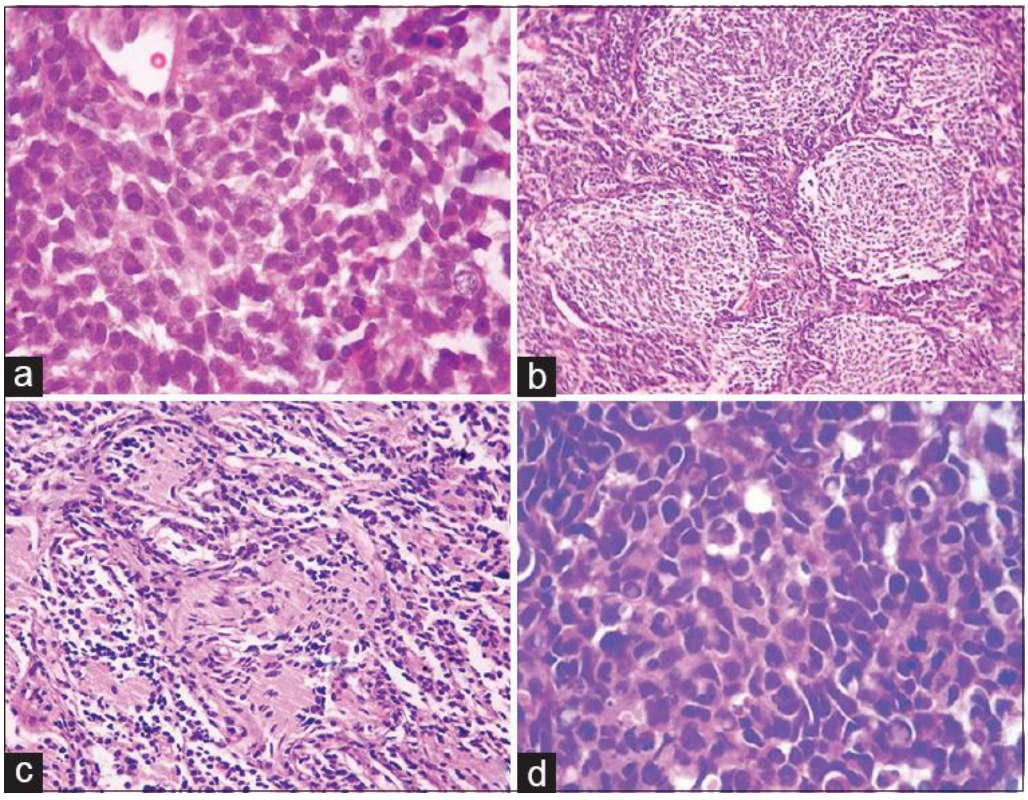

Figure 1.2 Histological subtypes of medulloblastoma

Microphotographs (hematoxylin and eosin stain showing) (a) classic medulloblastoma (b) desmoplastic/nodular medulloblastoma, (c) medulloblastoma with extensive nodularity and (d) large-cell/anaplastic medulloblastoma. All images shown at × 400 magnification which emphasizes the large cell phenotype. (Gupta *et al.,2017)*

Approximately 65% of tumours are classified as classic medulloblastoma (Polkinghorn and Tarbell, 2007). Classic medulloblastoma cells have small to medium-sized, round to oval-shaped hyperchromatic nuclei and minimal cytoplasm. (Millard and Braganca, 2015). About 25% of tumours are of desmoplastic subtype, consisting of reticulin-free nodules (also called pale islands) surrounded by proliferating cells that produce a reticulin-rich extracellular matrix (Polkinghorn and Tarbell, 2007). MBEN subtype comprises approximately 5% of tumours, occurring almost exclusively in infants (Polkinghorn and Tarbell, 2007). It has an expanded lobular architecture with more prominent reticulin-free zones that are more elongated and richer in neutrophil-like tissue. Compared to classic medulloblastomas, desmoplastic/nodular and MBEN variants have improved prognosis. LC/A subtype comprises the most undifferentiated tumours, constituting approximately 5% of tumours. Cells here have large, round, vesicular nuclei and prominent nucleoli. They exhibit poor prognoses when compared to classic medulloblastomas as shown in Figure 1.2 (Millard and Braganca, 2015).

1.1.1.2 Molecular classification of medulloblastoma

Pomeroy *et al.,* 2002 highlighted the presence of distinct molecular subgroups in medulloblastoma. The outcome of their study led several other studies to subgroup medulloblastoma based on the differences in their transcriptome. Thompson *et al* 2006, and Kool *et al* 2008, concluded the existence of five distinct molecular subgroups named A, B, C, D, and E. Cho *et al* concluded in 2011 the existence of six distinct molecular subgroups named C1 to C6, and Northcott *et al* 2011 concluded the existence of four distinct molecular subgroups named SHH, WNT, Group C, and Group D. These variations in subgrouping led to a consensus conference which was held at Boston during the autumn of 2010 at which it was agreed there were four main transcriptional subgroups of medulloblastoma named WNT, SHH, Group 3, and Group 4. (Figure 1.3) (Thomas and Noël, 2019).

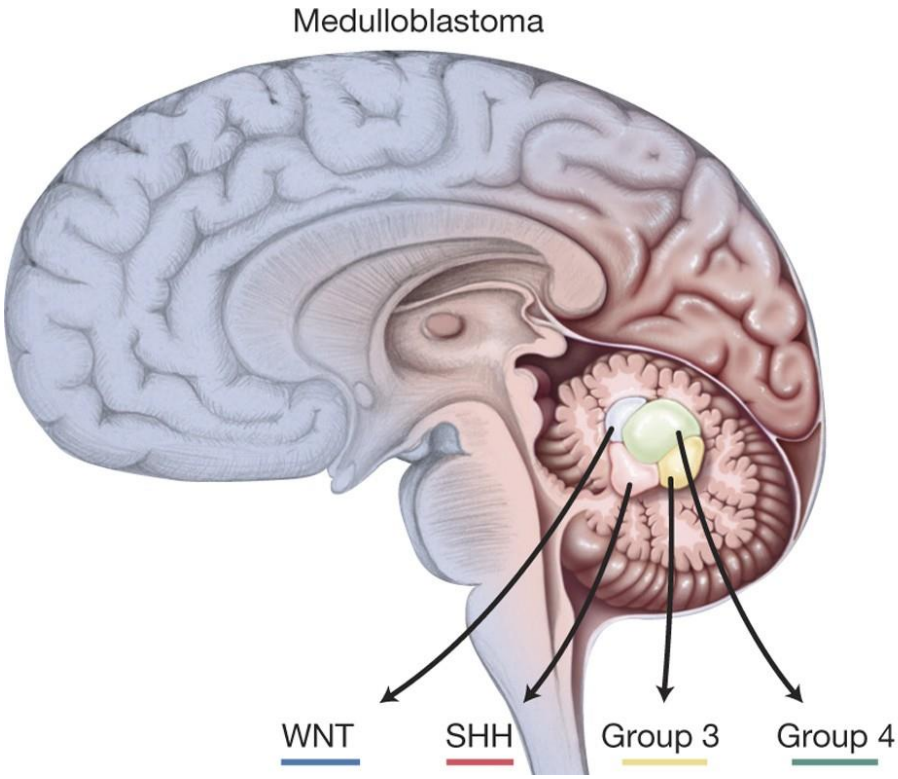

Figure 1.3 Molecular subtypes of medulloblastoma

A section of the cerebellum and brainstem showing common locations was observed for subgroups: WNT (blue); SHH (red), Group 3 (yellow) and Group 4 (green). (Northcott *et al.*, 2017)

WNT subgroup

Wingless-related integration site (WNT)-activated tumours constitute 10%-15% of medulloblastoma cases. They are mostly detected in children between 7 and 14 years of age with the incidence peaking between 10-12 years of age (Orr *et al.*, 2020). The male-to-female incidence ratio is balanced (Northcott *et al.*, 2019). Almost all WNT medulloblastomas exhibit classic histology, in some rare cases LC/A histology is seen (Orr *et al.*, 2020). Tumours are typically located in the midline of the brain, occupying the fourth ventricle and infiltrating the brain stem but can also arise from the cerebellar peduncle or the dorsal brain stem (Hennika and Gururangan, 2015) as shown in Figure1.1. WNT-activated medulloblastomas are mostly non-metastatic at the time of diagnosis. The prognosis in children below the age of 16 is very good with the overall 5-year survival rate being over 95% (Northcott *et al.*, 2019).

In 85–90% of cases, the WNT signalling pathway activation occurs due to the activation of somatic mutations in exon 3 of *CTNNB1 (*Catenin Beta 1*)*, leading to the overexpression of β-catenin. Monosomy 6 is seen in almost 70–80% of the cases (Thomas and Noël, 2019). *WNT* medulloblastomas lacking *CTNNB1* mutations exhibit high levels of *APC* (Adenomatous Polyposis Coli , gene coding for a tumour suppressor protein) mutations. WNT-activated medulloblastomas have poorly developed blood-brain barrier (BBB) and hence are associated with a high degree of haemorrhage (Orr *et al.,* 2020). These clinical and molecular characteristics are summarized below (Table 1.2).

Cavalli et al. suggested two subtypes for WNT: WNTα and WNTβ. The WNTα subtype primarily occurred in children and 98% of these cases exhibit monosomy 6, whereas the WNTβ subtype occurred in older children and adults and only around 29% of the cases exhibit monosomy 6 (Juraschka and Taylor, 2019).

SHH subgroup

Sonic Hedgehog (SHH) subgroup tumours constitute around 30% of the medulloblastoma cases. They typically occur in children below the age of 3 and young adults above the age of 16 (Millard and Braganca, 2015). SHH medulloblastomas arise mostly in the cerebellar hemisphere but also can arise in the cerebellar vermis (Orr *et al.,* 2020) (Figure1.1). The male-to-female incidence ratios here are equal (Millard and Braganca, 2015). SHH subgroup can exhibit all the histologic variants of medulloblastoma with desmoplastic being the most commonly seen (over 50%) followed by classic and LC/A histology (Orr *et al.,* 2020). They are more likely to metastasize than WNT subgroup tumours in infants and children, but less likely when compared to Group 3 or Group 4. Survival varies based on the age and histological subtype. Amongst SHH subgroup tumours, infants with desmoplastic/nodular tumours have the best prognosis, with ten-year overall survival of 84% (Millard and Braganca, 2015). SHH medulloblastomas are characterised by activation of the SHH signalling pathway. Most of the patients have germline or somatic mutations in critical genes of the pathway. These mutations include loss-of-function mutations or deletions in *PTCH1* (Protein Patched Homolog 1) (43%

of patients), loss-of-function mutations or deletions in *SUFU* (Suppressor of Fused Homolog) (10%), *MYCN* (proto-oncogene*)* amplification (7%) etc (*PTCH1* and *SUFU* are genes associated with the negative regulation of the SHH signalling pathway) (Northcott et al., 2012; Kool et al., 2014). Recurrent alterations in the *TP53* (Tumour protein P53, gene encoding tumour suppressor protein) signalling pathway (9.4%) and the PI3K pathway (10%) can also be a contributing factor toward tumorigenesis of this subgroup (Northcott et al., 2012). The 2016 WHO Classification of CNS Tumours separates SHH medulloblastoma with or without *TP53* mutation (Thomas and Noël, 2019). SHH-activated and *TP53* wild-type MBs are associated with intermediate risk disease and a 5-year overall survival of around 76%, whereas SHH MBs with *TP53* mutations are associated with high-risk disease, very poor prognosis and 5-year overall survival of 40% (Thomas and Noël, 2019; Orr *et al.*, 2020). Children with SHH-MB are mostly seen having *TP53* mutation enrichment (Orrego *et al.,* 2019)

Apart from the WHO subgrouping several other SHH subgroups have been proposed, reflecting the molecular, pathological and risk heterogeneity seen in this group. Schwalbe et al described two SHH subgroups based on the age; SHH-infant (<4·3 years) and SHH-childhood (≥4·3 years) (Schwalbe *et al.*, 2017). Cavalli *et al*, described four subtypes of SHH: SHHα, SHHβ, SHHγ, and SHHδ. SHHα occurs during childhood and is characterized by frequent TP53 mutations and *MYCN* amplifications. SHHβ occurs in infants, is frequently metastatic, and is associated with a poor outcome compared to that of SHHγ, which also occurs in infants and is associated with medulloblastoma with extensive nodularity (MBEN) histology. SHHδ subtype occurs in adults and is enriched for TERT promoter mutations (Juraschka and Taylor, 2019).

Group 3

Group 3 constitutes approximately 25% of the medulloblastoma cases, which occur commonly in children and infants (Hennika and Gururangan, 2015). The incidence in males is twice when compared to that of females (Northcott *et al.*, 2019). Group 3 MBs often have classic histology. However, a high ratio of LC/A histology (40%) is seen especially in infants (Cassia *et al.*, 2018).

Radiographically, these tumours typically demonstrate a midline vermian location adjacent to the fourth ventricle (Figure1.1). Group 3 tumours likely arise from a neural stem cell population (Juraschka and Taylor, 2019). Group 3 MB is considered the most aggressive subgroup of medulloblastoma, with 5-year overall survival of <60% and has a high incidence of metastasis at diagnosis (Northcott *et al.*, 2019; Udaka & Packer, 2018).

Unlike WNT and SHH subgroup, integrated molecular analysis has not identified any specific driver pathway for group 3 medulloblastomas. However, proto-oncogene *MYC* amplification is seen occurring in 17% of the group 3 medulloblastoma cases with frequent *PVT1-MYC* fusion. Recurrent somatic mutations are rare in group 3 medulloblastomas, with only four genes mutated in over 5% of cases (Juraschka and Taylor, 2019). Group 3 medulloblastomas expressing high levels of the transcription factor *TWIST1* exhibit the worst overall survival (Cardall 2021). Cytogenetically, Group 3 medulloblastomas exhibit extensive aneuploidy, characterized by frequent isochromosome 17q (~40–50%; whereby the q arm is duplicated, and the p arm is lost); gain of chromosomes 1q and 7; and loss of chromosomes 8, 10q and 16q (Northcott et al., 2019). These clinical and molecular characteristics of group 3 medulloblastoma are summarized in the table below (Table 1.2).

Multiple different subtypes of Group 3 medulloblastomas have been proposed. Based on the gene expression profiles group 3 medulloblastoma patients were divided into two subclasses, c1 and c5. The c1 class was strongly associated with *MYC* amplification or overexpression and was characterized by a poor outcome, whereas c5 had genome-wide aneuploidy and a more favourable outcome. Another study divided group 3 medulloblastoma patients into High-Risk group and Low-Risk group, whereas a third study subtyped group 3 medulloblastomas to Group 3α, Group 3β and Group 3γ. In both studies, subtypes with *MYC* amplification or overexpression were associated with poor outcomes, and additional subtypes with intermediate to favourable subtypes were identified (Northcott et al., 2019; Cavalli *et al.*, 2017; Schwalbe *et al.*, 2017).

Group 4

Group 4 medulloblastomas are the most prevalent and account for about 35% of all medulloblastoma cases. Children between the age of 3 and 16 are affected and it is less common in infants. Group 4 medulloblastoma is said to be more predominant in males when compared to females (3:1) (Menyhárt *et al.,* 2019). Tumours typically have midline vermian location (Figure1.1) (Juraschka and Taylor, 2019). The majority of group 4 medulloblastomas are of classic histology, although cases of LC/A have been observed (Hennika and Gururangan, 2015). The prognosis of group 4 medulloblastoma patients is intermediate and with standard therapy, the 5-year overall survival amounts to 80%. Non-metastatic group 4 patients with chromosome 11 loss have an excellent prognosis, with > 90% survival. Approximately 30–40% of group 4 medulloblastoma patients are metastatic at diagnosis and are currently treated as high risk, including those with an LC/A histology. The 5-year survival of high-risk patients is approximately 60% (Menyhárt *et al.,* 2019).

The cell of origin of group 4 medulloblastoma has not been definitively established; however, these tumours appear to have transcriptional similarities to unipolar brush cells. Common somatic mutations are also rare in this subgroup. Amplifications in *MYCN* is seen in group 4 tumours as well. Cytogenetic events seen in Group 4 MBs are isochromosome 17q, the gain of chromosomes 7 and 18q, and loss of 8q, 8p, 11p, and X. Table 1.2 gives the summary of these clinical and molecular characteristics. Schwalbe *et al*., characterized group 4 medulloblastomas into high-risk and low-risk subtypes. The high-risk group show isochromosome 17q enrichment and their 10-year survival is approximately 36%, whereas the low-risk group exhibit chromosome 11 loss and with a 10-year survival of approximately 72%. Cavalli et al. subdivided group 4 tumours into three subtypes: 4α, 4β and 4γ. Molecular features associated with these subtypes include *MYCN* amplification in group 4α (Juraschka and Taylor, 2019).

Table 1.2 Molecular Subtypes of Medulloblastoma (Juraschka and Taylor, 2019)

	Subgroup	WNT	SHH	Group 3	Group 4
Clinical Characteristics	% of Cases	10	30	25	35
	Age at Diagnosis				
	Gender Ratio (M:F)	1:1	1:1	2:1	3:1
	Anatomic Location				
	Histology	Classic, Rarely LCA	Desmoplastic, Classic, LCA	Classic, LCA	Classic, LCA
	Metastasis at Diagnosis (%)	5-10	15-20	40-45	35-40
	Recurrence Pattern	Rare; Local or metastatic	Local	Metastatic	Metastatic
	Prognosis	Very good	Infants good, others intermediate	Poor	Intermediate
Molecular Characteristics	Proposed Cell of Origin	Progenitor cells in the lower rhombic lip	Granule precursors of the external granule layer	Neural stem cells	Unipolar brush cells
	Recurrent Gene Amplifications	-	*MYCN* *GLI1* or *GLI2*	*MYC* *MYCN* *OTX2*	*SNCAIP* *MYCN* *OTX2* *CDK6*
	Recurrent SNVs	*CTNNB1* *DDX3X* *SMARCA4* *TP53*	*PTCH1* *TERT* *SUFU* *SMO* *TP53*	*SMARCA4* *KBTBD4* *CTDNEP1* *KMT2D*	*KDM6A* *ZMYM3* *KTM2C* *KBTBD4*
	Cytogenetic Events ■ Gain ■ Loss	6	3q, 9p 9q, 10q, 17p	1q, 7, 18 8, 10q, 11, 16q i17q	7, 18q 8, 11p, X i17q
	Other Recurrent Genetic Events	-	-	*GFI1* and *GFI1B* enhancer hijacking	*PRDM6*, *GFI1*, and *GFI1B* enhancer hijacking

Age: Infant Child Adult

1.1.2 Clinal Risk stratification of medulloblastoma

A final classification of medulloblastoma patients stratifies according to risk and was adopted after a consensus meeting of scientists and clinicians in Heidelberg (Ramaswamy *et al.*, 2015).Based on the new stratification protocol, patients are classified into very high risk, high risk, standard risk and low-risk patients. Group 3 medulloblastoma patients who are metastatic and exhibit *MYC* amplification as well as SHH patients who are metastatic with *TP53*

mutation are classified as very high-risk patients and have less than 50% chance of survival. High-risk patients are patients with metastatic or *MYCN* amplified this is seen in SHH subgroup as well as group 4 medulloblastoma patients with leptomeningeal dissemination. Patients with non-*MYCN* amplified, non-*TP53*-mutated SHH medulloblastoma, non-*MYC* amplified group 3 tumours and group 4 tumours without chromosome 11 loss are classified as standard-risk patients. Low-risk patients are non-metastatic WNT patients as well as patients with non-metastatic group 4 tumours and whole chromosome 11 loss (Table 1.3) (Kuzan-Fischer CM *et al.*, 2018).

Table 1.3 Clinal Risk stratification of medulloblastoma

Subgroup	WNT	SHH	Group 3	Group 4
Low risk (<90% survival)	Non-metastatic			Non-metastatic and chromosome 11 loss
Standard risk (75-90% survival)		Non- metastatic and *TP53* Wild Type and No *MYC* amplification	Non- metastatic and No *MYCN* amplification	Non-metastatic and chromosome 11 loss
High risk (50-75 % survival)		Metastatic and *TP53* Wild Type Or Metastatic and No *MYCN* amplification		Metastatic
Very high risk (<50% survival)		*TP53* mutation	Metastatic and *MYC* amplification	

Patient risk stratification based on molecular and outcome criteria (Kuzan-Fischer CM *et al.*, 2018).

1.2 Metastasis

Metastasis is regarded as the deadliest event of tumorigenesis and distant metastasis was regarded as the end stage of tumorigenesis but recent advances in research have shown that metastasis also occurs during the early stages of tumorigenesis. Metastasis is an organ-specific, multistep process. It starts with the tumour cells leaving their primary tumour and ends with them colonising as

secondary tumours in distant sites. Being a multistep process makes drug development hard (Majidpoor and Mortezaee, 2021).

1.2.1 Metastasis cascade

1. Invasion

   Invasion is the first step of metastasis where the cancer cells leave the primary tumour and move into the surrounding tumour-associated stroma and then into the adjacent normal tissue parenchyma. For the cells to reach the stroma they must invade the basement membrane- a specialised extracellular matrix (ECM) (Valastyan and Weinberg, 2011). Epithelial cells are immotile and tightly bound to each other and to the neighbouring ECM. Epithelial-Mesenchymal Transition (EMT) permits epithelial cells to attain mesenchymal phenotype with increased migratory capacity and invasiveness making EMT the key mechanism in the promotion of cancer metastasis. (Fares *et al.*, 2020, Majidpoor and Mortezaee 2021). The completion of an EMT is marked when the epithelial cells attain mesenchymal phenotype which allows them to migrate away from the epithelial layer in which they originated (Kalluri and Weinberg, 2009).

2. Intravasation

   When the locally invasive cancer cells enter the lumina of lymphatic or blood vessels it is known as intravasation. The lymphatic spread of cancer cells is routinely observed in human tumours making it an important prognostic marker for disease progression – dissemination via the hematogenous circulation appears to represent the major mechanism by which metastatic carcinoma cells disperse (Valastyan and Weinberg, 2011).

3. Circulation

   Once cancer cells have successfully intravasated into the lumina of blood vessels, they can disseminate widely through venous and arterial circulation (Valastyan and Weinberg, 2011). Circulation is one of the most difficult stages for cancer cells. Interactions between circulating tumour cells (CTC) and the microenvironmental components of circulation determine the survival of the CTCs and their ability to

eventually extravasate in distant sites. Most CTCs circulate as single cells, whereas others travel in clusters. However, circulating clusters are much more likely to form metastases because they have stromal cells and immune components from the original microenvironment that contribute to their heterogeneity and enhance their survival. Neutrophils participate in cluster formation and suppress leukocyte activation, which increases the chances of CTC survival. Moreover, CTC and platelet interaction leads to the formation of a coating shield of platelets around cancer cells that prevents CTC detection by immune cells and provides the structure needed to bear the physical stresses of circulation (Fares *et al.,* 2020).

4. Extravasation

   Extravasation is a stage where the CTC's that survived the circulation exit the circulation through the endothelial vasculature. Into the target tissue. Exactly when the CTC's exit varies from tumour to tumour (Gupta and Massague, 2006).

5. Colonisation

   The extravasated cancer cells must survive the microenvironment of the distant tissue because the microenvironment of the primary tumour site differs from that of the distant tissues. However, it has been proposed that tumour cells can establish a pre-metastatic niche via exosomes which are extracellular vesicles that communicate signals to local and remote cells, and tissues in order to form micro metastatic lesions and eventually macroscopic tumours (Guo *et al.,* 2019, (Valastyan and Weinberg, 2011) (Figure 1.4). Extracellular vesicles are lipid bound vesicles secreted into the extracellular space by the cell (Doyle and Wong, 2019). Tumour-secreted extracellular vesicles mediate intercellular communication between tumour cells and stromal cells in the adjacent and distant microenvironments. They play a vital role in the growth of the primary tumour and the evolution of metastasis. They are also responsible for multiple systemic pathophysiological processes such as vascular leakiness, coagulation, and reprogramming of stromal recipient cells to support pre-metastatic niche formation and subsequent metastasis (Becker *et al.,* 2016).

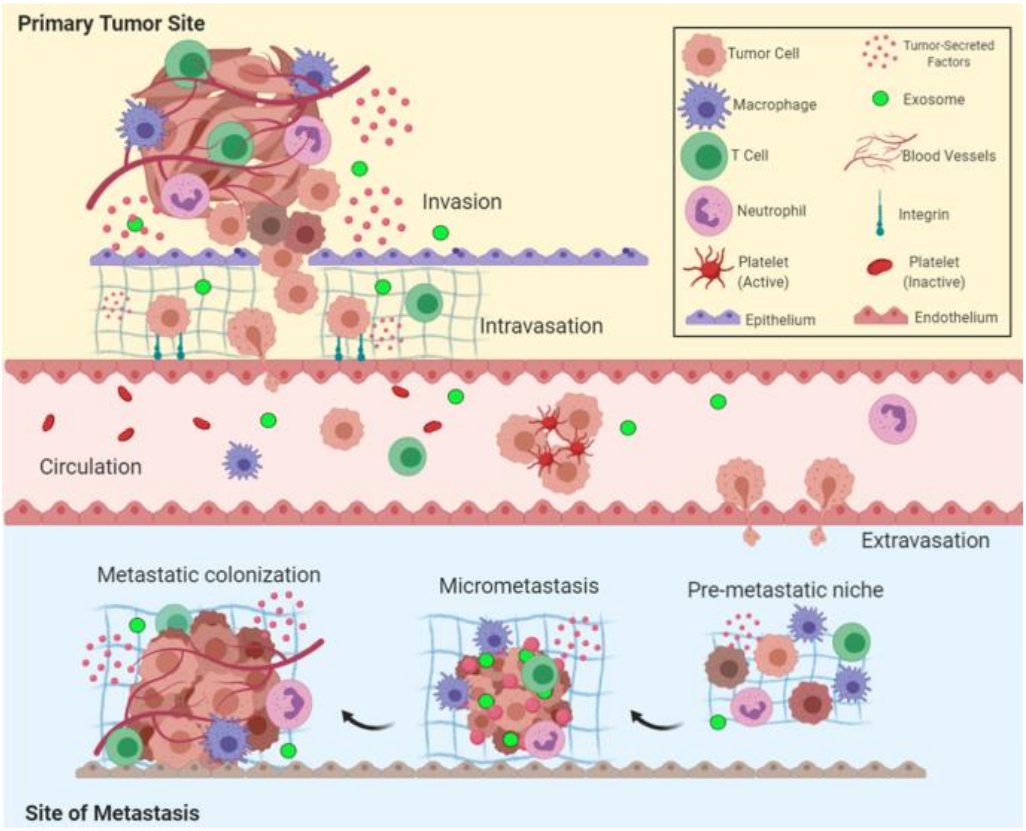

Figure 1.4 Overview of the metastatic cascade

The five key steps of metastasis include invasion into the adjacent tissue, intravasation into the lymphatic or blood vessels, circulating through the lymphatic or blood vessels, exiting the circulation (extravasation), and colonization in the distant tissue (Fares *et al.*, 2020).

1.2.1 Metastasis in Medulloblastoma

Metastasis and recurrence are responsible for 95% of medulloblastoma-associated deaths (Menyhárt and Győrffy, 2020). Metastatic dissemination at the time of initial diagnosis may be present in up to 50% of cases. Metastatic dissemination can be systemic or limited to the CSF. The former is rare with an overall incidence rate of 7% to 10% but is always associated with a very poor prognosis, the latter being the most common, but the mechanisms of dissemination are poorly understood. (Cassia *et al.*, 2018). The incidence of metastatic dissemination in medulloblastoma is also highly subgroup-specific; metastatic dissemination at diagnosis is high in Group 3 and 4 tumours and relatively rare in WNT and SHH medulloblastomas. The pattern of relapse is also seen to be highly subgroup-specific: SHH medulloblastomas recur more

frequently in the previously treated resection cavity, whereas Group 3 and 4 tumours recur almost exclusively with metastatic dissemination (Zapotocky *et al.,* 2017). Since medulloblastomas commonly metastasise to the spinal and intracranial leptomeninges it has fostered the long-held belief that medulloblastoma cells spread directly through the CSF, not the bloodstream. The absence of lymphatic channels in the brain rules out the alternative of lymphatic metastasis. Fults *et al* proposed a leptomeningeal dissemination (LMD) cascade, a 3-stage process:

i. Initiation: medulloblastoma cells escape from the primary tumour mass in the cerebellum and enter the CSF.
ii. Dispersal: surviving cells spread through the CSF channels.
iii. Colonisation: disseminated cells or cell aggregates implant on a distant pial surface and establish a thriving metastatic nidus.

Medulloblastomas arise in the cerebellum allowing them to be in close proximity to the CSF-filled fourth ventricle (Figure1.1). To metastasise, medulloblastoma cells must acquire enhanced migration and invasive properties and be able to weaken cell-cell adhesions so that they can loosen their attachment to neighbouring tumour cells, invade the ECM, and gain access to the CSF (Fults *et al.,* 2019). For this LMD cascade to begin, the cells must be able to invade and migrate; for Group 3 medulloblastoma insights into the process can be garnered from consideration of the genetic alterations that can be seen in this group (Zhou et al., 2010).

The primary molecular signature of Group 3 medulloblastoma is the upregulation of the gene coding for *MYC*. The upregulation of *MYC* suppresses the expression of Thrombospondin-1 (Tsp-1, an adhesive glycoprotein) thereby weakening the intercellular adhesive forces sufficiently to cause individual cells or small aggregates of cells to detach from the tumour mass and enter the CSF (Fults *et al.,* 2019; Resovi *et al.,* 2014). Group 3 medulloblastomas that exhibit chromosome 17q gain are seen to overexpress the cytoskeleton reoganising protein *LASP1 (17q21)*. Overexpression of *LASP1* is strongly correlated with metastatic dissemination and inferior survival (Traenka *et al., 2010*). *WIP1* is another gene seen on chromosome 17q. Overexpression of *WIP1* stimulates C-X-C chemokine receptor type 4 (CXCR-4) on the cell

surface which in turn activates PI3K/AKT signalling and promotes proliferation and invasion (Buss *et al.,* 2015). *PRUNE1* (negative regulator of NME1) promotes metastasis by binding to metastasis-suppressor *gene NME1* and activating Transforming growth factor - β (TGF-β) signalling and then enhances the transcription factor *OTX2* expression and tumour suppressor gene *PTEN* inhibition, which together constitute a signalling axis to promote metastasis (Ferrucci *et al.,* 2018). *NOTCH1* (Translocation-Associated Notch Protein TAN-1) is seen to initiate metastasis in Group 3 medulloblastomas with *TWIST1* and *BMI1* (proto-oncogene) as the downstream mediators. *BMI1* has been proven to promote medulloblastoma invasion and metastasis (Bakhshinyan *et al.,* 2019; Merve *et al,* 2014). TWIST1 in Group 3 medulloblastoma tumours has been shown to regulate pathways linked to metastatic pathways and outcomes (Cardall 2021). Finally, Taylor et al showed that YB-1 regulates traits associated with invasion in group 3 medulloblastoma by establishing *YBX1* knockdown cell lines making YB-1 a worthy target for further investigation. (Taylor 2022).

1.3 Y-Box Binding Protein (YB-1)

YB-1 is a multifunctional protein that got its name from the ability to bind to a sequence in the DNA called a Y-Box (5'-CTGATTGGC/TC/TAA-3') located in the promoter region of the major histocompatibility complex II gene (Lyabin *et al.,* 2013). It is a member of a large family of proteins with an evolutionarily ancient cold shock domain (Eliseeva *et al.,* 2011). YB-1 is involved in various cellular processes like proliferation, differentiation and stress response. YB-1 functions in the cytoplasm as well as in the nucleus. It is a DNA and RNA binding protein and also interacts with a variety of other proteins. Because of its ability to bind to nucleic acids, YB-1 is seen to be involved in almost all DNA and mRNA-dependent processes including DNA replication and repair, transcription, pre-mRNA splicing, and mRNA translation (Taylor *et al.,* 2021).

YB-1 activates the transcription of genes of several protective proteins when moving from the cytoplasm into the nucleus, including proteins that provide multidrug resistance in cells. During DNA repair in the nucleus, YB-1 also

enhances the resistance of cells to xenobiotics and ionizing radiation thereby making YB-1 nuclear localization an early marker of multidrug resistance in malignant cells. Increased levels of YB-1 in the cytoplasm prevent oncogenic cell transformation by the PI3K/Akt signalling pathway, and simultaneously it can promote EMT thereby making it favourable for the cells to spread within the organism and metastasize. Thus, YB-1 in the cytoplasm can be a marker of metastasis in remote organs (Eliseeva *et al.,* 2011).

1.3.1 YB-1 Structure

YB-1 is a 36 kDa protein coded by the gene *YBX1* located on chromosome 1 at position 1p34 (Bergmann *et al.,* 2005). YB-1 consists of three domains: an alanine/proline-rich N-terminal domain (A/P domain), a cold shock domain (CSD), and a large C-terminal domain (CTD) with alternating clusters of positively and negatively charged amino acid residues as shown in Figure 1.5 (Alkrekshi *et al.,* 2021). CSD's have tertiary structures similar to the bacterial major cold shock protein domain whose structure is represented by a closed five-stranded antiparallel β-barrel (Lyabin *et al.,* 2013 and Taylor *et al.,* 2021). This has been suggested by bioinformatics analysis and confirmed by circular dichroism (CD) spectroscopy. Lyabin *et al.,* also showed that the A/P domain and CTD have no secondary structures and appeared to be intrinsically disordered. CTD's binding to nucleic acids was thought to be due to the disordered structure of this domain (Lyabin *et al.,* 2013) but recent DNA structural analyses have revealed that CTD's react with residues in CSD and attain a rigid structure which helps them recognise more DNA binding sites than previously thought (Zhang *et al.,* 2020).

DNA binding was seen to reduce significantly due to the phosphorylation of serine 102 (S102) showing that YB-1's interaction with DNA and RNA is regulated by S102 phosphorylation (Zhang *et al.,* 2020). The distribution of YB-1 between the cytoplasm and nucleus is thought to be regulated by the cytoplasmic retention site (CRS): CRS1 (247–267) and CRS2 (264–290) and by a set of nuclear localisation signals (NLS): NLS-1 (149-156), NLS-2 (185-194), and NLS-3 (276-292) shown in Figure 1.5 (Talyor *et al.,* 2021). Under normal growth conditions, CRS was found to be more prevalent than NLS

making YB-1 localized in the cytoplasm but under certain stress 20S proteasome can cleave off the CRS-containing portion leading to the translocation of YB-1 into the nucleus (Mordovkina *et al.*,2016).

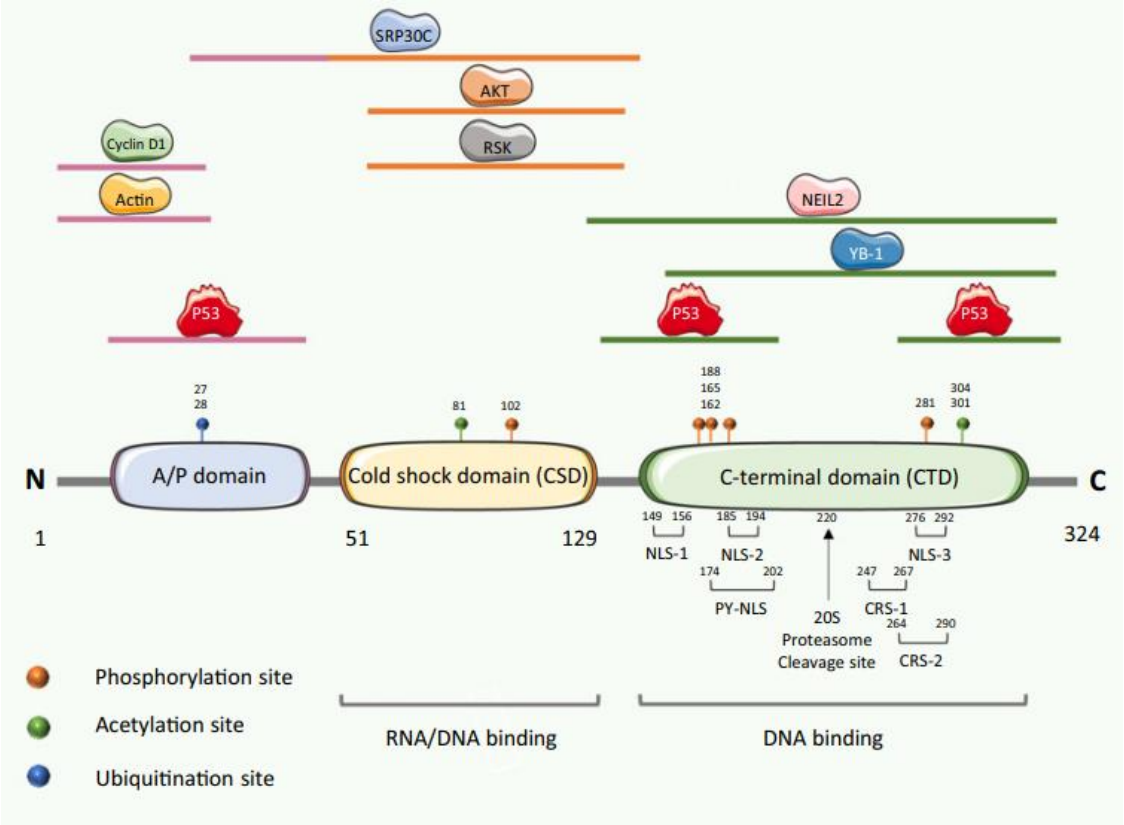

Figure 1.5 YB-1 protein domain organization

YB-1 has a disordered Alanine/Proline rich (A/P) domain, a universally conserved cold shock domain (CSD) and an elongated, disordered C-terminal domain (CTD). Each domain contains binding sites for various protein interactors, some of which are illustrated, with the coloured horizontal bars indicating the region of YB-1 thought to be involved in the interaction denoted. The possibility of YB-1 dimerisation through the CTD is one such interaction. The CTD consist of two cytoplasmic retention signals (CRS) and three nuclear localization signals (NLS) (Talyor *et al.*, 2021)

1.3.2 YB-1 as a DNA Binding Protein

YB-1 was recognized as a transcription factor when it was found to bind to the promotor of two genes: the major histocompatibility complex (MHC) class II and the epidermal growth factor receptor (EGFR) enhancer gene. Though YB-1 acts as a transcription factor for specific genes, the story is far from complete because, in genome-wide chromatin immunoprecipitation (ChIP)-on-chip

analysis of breast cancer cell lines, there were over 6000 potential target genes for YB-1 (Finkbeiner *et al.,* 2009). A study analysed the interaction of YB-1 with oligodeoxyribonucleotides immobilized onto a microchip and found that YB-1 had the greatest preference for the single-stranded motif GGGG, followed by single- and double-stranded motifs CACC and CATC, and a lower affinity for the sequences occurring in Y-boxes. Many studies showed that YB-1 had a higher affinity for single-stranded DNA than double-stranded DNA. YB-1 when translocated from the cytoplasm to the nucleus under stress brings about multidrug resistance, DNA repair etc (Yin *et al.,* 2022) YB-1's role in DNA repair is due to its high affinity to cisplatin-modified DNA, DNA with apurinic sites, DNA with unpaired bases or DNA-containing mismatches (Eliseeva *et al.,* 2011). Studies have shown that the nuclear expression of YB-1 and the expression of the multidrug pump ATP binding cassette subfamily B member 1 (ABCB1) following exposure to therapeutics links YB-1 expression to multidrug resistance mechanisms (Taylor *et al.,* 2023).

1.3.3 YB-1 as an RNA Binding Protein

YB-1's ability to bind to RNA was discovered before its ability to bind to DNA was discovered. YB-1 interacts with numerous mRNAs and is also a potent cap-dependent mRNA stabilizer. YB-1's role as a ribonuclear protein depends on its phosphorylation status. YB-1 when not phosphorylated binds to translationally inactive messenger ribonuclear protein particles (mRNPs) and inhibits internal ribosome dependant mRNA translation but this mRNA binding ability reduces when it is phosphorylated at S102 thereby permitting the translation of mRNAs (Alkrekshi *et al.,* 2021). Non-coding RNA (ncRNA) such as microRNA (miRNA), circular RNA (CircRNA), and long non-coding RNA (LncRNA) are recognized as central regulators of cellular processes, and expression alterationis associated with several cancers (Anastasiadou *et al.,* 2018). Genome-wide analysis of YB-1 and RNA interaction in glioblastoma multiforme revealed that YB-1 regulates miRNA by binding to pri/pre-miR-29b-2 and regulates the biogenesis of miR-29b-2 by blocking its interaction with Dicer (Lai Wu *et al.,* 2015). LncRNA AATBC in breast cancer leads to metastasis by activating Hippo/YAP1 signalling pathway through AATBC-

YB-1-MST1 (Yin *et al.,* 2022). In breast cancer, LncRNA MIR200CHG binds directly to YB-1, inhibits its ubiquitination and degradation and increases YB-1 pS102 expression in the nucleus and cytoplasm thereby promoting proliferation, invasion and drug resistance (Tang *et al.,* 2021). In renal cell carcinoma cells, circ-SAR1A was seen to promote growth and invasion by controlling the miR-382/YBX1 axis (Zhao *et al.,* 2020). YB-1 showed a higher affinity to RNA containing an oxidized base of 8-oxoguanine which is discussed in detail in section 1.3.5. (Hayakawa *et al.,* 2002).

1.3.4 YB-1 and metastasis

YB-1's role in the invasion and metastasis of various other tumours has been studied as well. shRNA-mediated silencing of YB-1 decreased the proliferation, migration, and invasion of neuroblastoma cell line SH-SY5Y (Wang *et al.,* 2017). Knockdown of YB-1 both stably and transiently in pGBM cell line SF188 significantly reduced cell invasion in transwell invasion assays (Gao *et al.,* 2009). Taylor 2022 through modified Boyden chamber assay saw a reduction in the invasive capacity of group 3 MB's upon knocking down YB-1(Taylor 2023). A study in lung cancer showed that YB-1 activated the transcription of *Nanog* thereby increasing the metastatic cells and the formation of new colonies. A study in malignant pleural mesothelioma showed YB-1 knockdown significantly reduces tumour cell migration and invasion (Yin *et al.,* 2022). A study showed that YB-1 overexpression in mammary epithelial cells MCF10AT resulted in their epithelial-mesenchymal transition (EMT). Especially YB-1 synthesized from a plasmid-triggered translation of mRNAs coding for the EMT-providing transcription factors (Snail 1 and 2, HIF1α, LEF-1, ZEB2, etc.) (Laybin *et al.,* 2013). Over-expression of YB-1 in breast cancer cells is associated with loss of E-Cadherin and tight junction protein ZO-1, increased expression of N-cadherin and vimentin and the emergence of a mesenchymal phenotype (Evdokimova *et al.,* 2009). Studies in epithelial tumours showed that YB-1 can regulate the expression or enhance the activity of various matrix metalloproteinases (MMPs) including MMP-11, MMP-14, MMP-2, MMP9 and (MT1)-MMP (Taylor 2022). MMP's degrade ECM promoting the invasion of tumour cells (Gonzalez-Avila *et al.,* 2019).

1.3.5 YB-1 and Oxidative Stress

YB-1 is linked with the cell's response to oxidative stress. The cold shock domain is said to be involved in stress response. YB-1 is said to localize to the cytoplasmic stress granules (SG's) under acute oxidative stress (Guarino *et al.,* 2018). SG's are one mechanism by which cell responds to protein synthesis under stress. SG's require specific RNA-binding proteins like G3BP1. YB-1 is said to bind to the 5'untranslated region (UTR) G3BP1 mRNAs, thereby controlling the availability of the GTPase G3BP1 which activatesSG assembly (Somasekharan *et al.,* 2015). 8-oxoguanine modification occurs due to oxidative stress conditions and can cause different errors during protein biosynthesis. It is assumed that YB-1 blocks the translation of the 8-oxoguanine containing mRNA by binding to it.

1.4 Oxidative stress

Cellular homeostasis is maintained when there is a balance between the production and degradation of reactive oxygen species (ROS). Oxidative stress is the imbalance between excessive oxidant formation and the scavenging of those radicals by antioxidants (Daenen *et al.,* 2019). The brain is more susceptible to oxidative stress due to its high oxygen consumption (Salim 2016). ROS can be mutagenic and promote tumour formation through the oxidation of the guanine base in the DNA and RNA producing 8-Oxoguanine (Figure 1.6) (Gill *et al.,* 2016). 8-Oxoguanine can base-pair to both cytosine(C) and adenine(A) (Boogard *et al.,* 2020) thereby resulting in G to T and C to A substitutions, potentially introducing missense mutations (Gill *et al.,* 2016).

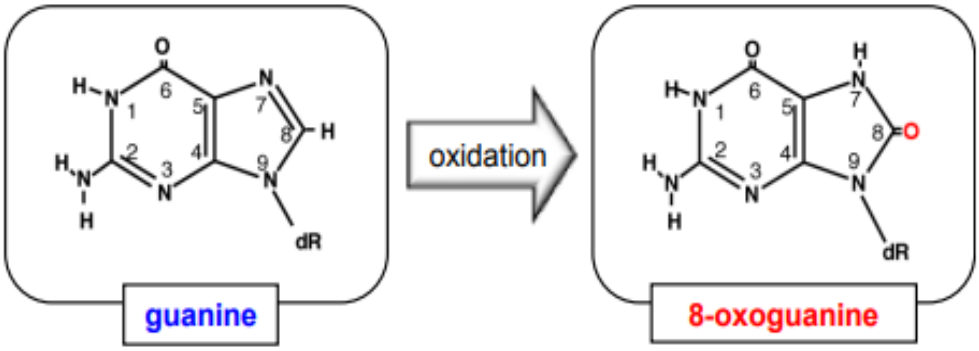

Figure 1.6 Oxidation of guanine base

Reactive oxygen species (ROS) generate 8-oxoguanine by oxidation of guanine base in the C8 position. 8-oxoguanine is highly mutagenic as it can pair to both adenine and cytosine. After two rounds of replication it increases the occurrence of A:T to C:G or G:C to T:A transversion mutations. (Nakabeppu 2014).

1.4.1 8-Oxoguanine in cancer

8-oxoguanine serves as a promising biomarker for predicting the prognosis and survival outcomes of various cancers due to their high levels in in tumours, blood samples or urine (Qing *et al.,* 2019). Karihtala *et al.,* showed that 8-hydroxydeoxyguanosine (8-OHdG) plays a significant role in ovarian carcinogenesis suggesting 8-hydroxydeoxyguanosine to be a novel prognostic marker in ovarian cancer (Karihtala *et al.,*2009). Li *et al.,* reported 8-hydroxydeoxyguanosine levels to be associated with hepatocellular carcinoma characteristics, including tumour size, tumour quantity, clinical staging, child classification, portal vein thrombosis and ascites. Therefore suggested 8-hydroxydeoxyguanosine to be a novel prognostic factor in hepatocellular carcinoma when taken together with the other clinical characteristics (Li *et al., 2012*). Studies have also reported 8-oxoguanine as prognostic markers for breast cancer as well as renal cell carcinoma (Qing *et al.,* 2019). In colon cancer, oxidative stress is induced at an early and is intensified during cancer progression based on which a study conducted by Diziaman *et al.,* showed 8-oxoguanine to be an effective predictor of survival in colon cancer patients (Diziaman *et al.,*2014).Studies on several cancer groups like nonsmall-cell lung cancer, cutaneous melanoma, colorectal cancer have shown 8-oxoguanine to be

a suitable marker to be used to determine the survival outcomes (Qing *et al.*, 2019).

1.4.2 8-Oxoguanine in DNA

In the DNA over 100 oxidative adducts have been identified, ranging from modifications of the bases (e.g., 8-oxo-dG, 8-oxo-dA, thymidine glycol, 5-hydroxylcytosine, and 5-hydroxyuracil) and nucleotides (abasic or cyclic forms; e.g., 2-deoxyribonolactone, 5′,8-cyclo-2’-deoxyguanosine, and 5′,8-cyclo-2’-deoxyadenosine) to those with breakage of the phosphate backbone. Guanine has the lowest redox potential compared to the other bases making 8-oxo-dG the most prevalent oxidized form generated by reacting with oxygen at the C8 position, of which the double bond in guanine is directly attacked by the hydroxyl radical (J.Y. Hahm et al., 2022). 8-Oxoguanine was first discovered in DNA during the characterization of carcinogenic molecules related to oxidative stress owing to which they are widely used as a ROS biomarker (Ock *et al.*, 2012). 8-Oxoguanine can be either produced directly at the DNA or at the free nucleotide level (8-oxo-dG or 8-oxo-dGTP), which can be incorporated through DNA replication. As stated above, 8-Oxo-dG is highly mutagenic because of its ability to pair with adenine causing a guanine-to-thymine mutation (G > T, the same as C > A) during DNA replication (J.Y. Hahm et al., 2022).

1.4.3 8-Oxoguanine in RNA

Guanine in the RNA is more vulnerable to producing 8-oxoguanine under oxidative stress than guanine in DNA as there are exposed (single stranded) and unsecured (lacks reductant defence mechanism), but the focus on 8-oxoguanine in the RNA is low because most RNAs are relatively unstable macromolecules (with rRNA and rRNA being notable exceptions). Therefore, 8-oxoguanine in the DNA has been studied more than 8-oxoguanine in the RNA, and the latter’s repair mechanisms and regulatory functions are largely unknown. Among the numerous forms of oxidized RNA (e.g., 8-oxoguanine, 8- oxoadenine, 5-hydroxyuridine, and 5-hydroxycytidine), 8-oxoguanine is the most abundant product and is susceptible to further oxidation, strand breakage,

and base removal. Due to the wide range of biological roles played by RNA , oxidation of RNA can critically lead to miscellaneous dysfunctions and regulation of both coding and noncoding RNAs, which are related to pathophysiological consequences under oxidative (J.Y. Hahm et al., 2022).

1.4.4 8-Oxoguanine repair Mechanism

DNA Repair Mechanism:

8-oxoguanine accumulates in DNA either due to the incorporation of 8-oxo-dGTP from the nucleotide pool or because of direct oxidation of guanine in the DNA (Nakabeppu 2014). In eukaryotes, MTH1 (also known as NUDT1), a homolog of the *Escherichia coli* MutT protein hydrolyzes oxidized purine nucleoside triphosphates like 8-oxo-dGTP, to the corresponding monophosphates and pyrophosphates (Sakai *et al.*, 2002) .8-oxo-dGMP is further converted to the nucleoside, 8-oxo-dG, thus avoiding their incorporation into DNA as shown in Figure 1.7 (Nakabeppu 2014).

8-oxoguanine incorporated in the DNA is removed by 8-oxoG DNA glycosylase, encoded by the *OGG1* gene,(Radicella *et al.,* 1997). OGG1 removes the oxidized base to initiate base excision repair (BER). OGG1 preferentially excises 8-oxoguanine opposite cytosine (Lu *et al.,* 1997). A DNA glycosylase encoded by *MUTYH,* a homolog of *E. coli* mutY, excises the adenine inserted opposite 8-oxoG in the template strand (Slupska *et al.*, 1999). When base excision repair (BER) is initiated by MUTYH, cytosine is inserted opposite 8-oxoguanine in the template DNA. OGG1 then removes the 8-oxoG residue opposite cytosine in DNA. MUTYH thereby contributes to minimising 8-oxoG accumulation in DNA as shown in Figure 1.7 (Nakabeppu 2014).

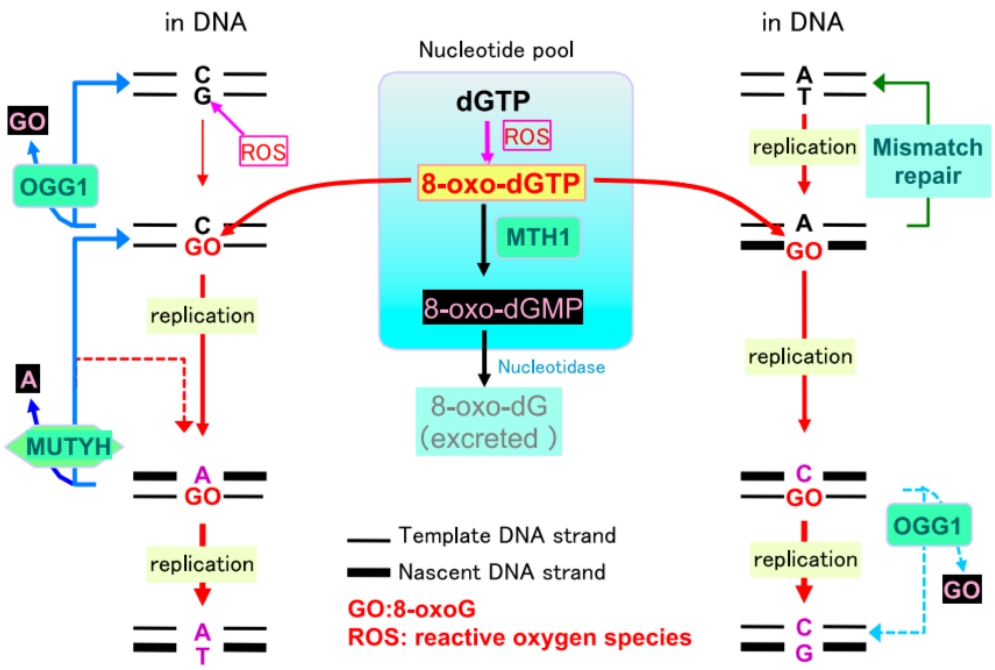

Figure 1.7 8-Oxoguanine repair in the DNA

8-oxoguanine gets repaired either in the nucleotide pool by MTH1/NUDT1 (black coloured arrow) or in the DNA by OGG1 and MUTYH (blue coloured arrows). Unrepaired 8-oxoguanine base leads to A:T to C:G or G:C to T:A transversion mutations (purple colour) (Nakabeppu 2014).

RNA Repair Mechanism:

Direct repair of 8-oxoguanine in the RNA is not well known (J.Y. Hahm et al., 2022). YB-1 is seen to bind specifically to RNA containing 8-oxoguanine and is assumed that by recognizing the modified mRNA, YB-1 is capable of blocking its translation (Hayakawa et al., 2002; Eliseeva et al., 2011).

1.5 Aims of this project

As a part of her PhD work, Taylor (2022) aimed to identify the transcriptional targets regulated by YB-1 under acute and chronic treatment of cisplatin and vincristine in Group 3 MB's by performing ChIP Sequencing. Unfortunately, all the input samples irrespective of their cell line or treatment state exhibited unexpected peak enrichment which led to poor alignment of the input samples to the human genome and problematic peak calling analysis. PCR errors and sequencing mis-calls which are the common causes for poor alignment were ruled out. Similarly, the data was not affected by the so-called Exclusion List, a

list of regions in the human genome known to give high variance in mapping experiments. Further sequencing of Taylor 2022's samples was carried out by the University of Nottingham DEEP-SEQ facility and a prevalent 8-oxoguanine signal was detected leading the poor alignment with its reference genome. *The overarching aim of this thesis is to determine this enrichment of 8-oxoguanine is artefactual in the ChIP sequencing or is a general reflection of paediatric medulloblastoma samples.*

8-oxoguanine lesions can be either naturally occurring in the tumour cells or can occur artifactually (Van den Boogaard *et al.,* 2020). Van den Boogaard *et al.,* confirmed the presence of naturally occurring 8-oxoguanine in neuroblastoma by performing Sanger sequencing and Lida *et al.,* confirmed the presence of 8-oxoguanine in various brain tumour tissues by immunohistochemistry (Van den Boogaard *et al.,* 2020; Lida *et al.,* 2001). In contrast, Costello *et al.,* in their work, showed that 8-oxoguanine lesions can occur during due to the shearing of samples during sample preparation for sequencing (Costello *et al.,* 2013) (chromatin shearing was used in Taylor's ChIP Sequencing study). Therefore, the study's first aim is to check if the 8-oxoguanine lesion detected is natural or artefactual by performing immunofluorescence in the parental and the drug-tolerant Group 3 MB cell lines.

In their study, van den Boogaard *et al*. showed that defects in the base excision repair (BER) pathways increased the levels of 8-oxoguanine lesions in Neuroblastoma (Van den Boogaard *et al.,* 2020). Hence the next aim of the work is to determine if there are any defects in the 8-oxoguanine defence mechanism in Group 3 MB's.

Hiroshi *et al.* showed that YB-1 binds specifically to 8-oxoguanine containing RNA and is assumed to prevent its translation (Hiroshi *et al* 2002; Eliseeva *et al*., 2011) and 8-oxoG DNA glycosylase (OGG1) specifically excises 8-oxoguanine incorporated in the DNA (Lu *et al.,* 1997). Therefore, the next aim is to determine if YB-1 regulates 8-oxoguanine levels and how the presence and reduction of OGG1 and/or YB-1 relates to 8-oxoguanine levels.

Lin *et al.,* showed that 8-oxoG is associated with the lymphatic metastasis of cervical carcinoma (Lin *et al.,* 2022) and several studies have shown the involvement of YB-1 in the metastasis of various cancers. With 8-oxoguanine and YB-1 having been seen involved in metastasis, the next aim of the work is to study the colocalization of YB-1 and 8-oxoguanine between Group3 MB's primary tumour cell line and their corresponding metastatic cell line.

Aim 1: To determine whether the 8- oxoguanine lesion detected in Taylor's ChIP Seq data is natural or artefactual.

Aim 2: To determine if there are any defects in the 8-oxoguanine defence mechanism in Group 3 MB's.

Aim 3: To determine if YB-1 can regulate 8-oxoguanine levels and to check if the presence and reduction of OGG1 and/or YB-1 relates to 8-oxoguanine levels.

Aim 4: To determine the colocalization of YB-1 and 8-oxoguanine between Group 3 MB's primary tumour cell line and their corresponding metastatic cell line.

Chapter 2. MATERIALS AND METHODS

2.1 Genome analysis of publically available datasets

The R2 Genomic Analysis and Visualization Platform (https://r2.amc.nl/) was used the analyse the expression of the gene of interest in publically available datasets. The datasets used in this study are listed in Table 2.1

Table 2.1 Gene expression dataset used in this study

Dataset	**Sample/Tumour Type**	**Number of samples**	**Reference**
Roth	Normal Cerebellum	9	Roth *et al.,* 2006
Pfister	Medulloblastoma	223	Northcott *et al.,* 2017
Cavalli	Medulloblastoma	763	Cavalli *et al.,* 2017

2.2 Cell Culture

2.2.1 Cell Maintenance

Eight cell lines were used for this study and their clinical information can be found in Table 2.2. The cells were grown at 37℃ and 5% CO_2 using suitable flaks and medium and the details of which can be found in Table 2.2. The cells were subcultured after they reached 70% confluency. All the cell lines were from the local stocks originating from donations from authors in the reference column of Table 2.2

Table 2.2 Cell Lines used in this study

Subgroup	Cell Line	Metastatic State	Growth Type	Media	Reference
Group 3 MB	HD-MB03	Spinal metastasis at diagnosis (M3)	Semi-Adherent	Roswell Park Memorial Institute-1640 (RPMI-1640; Sigma-Aldrich; R8758) + 10% foetal calf serum (FCS)	Milde *et al.*, 2012
	D425*	Non-metastatic (M0)	Semi-Adherent	Dulbecco's Modified Eagle Serum (DMEM;Sigma-Aldrich;D6429)+ 10% FCS	He *et al.*, 1991
	D458*	Metastatic (M+)	Semi-Adherent		
HEK293A	Human Embryonic Kidney	N/A	Adherent	DMEM+ 10%FCS	DuBride RB *et al.*, 1987
Drug Tolerant and Vehicle MB	DT-HD-MB03-CIS	N/A	Semi-Adherent	RPMI +10%FCS + 0.5µM cisplatin (Merck;C2210000)	Taylor 2022
	DT-HD-MB03-DMF	N/A	Semi-Adherent	RPMI +10%FCS + 0.005% DMF (Sigma-Aldrich;D4551)	
YB-1 Knockdown cell lines and Vehicle MB	KD-HD-MB03 or NS-HD-MB03	N/A	Semi-Adherent	RPMI +10%FCS + 2µg/ml puromycin (Sigma, P8833)	Taylor 2022

MB – Medulloblastoma; *- Primary cell lines and their matched metastatic cell line

2.2.2 Culturing Adherent Cell lines

The HEK293A cell line grew adherently in standard culture. Medium, PBS (10x PBS; Lonza 17-517Q) and trypsin were pre-warmed before sub-culturing. To sub-culture these cells, the growth medium was removed and discarded, and the cells were washed with 1x PBS once and discarded. The cells were detached by incubating them with 3ml Trypsin-EDTA (Sigma-Aldrich; T4174) at 37°C for 3 to 4 minutes. The trypsinisation was stopped by the addition of double the volume of the dissociating solution and the contents were transferred to a 20ml tube. The cell suspension was centrifuged at 500 x g for 5 minutes. The supernatant was discarded, and the pellet was re-suspended in its respective medium (Table 2.2) at a ratio of 1:10 and seeded into a new T75 flask (Thermo Scientific; 130190) containing 10-12ml of the medium.

2.2.3 Culturing Semi-Adherent Cell lines

Group 3 Medulloblastoma cell lines HD-MB03, D425 and D458 grew semi-adherently in standard culture consisting of a mixed population of adherent cells, semi-adherent cells and suspension cells. To sub-culture these lines, the growth medium was transferred to a 20ml tube. The cells were washed using 1x PBS and transferred to the same tube. The cells were detached by incubating them with 2ml Trypsin-EDTA at 37°C for 3 to 4 minutes. The trypsinisation was stopped by the addition of double the quantity of the medium. The contents were transferred to the same tube. The cell suspension was centrifuged at 100 x g for 5 minutes. The supernatant was discarded, and the pellet was re-suspended in its respective medium (Table 2.2) at a ratio of 1:10 or 1:20 and seeded into a new T75 flask containing 10-12ml of the medium.

2.2.5 Maintaining Drug-Tolerant Cell lines

DT-HD-MB03-CIS, the drug-tolerant cell line of group 3 medulloblastoma cell line HD-MB03 and its respective vehicle cell line DT-HD-MB03-DMF grew semi-adherently and were cultured similarly to their parental cell line. Cisplatin tolerant cell lines were generated by Taylor 2022 by continuous selection

model. The cells were grown in gradually increasing concentrations of the cytotoxic drug starting at 1/100th the IC_{50} and doubling it from there with subsequent passages until a stable tolerance was obtained and quantified with cytotoxicity assays (Taylor 2022). The drug tolerant cell lines were cultured with media containing 0.5µM Cisplatin and vehicle treated cell line were cultured with media including 0.005% of DMF.

2.2.6 Culturing Knockdown Cell Lines

Taylor 2022 generated cell lines with stable knockdown of *YBX1* expression through shRNA mediated gene silencing using the GIPZ Lentiviral particle starter kit for YBX1. The *YBX1* gene expression was reduced by 93% and the protein levels were reduced by 83% after knockdown (Taylor 2022). KD-HD-MB03, the *YBX1* Knockdown cell line of group 3 medulloblastoma cell line HD-MB03 and its respective vehicle cell line NS-HD-MB03 grew semi-adherently and were cultured similar to their parental cell line with puromycin (2µg/mL).

2.2.7 Stock Preparation

The cells were trypsinised and the pellet was obtained as previously described. The pellet was resuspended in the desired quantity of freezing medium. The freezing medium was made from 90% v/v FCS and 10% v/v DMSO (Sigma-Aldrich; D8418). 0.5ml or 1ml of the cells suspended in the freezing medium were transferred to cryogenic vials. The cryogenic vials were then placed in a controlled cooler container at -80℃ for 24 hours and the cryovials were then transferred to the liquid nitrogen store.

2.2.8 Recovering cells from liquid-nitrogen storage

The cryogenic vials were thawed in a water bath set at 37^{o}C. Once thawed, the cells were transferred into a T25/T75 flask containing 5-7ml/10-12ml of fresh medium respectively. In the case of drug-tolerant cell lines and vehicle cell lines, the cell suspension was transferred to a T25/T75 flask containing drug-free medium, and once recovered drug/vehicle-containing medium was used.

In case of knockdown cell lines, the cells were recovered in media containing the desired amount of puromycin. Once the cells reached 60% confluency, they were further cultured using the respective medium as mentioned above.

2.2.9 Cell Counting

For counting cells, they were washed, trypsinised, pelleted and re-suspended in the required amount of medium. The cells were counted using ths CellDrop Automated Cell Counter (DENovix). The lower arm was brought to its resting position. 15µl of 70%ethanol was pipetted between the sample surfaces. The arm was lifted and the top and the bottom arm were wiped using a dry laboratory wipe. The arm was then lowered and 10µl of the cell suspension was pipetted between the sample surfaces. Using the Trypan Blue software, the number of cells in 10µl of the cell suspension was measured.

2.3 Assessing Cell Viability

PrestoBlue assay was used (ThermoFisher; A13262) to determine the changes in cell viability. The PrestoBlue Cell Viability Reagent is a resazurin-based solution that helps measure the viability of the cells based on the living cells reducing ability. Once PrestoBlue reagent enters the living cells it is reduced to resorufin which is red in colour and highly fluorescent. The viability of the cell can be monitored by the change in fluorescence. Non-viable cells cannot reduce this dye and hence produce no fluorescence.

Cells were plated in complete medium at 5000 cells per well in clear-bottomed, black-walled 96-well plates (Greiner; 655090) and left to settle for 24 hours. Cells were then treated with 2.5µM, 5µM ,10µM, 20µM and 50µM concentrations of TH5487 and incubated at 37℃ and 5% CO_2 for 24, 48 and 72 hours. Following treatment, surviving cells were assayed with PrestoBlue at a final dilution of 1:10 for 30 minutes at 37℃ and 5% CO_2 and fluorescence was measured at 555/595nm using SpectraMax^{R} iD3 Multi-Mode Microplate Reader.

2.4 Immunofluorescence

2.4.1 Single Staining

For immunofluorescence (IF), cells were seeded in chamber slides (Ibidi; 80841) at 20,000 cells/well (HD-MB03, DT-HD-MB02-CIS, DT-HD-MB03-DMF) and were incubated overnight. For these semi-adherent cell lines, in order to let the suspension cell population settle the chamber slides were taken out of the incubator 15 minutes prior to fixing. After 15 minutes, 3/4ths of the medium was removed by careful aspiration, leaving a thin layer ($1/4^{th}$) of the suspension cells. The cells were fixed using sterile filtered 4% w/v paraformaldehyde (PFA) for 20 minutes at room temperature. Following the fixation, the wells of the chamber slides were either washed with PBS and used immediately for immunofluorescence or washed with PBS, wrapped in parafilm and stored in PBS at 4°C for use within 4 weeks.

The cells were permeabilised by incubating the wells with PBX (PBS + 0.1% v/v Triton X-100) for 30 minutes. The wells were then washed with PBS and blocked for one hour with 10% v/v goat serum (Vector Laboratories; S1000)) at room temperature in a humidity chamber. Following blocking, the primary antibody diluted in blocking solution (Table 2.3) was added dropwise to the wells and incubated in a humidity chamber either for one hour at room temperature or overnight at 4°C. The wells were then washed in PBT (PBS + 0.1% v/v Tween-20) 5 minutes, 10 minutes and 15 minutes, after which the secondary antibody was added dropwise to the wells and incubated in a darkened humidity chamber for one hour at room temperature. The secondary antibody was washed off with PBT for 5 minutes, 10 minutes and 15 minutes. Following the PBT wash, the cells were equilibrated in PBS. Following the equilibration, 500nM 4′,6-diamidino-2-phenylindole dihydrochloride (DAPI) (Invitrogen; D1306) was added to the wells and incubated for 5 minutes. The cells after incubation with DAPI were washed thrice in a 5-minute period with PBS. The slides were dried and mounted in FluoroGel mounting medium (GeneTex; GTX28214). Following this, a 22 X 50mm cover slip was placed

carefully over the sample. After the mounting medium was set the slides were sealed using nail polish and stored at 4℃ in a slide box for imaging.

2.4.2 Double staining

For double staining immunofluorescence (IF), cells were seeded in chamber slides (Ibidi; 80841) at 40,000 cells/well (D425 and D458) and were incubated overnight. The cells were fixed, permeabilised and blocked as mentioned in section 2.4.1. Following blocking, both the primary antibodies were diluted together in the blocking solution (Table 2.3) was added dropwise to the wells and incubated in a humidity chamber either for one hour at room temperature or overnight at 4℃. The wells were then washed in PBT (PBS + 0.1% v/v Tween-20) for 5 minutes, 10 minutes and 15 minutes, after which the respective secondary antibodies were diluted together and added dropwise to the wells and incubated in a darkened humidity chamber for one hour at room temperature. The secondary antibody was washed off with PBT for 5 minutes, 10 minutes and 15 minutes. Following the PBT wash, the cells were equilibrated in PBS. Following the equilibration, 500nM 4′,6-diamidino-2-phenylindole dihydrochloride (DAPI) (Invitrogen; D1306) was added to the wells and incubated for 5 minutes. The slides were washed, dried and mounted with the mounting medium as mentioned in section 2.4.1.

2.4.3 Immunofluorescence Imaging

Slides were imaged using Zeiss Axiovert S100 Inverted Phase Contrast Fluorescence Microscope at phase 1 with a 32x air lens. All images were taken at 1300x 1030-pixel resolution. The resulting images were then viewed and analysed using Fiji (ImageJ) software (Schindelin *et al.*, 2012).

2.4.4 Software analysis

In order to quantify the intensity of multi-channel immunofluorescence images, Fiji (ImageJ) software was employed. To obtain the cell's total intensity the multichannel images were split into mono-channel images (Image>colour>split channel). Next, the red channel images were chosen. The staining in these channels was more cytoplasmic than nuclear so the Region of Interest (ROI)

for individual cells were marked using the freehand tool from the toolbar. The intensity of the ROI's were measured and were corrected for background by measuring the intensity for the same area as the ROI in a region without staining within the image. Mean Grey Value was chosen as the measure to analyse. The final intensity of the ROI was obtained by subtracting the background intensity from the actual intensity of the ROI. To analyse the fluorescence intensity in the nuclear region of the cells, DAPI channel image was selected from the split mono-channel images. "Process > Binary > Watershed" function was used to separate cells for better analysis. The following measurements were selected; output: mean grey value, area, integrated density. Next, the "analyse particles" command was executed with the parameters set at: size 50-infinity; pixel units; show outlines; add to ROI manager; show results. The resulting image contained outlined and numbered nuclei marked as individual regions of interest (ROI). The ROI's were over laid in the corresponding non-binary image and executing the measure command gave the fluorescence of the nuclear region of each cell (Taylor 2022). Fluorescence in the cytoplasmic region is obtained by subtracting the fluorescence of nuclear region from the total fluorescence of the cell (Kelley and Paschal 2019). The intensity of 20 cells for each cell line was determined in this manner and the average of these cells was obtained. To analyse the colocalization coefficients of the multi-channel immunofluorescence images, the split mono-channel images either the red or green channel image is threshold (Image> Adjust> Threshold) and the ROI is marked. Using the coloc2 tool (Analyse> colocalization>coloc2) mask the ROI on the other fluorescent channel and analyse. The resulting Pearson's coefficient gives the colocalization coefficient. The values were normalized and plotted using GraphPad Prism 9.

Table 2.3 Antibodies used in immunofluorescence

Antibody	Primary/Secondary	Host Species	Dilution	Source
N45.1 (8-Oxoguanine)	Primary	Mouse (monoclonal)	1:75	Abcam (ab48508)
YB-1	Primary	Rabbit (Polyclonal)	1:100	Cell Signalling Technology (4202S)
Alexa-Fluor 568 Anti-Mouse	Secondary	Goat	1:100	Life Technologies (A11031)
Alexa-Fluor 488 Anti-Rabbit	Secondary	Goat	1:500	Life Technologies (A11034)

2.5 Western Blot

2.5.1 Cell pellet preparation and cell lysis

The cell suspension was centrifuged at 100 x g for 5 minutes. The supernatant was discarded, and the cell pellet is resuspended in 1ml 1x PBS and transferred to a 1.5ml microfuge tube. The suspension was centrifuged again, and the supernatant was completely discarded. The cell pellet was then transferred to the -80℃ freezer if not being used immediately. For protein analysis, the cell pellets stored at -80℃ were thawed on ice for 5 minutes. The cells pellets were re-suspended in 500µl of ice-cold PBS+10% (v/v) Glycerol and 1x EDTA-Free Protease Inhibitor Cocktail Set III (MilliporeSigma, 539134-1SET) was added and the cell pellets were probe sonicated (Vibra Cell^{TM}, Jencons Scientific LTD) three times with 10-second interval between each sonication. The entire process was carried out on ice.

2.5.2 Determination of Protein Concentration

To ensure equal loading of protein for each well during sodium dodecyl sulphate-polyacrylamide gel electrophoresis (SDS-PAGE) a modified Lowry assay was performed. Using a Bio-Rad DC protein assay kit and a standard

curve of 0-10µg bovine serum albumin (BSA), the total protein concentration of the cell lysates was determined. All the cell lysate samples, and the standard curves were analysed in duplicates.

2.5.3 Protein Sample Preparation

A quantity of 50µg of each protein sample was made up to a standard well volume of 30-70µL with PBS and 1x sample loading buffer (50mM Tris-HCl pH 6.8, 2% (w/v) SDS, 10% (v/v) glycerol, 0.1% (w/v) bromophenol blue, 100mM 2-mercaptoethanol). The sample was then heated at 90℃ for 10 minutes and then cooled down prior to loading.

2.5.4 SDS-gel preparation

Gels were prepared with respect to the target size of the protein. For OGG1(47kDa), MUTYH (55 kDa), GAPDH (36kDa) a 10% gel was chosen. The separating gel was prepared first as described in Table 2.4 and pipetted into a gel casket set up consisting of 0.75mm plates and was overlaid with butanol to remove the air bubbles. Once the gel was set, the butanol was removed using filter paper and the stacking gel was prepared (Table 2.4) and pipetted over the separation gel. A 0.75mm comb was inserted into the gel. Once the gel was set, they were either used directly or stored in a running buffer-soaked towel (Table 2.5) and foil at 4℃ for up to one week.

2.5.5 Electrophoresis

For sodium dodecyl sulphate-polyacrylamide gel electrophoresis (SDS-PAGE), the gel casket was placed inside a tank containing the required volume of 1x running buffer. The comb was gently removed and 50µg of the sample prepared as mentioned in section 2.5.3 was loaded into each well alongside 3µl of molecular weight marker (SeeBlue^{TM} Plus2 Prestained Standard; LC5925). The gel was run at 120-150V until the dye front reached the bottom of the separating gel. The nitrocellulose membrane (Amershan Biosciences; RPN203E) was soaked in 1x transfer buffer (Table 2.5) for 1 minute and the gel was then carefully transferred onto it. The nitrocellulose membrane with the gel was placed between two filter papers and the assembled blot was placed

inside a tank filled with 1x transfer Buffer. The transfer was run at 200mA at 4℃ for 2 hours. The nitrocellulose membrane after the transfer was stained with Ponceau S to allow visualisation of the protein lanes and the marker ladder. The membrane was gently washed with the blocking solution made up of 5% (w/v) skimmed milk powder (Marvel) and PBS-Tween (0.1% (v/v) Tween-20 in PBS).

Table 2.4 Preparation of SDS-gels

Components	**Separating Gel**	**Stacking Gel**
ddH_2O	8.5ml	7.5ml
4 x Separating Buffer	4.5ml	N/A
4 x Stacking Buffer	N/A	3ml
30% Acrylamide	4.5ml	1.2ml
10% SDS	135µl	90µl
10% Ammonium Persulphate (APS; Sigma)	270µl	180µl
N,N,N′,N′-Tetramethylethylenediamine (TEMED; Sigma)	10µl	7.5µl

Table 2.5 Buffers used in Protein Electrophoresis

Buffer	Components	Storage
4x Separating Buffer	1.5M Tris.Cl pH 8.8 0.4% w/v SDS	Room Temperature
4x Stacking Buffer	0.5M Tris.Cl pH 6.8 0.4% SDS	Room Temperature
10x Running Buffer (1000ml)	250mM Tris base 1.9M Glycine 4% SDS	Room Temperature
10x Transfer Buffer (1000ml) SDS Free	250mM Tris base 1.9 M Glycine	Room Temperature
1x Transfer Buffer	100mL 10x transfer buffer 200mL Methanol 700mL ddH2O	4°C
PBS-Tween	1x PBS 0.1% Tween	Room Temperature

2.5.7 Detecting Target Proteins

The nitrocellulose membranes were blocked with a 5% blocking solution (5%Milk and PBS-Tween) for 1 hour at room temperature on a shaker. The blocking solution was discarded at the membrane were left overnight rolling at 4°C after the addition of the respective primary antibody which was diluted using the blocking solution (Table 2.6). The next day, the membrane was washed 3 x 10 minutes with PBS-Tween and the respective secondary antibodies were added and the membranes were incubated for 1 hour at room temperature. The membranes were then washed 3 x 10 minutes with PBS-Tween. The membrane was then incubated with enhanced chemiluminescence reagent, ECL (Thermo Scientific, SuperSignal^{TM} West Pico PLUS Chemiluminescent Substrate; 34580) for 1 minute and then imaged using FUJIFILM LAS-3000 mini.

Table 2.6 Antibodies used in Western Blot

Antibody	Primary/Secondary	Host Species	Dilution	Source
OGG1	Primary	Rabbit (Polyclonal)	1:1000	Proteintech (15125-1-AP)
MUTYH	Primary	Rabbit (Polyclonal)	1:1000	Invitrogen (PA5-27855)
GAPDH	Primary	Rabbit (Monoclonal)	1:1000	Cell Signalling Technology (2118S)
Anti-Rabbit IgG, HRP linked	Secondary	Swine (Polyclonal)	1:2000	Dako (P0217)

2.5.8 Band Density Quantification

In order to accurately quantify the band density Fiji (ImageJ) software was used. The rectangle tool from the toolbar was used to select the band and with the help of the gel option available under the analyse toolbar (Analyse>gels>select first lane). The rectangle was then moved over to the next band (Analyse>gels>select next lane) and the same steps were repeated until all the bands were marked. The intensity histogram of the bands was obtained by using plot lanes (Analyse>gels>plot lanes). Using the wand (tracing) tool in the toolbar the area of each peak was obtained. In order to calculate relative density, the area of each sample peak was divided by the area of the appropriate loading control peak. The bar graph was plotted and significant differences in relative density were then calculated by ordinary one-way ANOVA analyses using GraphPad Prism.

2.6 Statistical Analysis

All immunofluorescence data and western blot data were obtained from at least 3 independent passages ($n \geq 3$) of the cell lines mentioned in the relevant sections above and normal distribution was assumed prior to parametric test.

Chapter 3. RESULTS

3.1 Determination of 8-oxoguanine lesion in Group 3 MB's polynucleotides.

As discussed in section 1.5, Taylor (2022) in her work saw a lot of unexpected peaks caused by 8-oxoguanine lesions in the input sample during ChIP sequencing analysis. The only commercially available antibody (N45.1) recognizes 8-oxoguanine in both DNA and RNA. Group 3 MB parental cell line(HD-MB03) and the corresponding cisplatin-tolerant i.e.,drug-tolerant (DT-HD-MB03-CIS) cell line and vehicle-treated (HD-MB03-DMF) cell lines were used to determine if the 8-oxogunaine lesions were naturally occurring or artefactually caused by employing immunofluorescence.

As shown in Figure 3.1A, 8-oxoguanine lesions were seen occurring under conditions of normal cell culture across all the 3 cell lines. Automated immunofluorescence analysis revealed that the level of 8-oxoguanine lesions in HD-MB03 cell lines was significantly higher when compared to DT-HD-MB03-CIS and DT-HD-MB03-DMF cell lines with interestingly DT-HD-MB03-DMF having the lowest level of 8-oxoguanine lesions as shown in Figure 3.1B.

To further confirm the results of the automated analysis, images were also manually double scored by blinded investigators. These results correlated well with the results obtained from the automated scoring of the fluorescence intensities. The HD-MB03 cell lines had the highest level of overall 8-oxoguanine staining intensity with 68% of the cells being scored as high positive and DT-HD-MB03-DMF exhibited the lowest level of 8-oxoguanine staining intensity with 70% of the cells being scored as low positive shown in Figure 3.2

From section 1.4.3 we know that 8-oxoguanine detected in the DNA is repaired by OGG1 and MUTYH and YB-1 is said to have the capability to bind specifically to RNA containing 8-oxoguanine and is assumed to block the mistranslation of the modified mRNA by recognizing them (Hayakawa et al., 2002; Eliseeva et al., 2011). Since the parental cell line (HD-MB-03) had the

highest 8-oxoguanine staining intensity when compared to its corresponding cisplatin-tolerant (DT-HD-MB03-CIS) cell line and vehicle-treated (HD-MB03-DMF) cell lines, it essential to determine the expression levels of the known repair mechanism of 8-oxoguanine in publically available datasets.

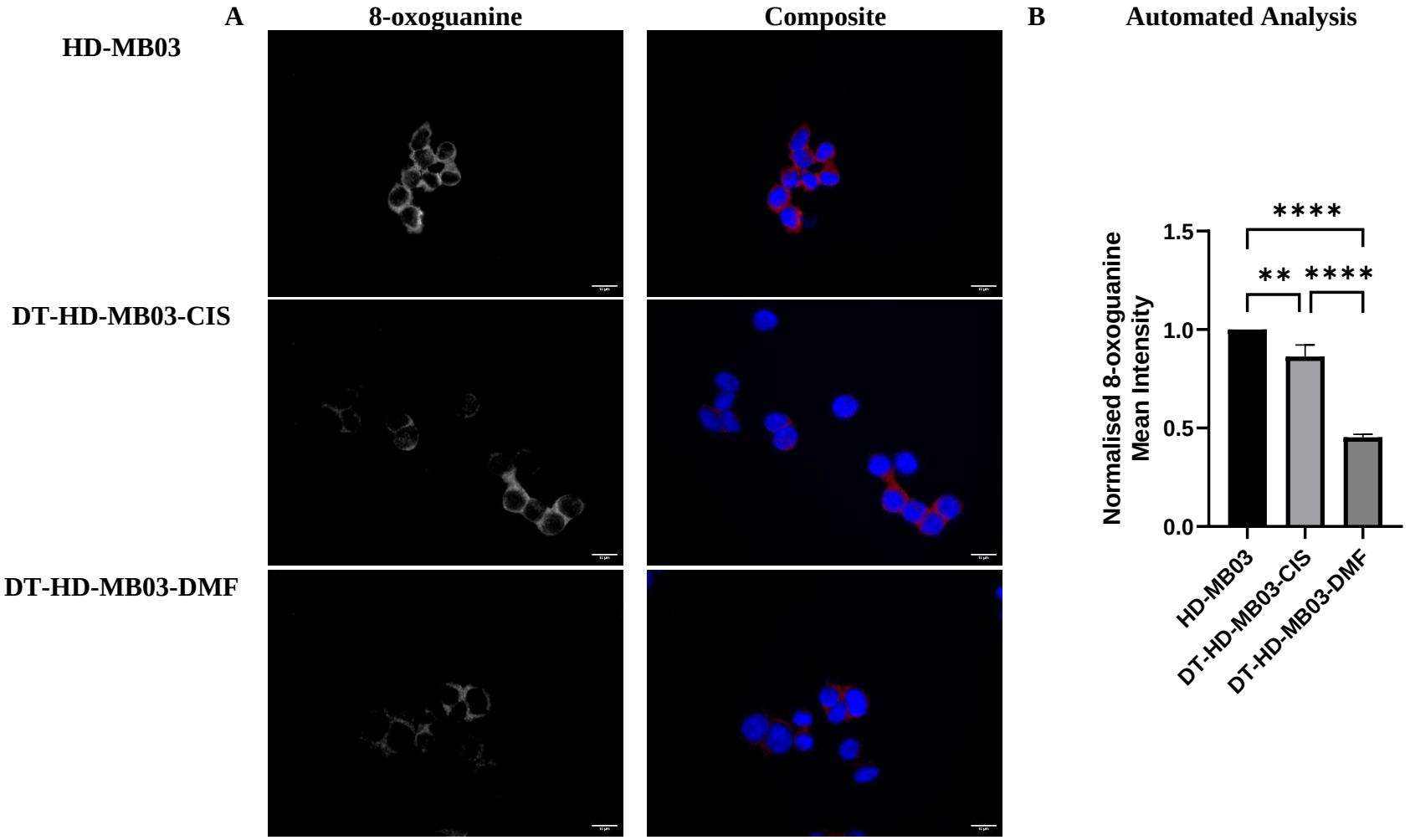

Figure 3.1 Automated analysis of 8-oxoguanine lesion in Group 3 MB

A) Immunofluorescence was employed to determine the presence of 8-oxoguanine lesions in Group 3 MB parental cell lines (HD-MB03), cisplatin-tolerant i.e., drug-tolerant (DT-HD-MB03-CIS) cell lines and vehicle-treated (HD-MB03-DMF) cell lines. Cells were fixed and immunostained for 8-oxoguanine (red) with DAPI (blue) used to identify the cell nuclei. Imaging was done using Zeiss Axiovert S100 Inverted Phase Contrast Fluorescence Microscope at phase 1 with a 32x air lens. 8-oxoguanine lesions were found predominantly in the cytoplasm compared to the nucleus. Images shown are representatives for n = 3 and all the scale bars represent 10µm. B) The immunostained cells were analysed automatically by using Fiji (ImageJ) software. The score of the individual cells was averaged and normalised with respect to HD-MB03. Average of the normalized 8-oxoguanine mean intensity of n=3. Mean ± SEM plotted; **P <0.01 ****P < 0.0001. Significance was assessed by ordinary one-way ANOVA analyses with Tukey's multiple comparisons test.

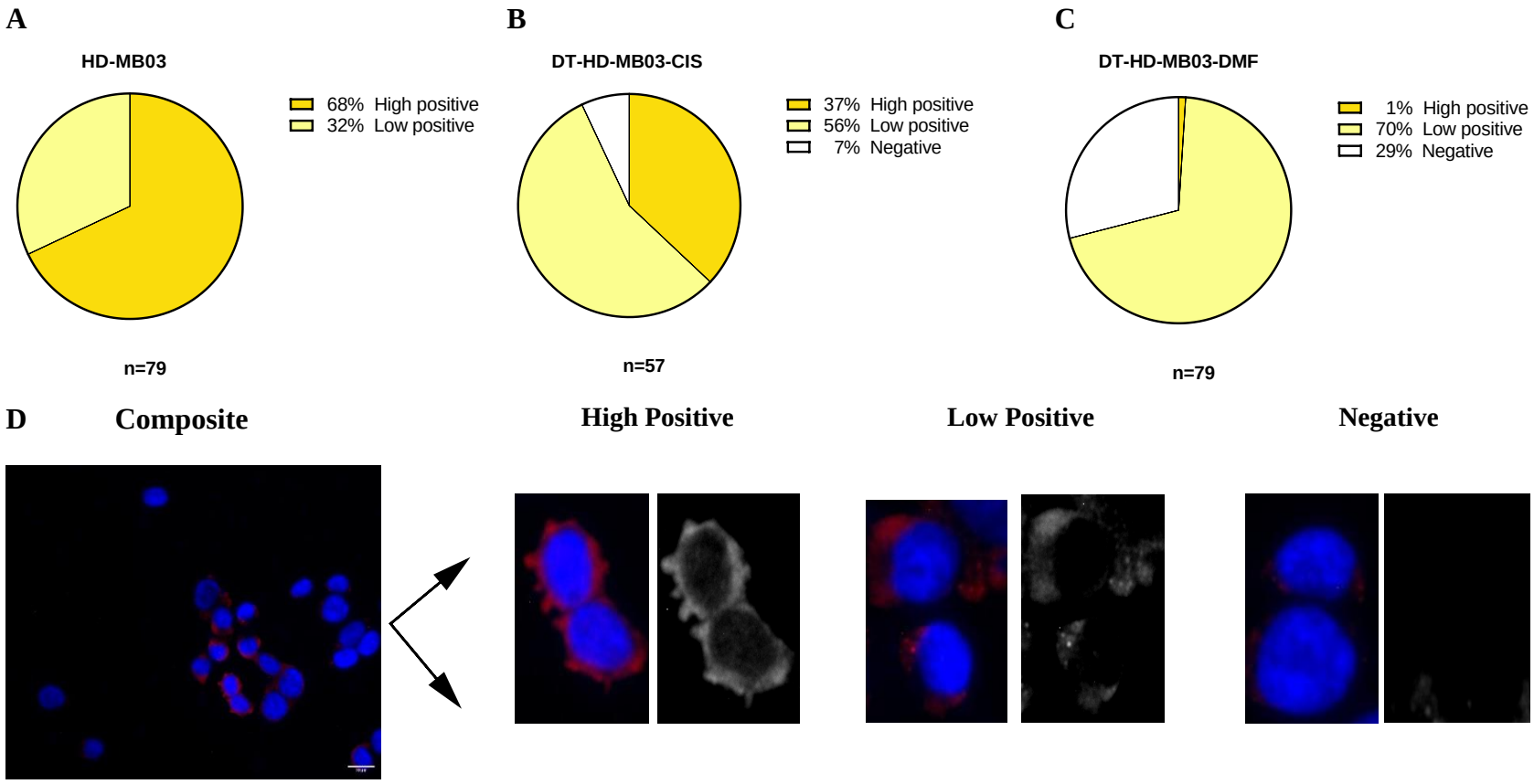

Figure 3.2 Manual analysis of 8-oxoguanine lesion in Group 3 MB

A) Majority of the HD-MB03 cell lines displayed high positive 8-oxoguanine staining 68% (n=79). B) The DT-HD-MB03-CIS cell lines exhibited intermediate levels of 8-oxoguanine staining (n=57) C) Majority of the DT-HD-MB03-CIS cell lines exhibited more low positive 8-oxoguanine staining 70% (n=79). D) Magnified representative images of high positive, low positive and negative scoring.

3.2 Analysis of 8-oxoguanine repair mechanisms across publically available datasets

3.2.1 Determining the expression of *OGG1*, *MUTYH* and *YBX1* genes in medulloblastoma and the normal cerebellum.

OGG1 (encoded by the *OGG1* gene on chromosome 3p25.3), MUTYH (encoded by the *MUYTH* gene on chromosome 1p34.1) and YB-1 (encoded by the *YBX1* gene on chromosome 1p34.2) and their involvement with 8-oxoguanine in medulloblastoma have not been extensively studied. From section 3.1 we know that 8-oxoguanine is naturally present in Group 3 MB's so next we wanted to assess the expression levels of its proposed repair mechanisms. From section 1.4.3 we know OGG1 and MUTYH are involved in the repair of 8-oxoguanine incorporated in the DNA and Hayakawa *et al.*, in their work showed that YB-1 has the ability to bind specifically to RNA containing 8-oxoguanine and is assumed that by recognizing the modified mRNA, YB-1 is capable of blocking its translation (Hayakawa et al., 2002; Eliseeva et al., 2011). So *YBX1* the gene coding for YB-1 has also been analysed in this section. In order to assess this first the expression levels of *OGG1*, *MUTYH* and *YBX1* across large-scale publicly available medulloblastoma patient datasets were analysed.

The R2: Genomics Analysis and Visualisation Platform (http://r2.amc.nl) was used to assess the expression levels of *OGG1*, *MUTYH* and *YBX1* between normal cerebellum and the molecular subgroups of medulloblastoma (Roth et al., 2006, Northcott et al., 2017). There was no significant difference in the expression levels of *OGG1* across WNT, SHH, Group 3 and Group 4 subgroups of medulloblastoma compared to the normal cerebellum (Figure 3.3A). The expression level of *MUTYH* is lower in all the medulloblastoma subgroups compared to the normal cerebellum. (Figure 3.3B). One way ANOVA analysis using Dunnett's multiple comparison test confirmed that Group 3 ($^{***}P<0.0001$) had the lowest expression levels followed by Group 4 ($^{***}P=0.0003$) and SHH ($^{*}P=0.0180$), there was no significant difference seen in the expression level of *MUTYH* between the WNT subgroup and the normal cerebellum. Whereas *YBX1* expression was found to be significantly elevated

across all molecular subgroups of medulloblastoma when compared with normal cerebellum ($^{****}P<0.0001$) (Figure 3.3C).

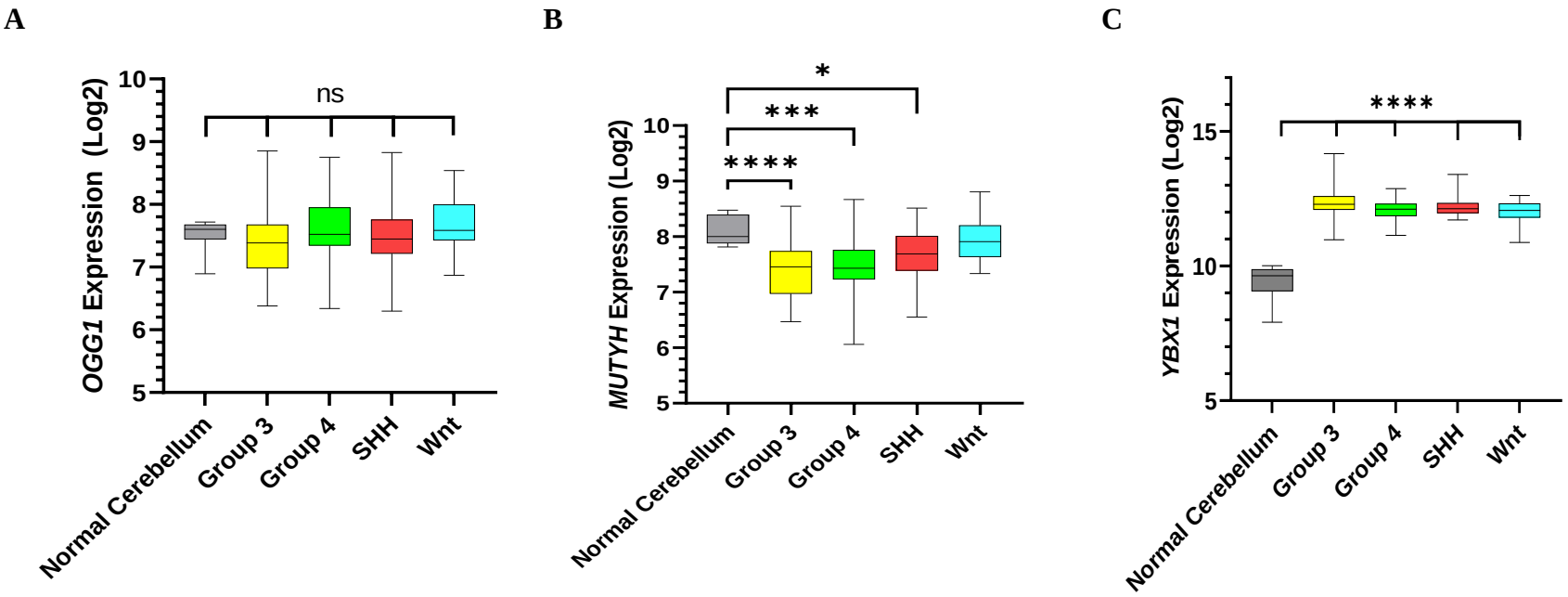

Figure 3.3 Expression levels of OGG1, MUTYH and YBX1 between normal cerebellum and the molecular subgroups of medulloblastoma

R2 Genomic Analysis was utilised to analyse differences in *OGG1, MUTYH* and *YBX1* expression in medulloblastoma A) *OGG1* expression levels exhibit no significant difference between the molecular subgroups of medulloblastoma (Pfister dataset, n = 223) and the normal cerebellum (Roth dataset, n = 9). B) *MUTYH* expression is lower in all four medulloblastoma subgroups when compared to the normal cerebellum ****P < 0.0001. C) *YBX1* expression is elevated in all four medulloblastoma subgroups ****P < 0.0001. Normal cerebellum (Roth dataset) n = 9; Group 3 n = 56, Group 4 n = 91, SHH n = 59 WNT n = 17 (Pfister dataset). Significance was assessed by one-way ANOVA with Dunnett's multiple comparison test

3.2.2 Correlation of *OGG1*, *MUTYH* and *YBX1* gene expression with the overall survival of Medulloblastoma patients

OGG1, MUTYH and *YBX1* gene expressions were correlated with the overall survival of the medulloblastoma patients using the Cavalli dataset, obtained from R2: Genomics Analysis and Visualization Platform (http://r2.amc.nl) , The Cavalli dataset has 763 patient samples (of which 612 have survival data, (Cavalli et al., 2017), and this was utilised to generate Kaplan-Meier survival curves using the 'Kaplan Scan' feature available in the R2 platform. This feature ranks patients from the lowest gene-expressing patient to the highest gene-expressing patient. Based on low vs high gene expression the patients are divided into as many binary group comparisons (i.e. high vs low) as possible. The negative log of the p-values is plotted for all these comparisons and the highest peak is chosen as the most significant cut-off point. Patient overall survival was assessed using the Cavalli patient dataset over a 120-month follow-up period for all molecular subgroups combined and individually.

Though the significance obtained from the raw p values and Bonferroni values differ, raw p values suggest that in all the subgroups combined, patients with higher expression of *OGG1* and *MUTYH* had the worse survival outcome (based on the raw p values) (Figure 3.4 and Figure 3.5) whereas, in the case of *YBX1,* lower expression of the gene resulted in the worse survival outcome (Figure 3.6). Further division of patient data by their molecular subgroups showed that Group 3 patients having a lower expression of *MUTYH* and *YBX1* gene expression had the worst survival outcome.

Out of all the subgroups of medulloblastoma Group 3 MBs are usually associated with poor prognosis and the 8-oxoguanine lesion picked up in *Taylor 2022* ChIP-sequencing data were also from Group 3 medulloblastomas (Taylor 2022). Data from section 3.1 also confirm the presence of 8-oxoguanine in Group 3 medulloblastomas so further studies in this work will be focused on Group 3 medulloblastomas, how the repair mechanisms of 8-oxoguanine are expressed in Group 3 medulloblastoma cell lines and the drug tolerant cell lines.

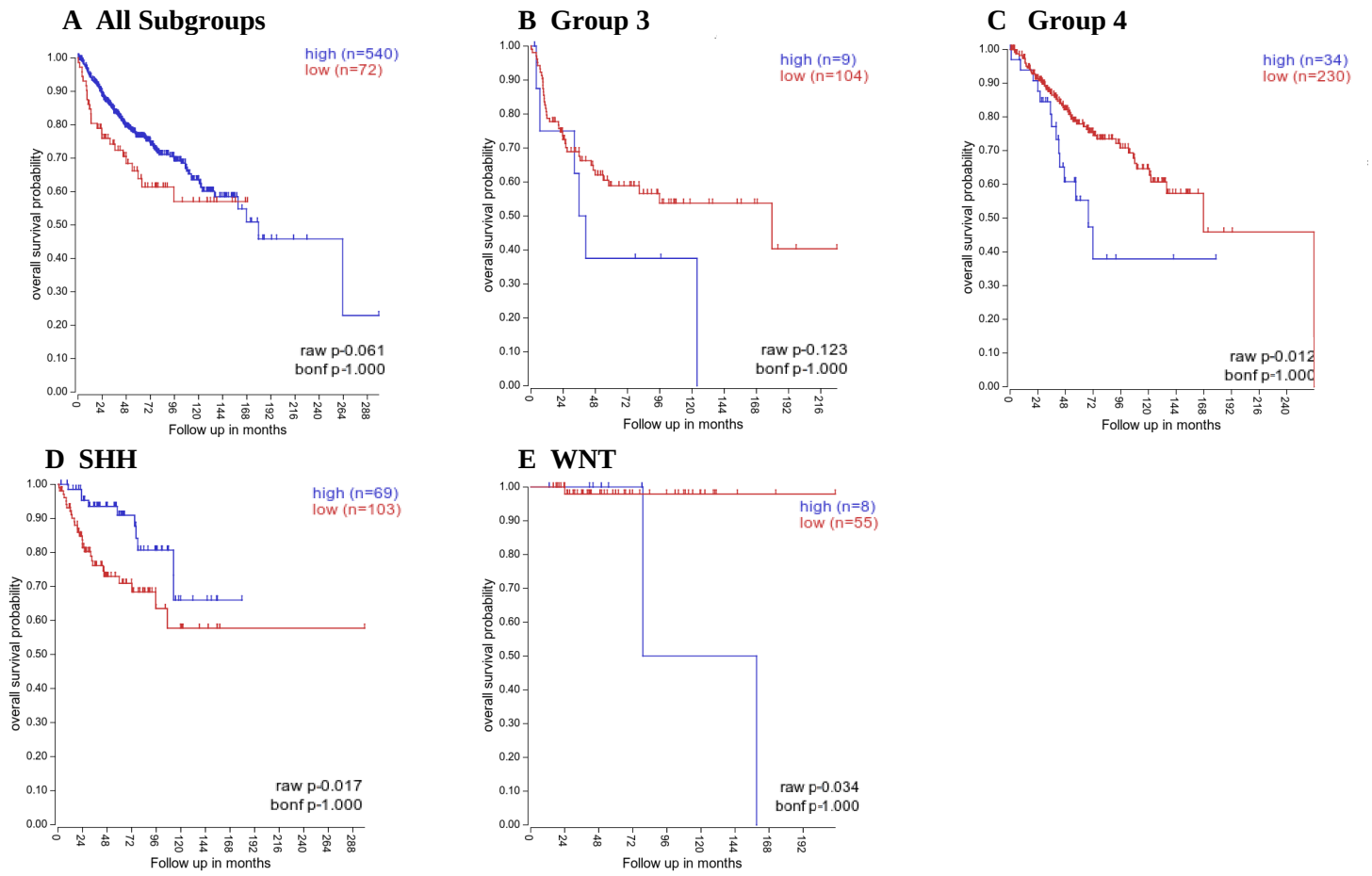

Figure 3.4 Kaplan Meier survival curves of the overall survival probability for high or low OGG1 gene expression in medulloblastoma patients

Kaplan Meier survival curves of the overall survival probability over a 120-month follow-up period based on high or low *OGG1* gene expression. Overall survival probability for all molecular subgroups A) All Subgroups B) Group 3 C) Group 4 D) SHH E) WNT were assessed using the Cavalli dataset.

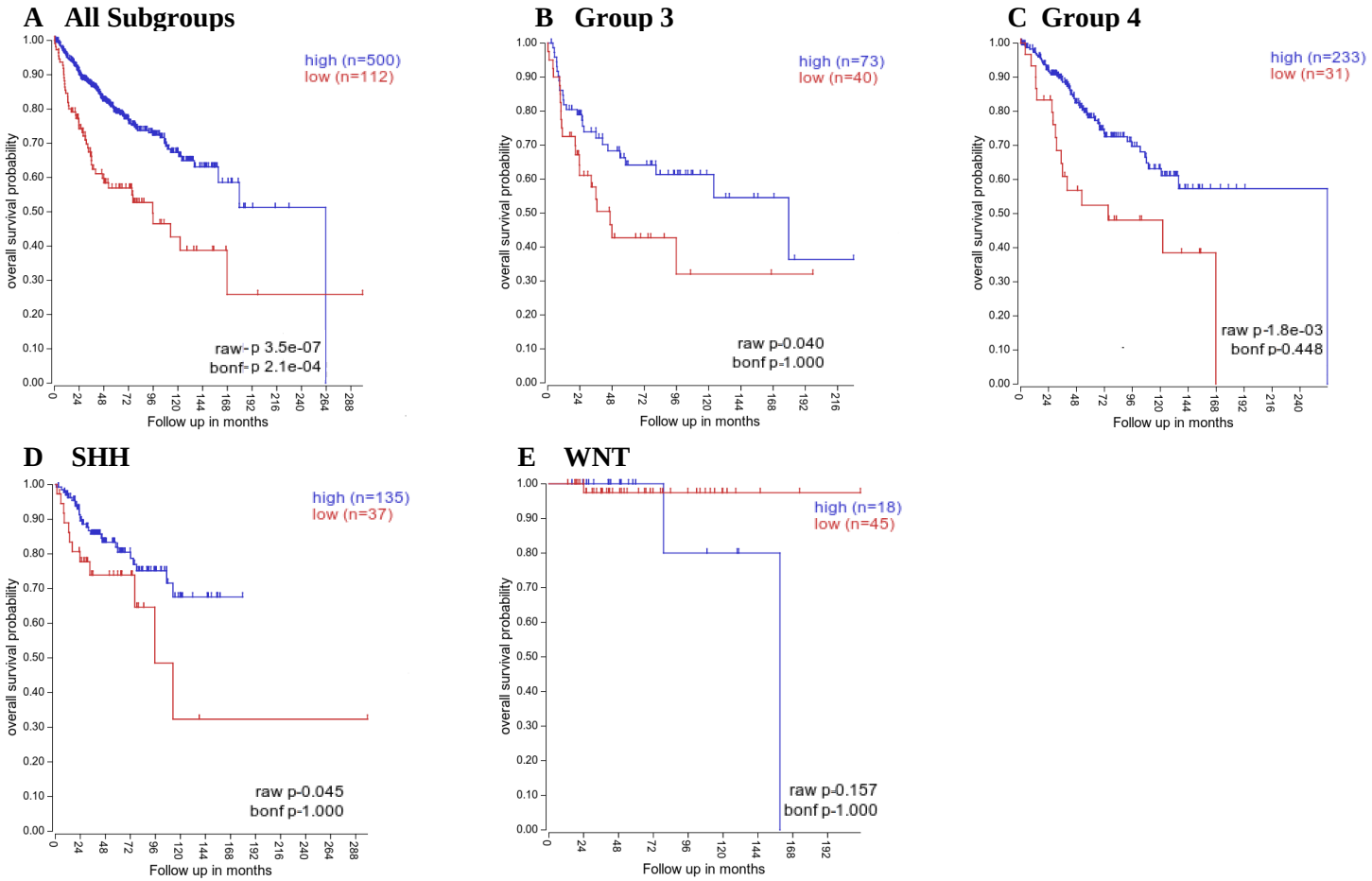

Figure 3.5 Kaplan Meier survival curves of the overall survival probability for high or low MUTYH gene expression in medulloblastoma patients

Kaplan Meier survival curves of the overall survival probability over a 120-month follow-up period based on high or low *MUTYH* gene expression. Overall survival probability for all molecular subgroups A) All Subgroups B) Group 3 C) Group 4 D) SHH E) WNT were assessed using the Cavalli dataset.

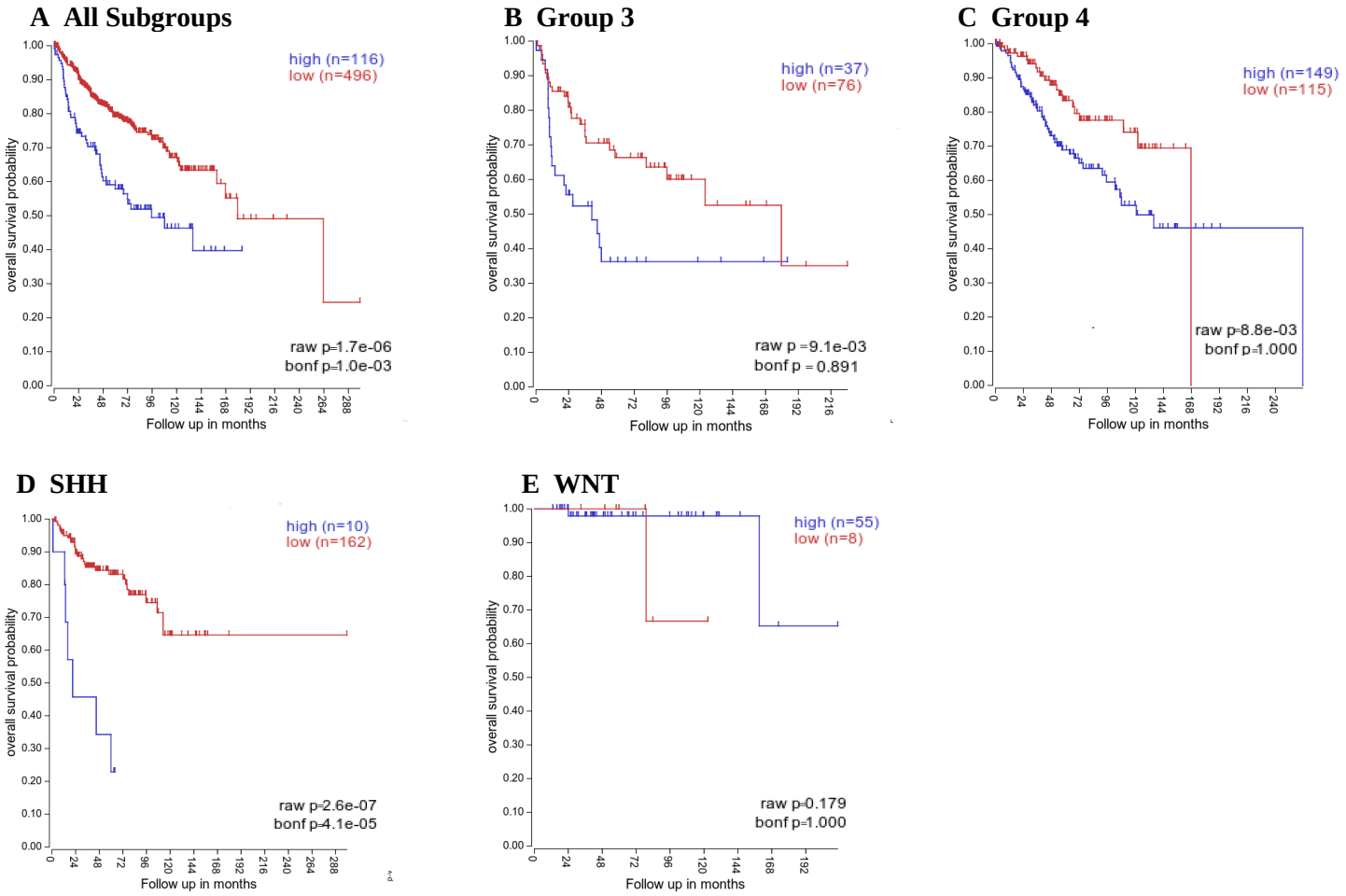

Figure 3.6 Kaplan Meier survival curves of the overall survival probability for high or low YBX1 gene expression in medulloblastoma patients

Kaplan Meier survival curves of the overall survival probability over a 120-month follow-up period based on high or low *YBX1* gene expression. Overall survival probability for all molecular subgroups A) All Subgroups B) Group 3 C) Group 4 D) SHH E) WNT were assessed using the Cavalli dataset.

3.3 Analysis of OGG1 and MUTYH expression in Group 3 medulloblastoma cell lines

The data obtained from R2 genomic analysis (section 3.2) showed that *OGG1* and *MUTYH* are expressed in group 3 medulloblastomas. From section 3.1 we know that 8-oxoguanine is naturally occurring in group 3 medulloblastomas but the level of 8-oxoguanine differed between the parental and drug-tolerant/vehicle cell lines. Does this mean that the repair mechanisms for 8-oxoguanine are differentially expressed across the parental and drug-tolerant/vehicle cell lines? This was investigated by performing western blot analysis across the parental and drug-tolerant/vehicle cell lines to determine the protein level expression of OGG1 and MUTYH.

Analysis of expression of OGG1 and MUTYH at a protein level in HD-MB03, DT-HD-MB03-CIS and DT-HD-MB03-DMF showed that OGG1 and MUTYH were expressed across all three cell lines and there was no significant difference in their expression levels across all the three cell lines (Figure 3.7A-D). The analysis of the expression level of YB-1 across all the three cell lines was not completed due to antibody related technical difficulties but Taylor 2022 had determined the expression levels of YB-1 across HD-MB03, DT-HD-MB03-CIS and DT-HD-MB03-DMF through immunofluorescence and it saw no significant differences in the expression levels between them.

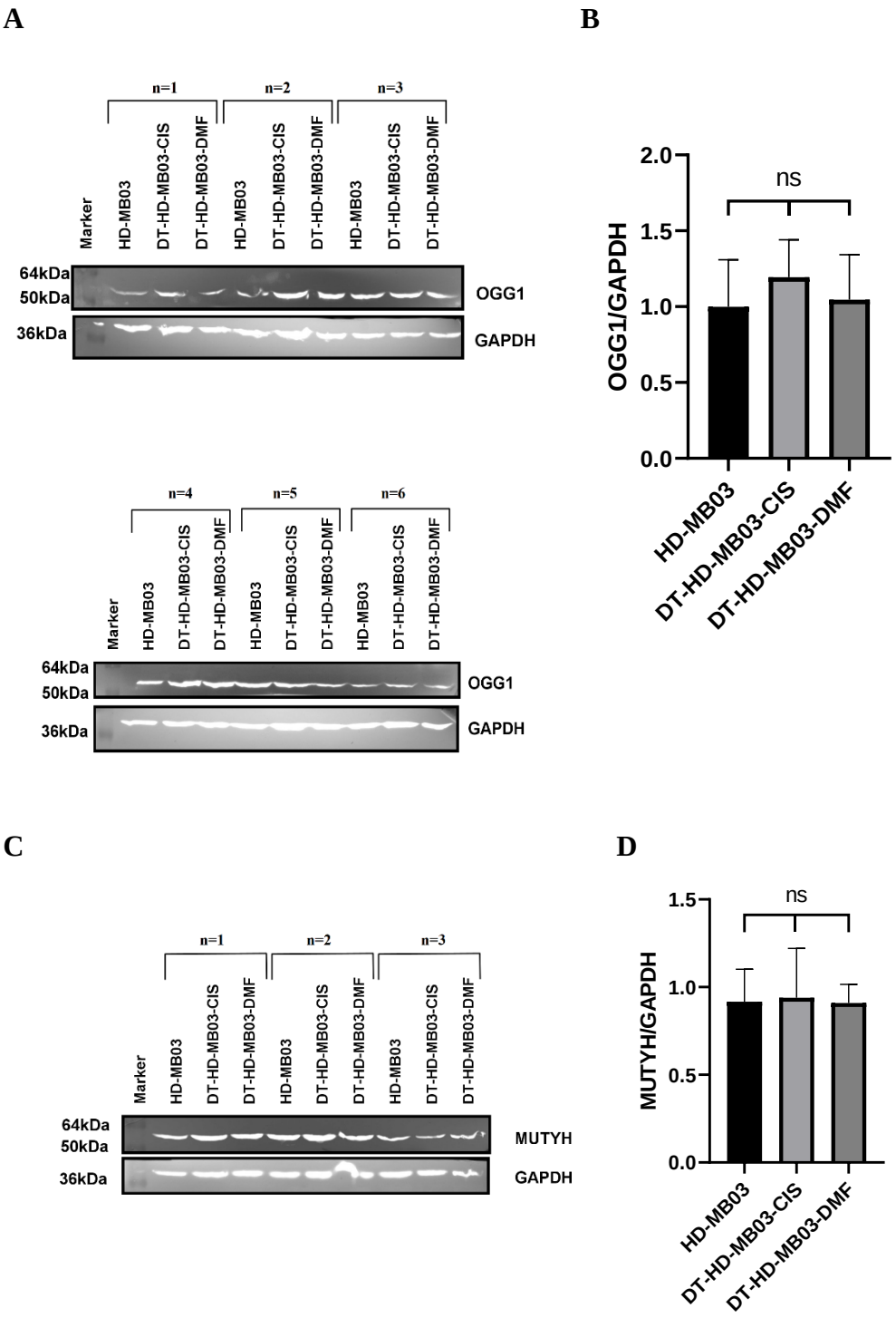

Figure 3.7 OGG1 and MUTYH expression in Group 3 MB cell lines

A) and C) A representative western blot for total OGG1 expression (n=6) and MUTYH (n=3) respectively. GAPDH served as a house-keeping protein. B) and D) Protein expression was quantified using Fiji imaging software and calculated relative to GAPDH to analyse OGG1 and MUTYH expression in all the three cell lines. Mean ± SEM plotted. No significant difference was seen in the expression of OGG1 and MUTYH across all three cell lines. Significance was assessed by ordinary one-way ANOVA analysis.

3.4 Determination of 8-oxoguanine levels in the presence and reduction of their repair mechanisms

3.4.1 Optimisation of an inhibitor of OGG1

From section 1.4.3 we know that OGG1 excises the 8-oxoguanine that gets paired opposite cytosine in the DNA and from sections 3.2 and 3.3 we know that OGG1 is expressed in group 3 medulloblastomas. We next wanted to see if 8-oxoguanine levels were senstive to OGG1 modulation. Visnes *et al.* developed a small molecule inhibitor TH5487 which is a selective active-site inhibitor of OGG1. TH5487 hinders the binding of OGG1 to and repair of 8-oxoguanine (Visnes *et al.,* 2018). In order to employ this, it was first necessary to determined concentration of the drug that is without toxicity to the cells.

The appropriate TH5487 concentration with which to treat each cell line was determined using the PrestoBlue cell viability assay. Group 3 medulloblastoma parental cell line (HD-MB03), the *YBX1* Knockdown cell line of group 3 medulloblastoma cell line HD-MB03 (KD-HD-MB03) and its respective vehicle cell line (NS-HD-MB03) were treated with different concentrations of TH5487 as mentioned in section 2.3 for 24hrs, 48hrs and 72hrs. Analysis of the resultant data showed that the highest concentration of TH5487 (50µM) showed some toxicity towards certain cell lines (the *YBX1* Knockdown cell line and its respective vehicle cell line which are the green and black symbols on the graphs respectively) (Figure 3.8) therefore 20µM TH5487 was chosen as the optimum drug concentration for further experiments similar to other works (Visnes *et al.,* 2018).

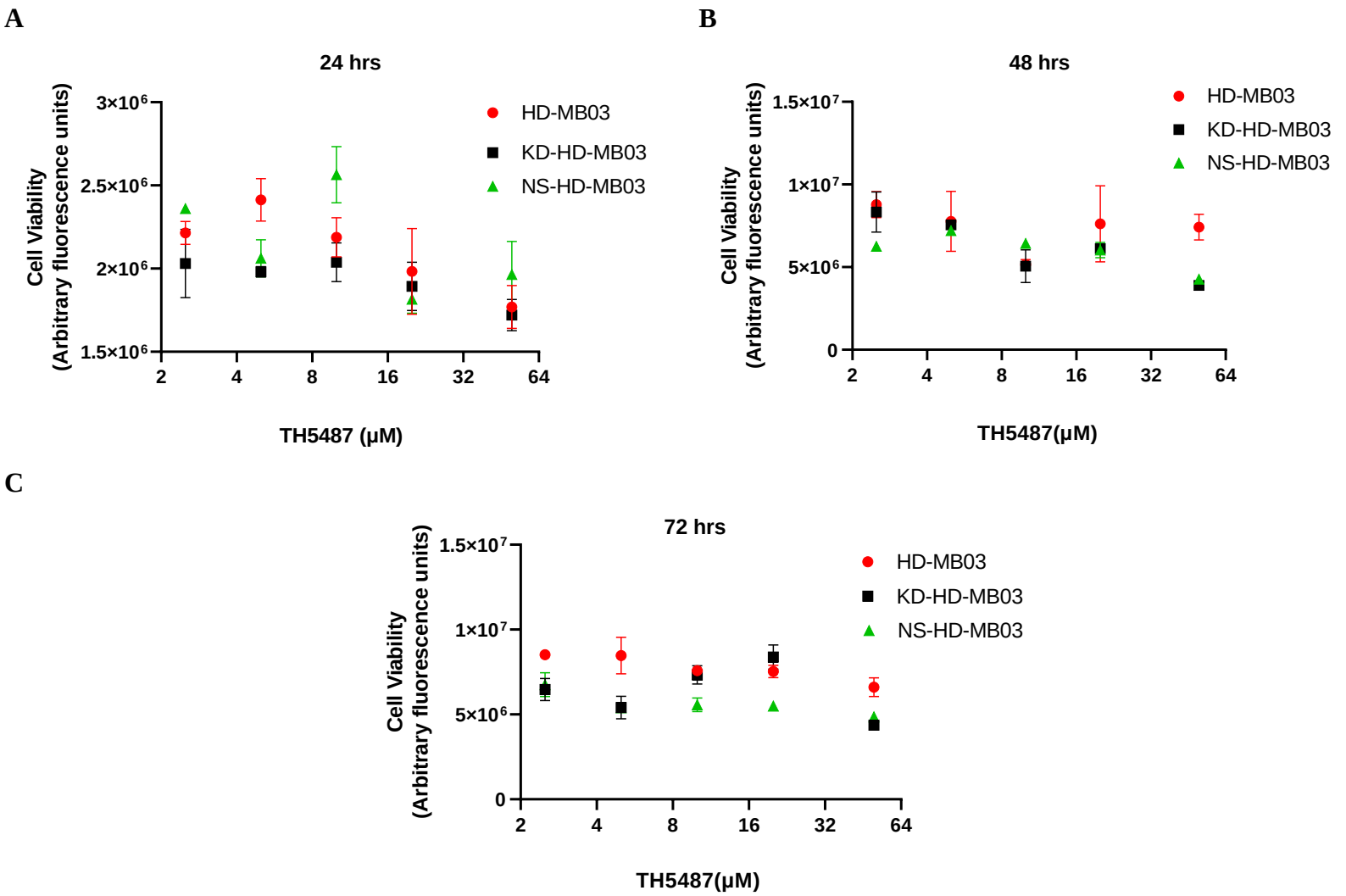

Figure 3.8 TH5487 cytotoxicity in HD-MB03, KD-HD-MB03 and NS-HD-MB03

HD-MB03, KD-HD-MB03 and NS-HD-MB03 cell lines were treated with indicated concentrations of TH5487 for A)24hrs, B)48hrs and C)72hrs respectively and the cell viability was assessed using the PrestoBlue cell viability assays. Only the highest concentration of TH5487 showed some toxicity to the cells. Mean ± SEM; Log2 graphs for duplicates plotted; n=1.

3.4.2 OGG1 inhibition and YB-1 depletion result in elevated 8-oxoguanine levels

Hiroshi *et al.,* showed that YB-1 binds specifically to 8-oxoguanine containing RNA and is assumed to prevent its mistranslation (Hiroshi *et al* 2002; Eliseeva *et al*., 2011) so we wanted to check if YB-1 has a role in the regulation of 8-oxoguanine lesions in the nuclear and cytoplasmic regions by employing immunofluorescence, using previously established YB-1 knockdown cell lines (Taylor, 2023). Additionally, having identified a non-cytotoxic concentration of TH5487 (section 3.4.1) we were also able to investigate the impact of OGG1 inhibition on 8-oxoguanine levels in the cytoplasmic and nuclear regions of group 3 medulloblastoma cell lines through immunofluorescence. Images obtained showed a visible increase in the 8-oxoguanine levels in the YB-1 knockdown cell line KD-HD-MB03 compared to the parental cell line HD-MB03 with the 8-oxoguanine staining being much higher in the cytoplasmic region compared the nuclear region. Additionally, it was observed that Figure 3.99. Through the automated analysis of the immunofluorescence images, we quantified the significant elevation in 8-oxoguanine lesion levels in the cytoplasmic and nuclear region s in the YB-1 knockdown cell lines compared to its parental cell lines suggesting that YB-1 has a role in the regulation of 8-oxoguanine (Hayakawa et al., 2002; Eliseeva et al., 2011). In the case of OGG1 inhibition, a significant increase in the 8-oxoguanine lesion is seen in the nuclear region compared to the parental cell lines but no significant change is seen in the cytoplasmic region correlating with section 1.4.3 that OGG1 is involved in repairing 8-oxoguanine in the DNA (Figure 3.10 A and B).

.

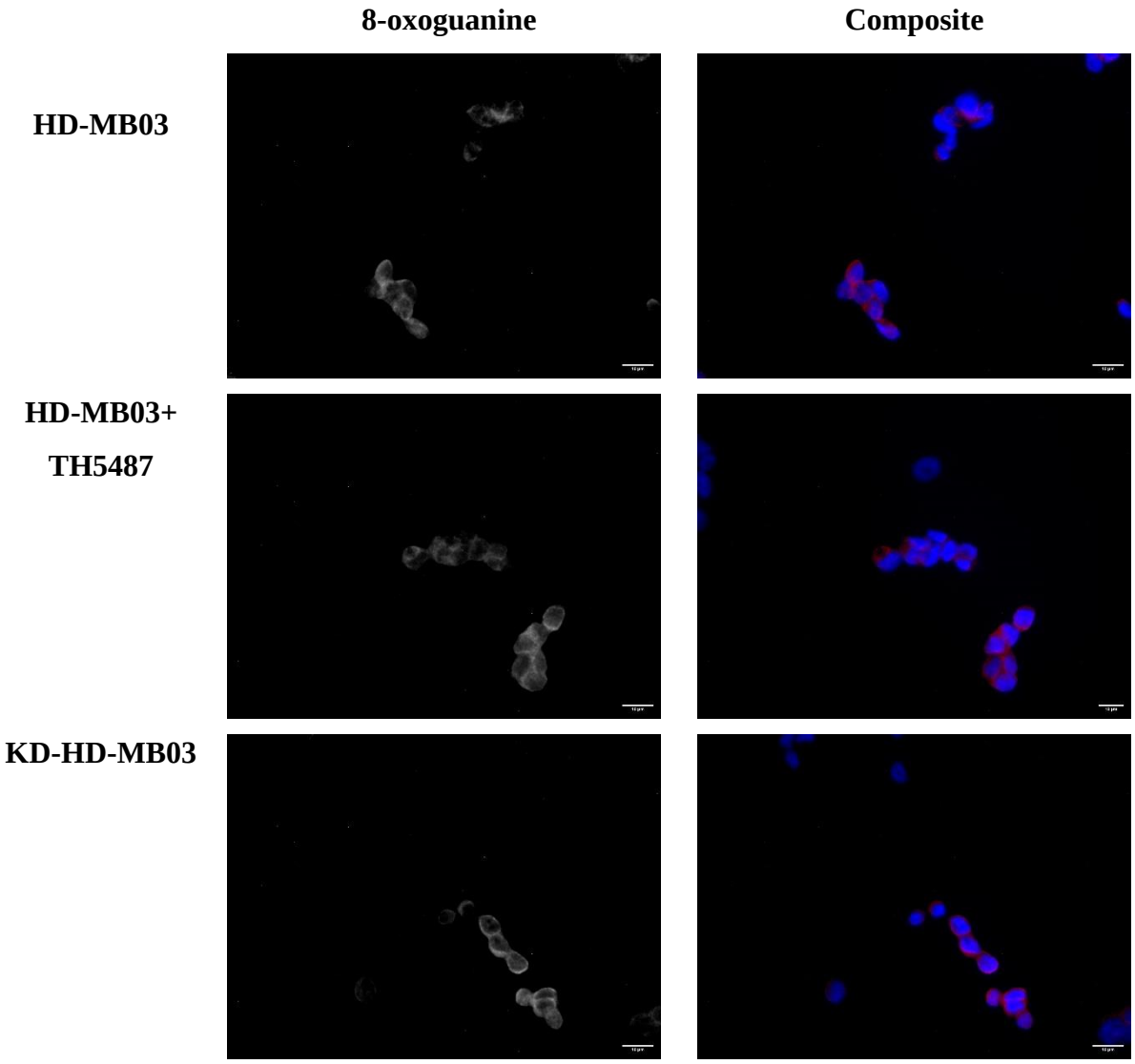

Figure 3.9 8-oxoguanine lesion levels change in YB-1 Knockdown cell lines and parental cell lines under conditions of OGG1 inhibition

Immunofluorescence was employed to determine the presence of 8-oxoguanine lesions in Group 3 MB cell lines. Cells were fixed and immunostained for 8-oxoguanine (red) with DAPI (blue) used to identify the cell nuclei. The individual reduction in OGG1 and YB-1 increased the 8-oxoguanine lesion intensity levels. Representative images are shown; n=3, all the scale bars represent 10µm.

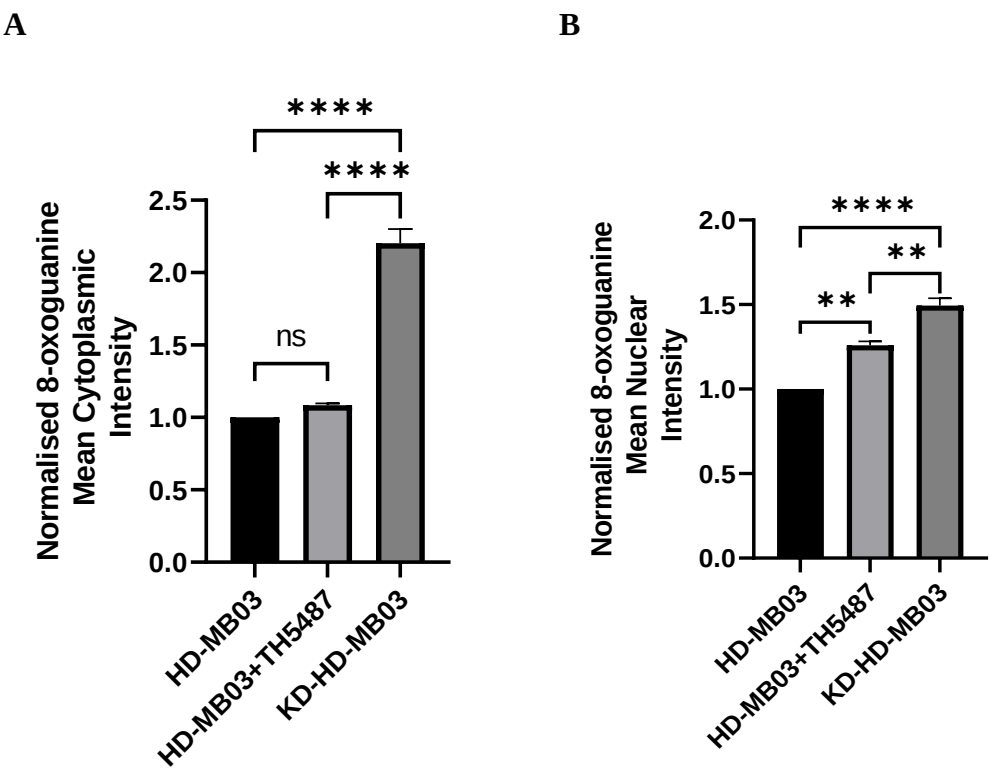

Figure 3.10 Automated analysis of 8-oxoguanine lesion levels in the cytoplasm and nucleus of YB-1 knockdown cell lines and parental cell lines under conditions of OGG1 inhibition

The immunostained cells were analysed automatically by using Fiji (ImageJ) software. The score of the individual cells was averaged and normalised with respect to HD-MB03. Total number of cells analysed for n=3 is 180, with 60 cells being analysed in each independent experiment. A) Automated quantification of the images revealed that the cytoplasmic staining intensity of 8-oxoguanine significantly increased in the KD-HD-MB03 cell line compared to the parental HD-MB03 cell line ****P < 0.0001; whereas no significant difference was seen in the case of OGG1 inhibition. B) Automated quantification of the images revealed that the nuclear staining intensity of 8-oxoguanine significantly increased in both TH5487 treated cell lines (**P = 0.0016) as well as KD-HD-MB03 cell lines (****P < 0.0001) compared to the parental HD-MB03 cell line. Mean ± SEM plotted; n=3; total number of cells analysed=180.Significance was assessed by ordinary one-way ANOVA analyses using Tukey's multiple comparisons test

3.4.3 Overall effect of the reduction of OGG1 and YB-1 on the 8-oxoguanine lesion levels

We know that YB-1 and OGG1 (section 3.4.2) 8-oxoguanine have a role in regulating 8-oxoguanine individually. We wanted to investigate the impact of OGG1 inhibition on 8-oxoguanine levels in the absence of YB-1 (KD-KD-MB03) by employing immunofluorescence. As shown in Figure 3.11 and Figure 3.12 the overall levels of 8-oxoguanine lesions significantly increased under individual conditions of either OGG1 inhibition or YB-1 knockdown but the combination of both (i.e. TH5487 treatment of knockdown cell lines) had a modest but statistically insignificant effect on 8-oxoguanine levels when compared to the 8-oxoguanine levels in the knockdown cell lines suggesting that YB-1 and OGG1 could have a coordinated response. To check if YB-1 directly regulates OGG1, Taylor 2022's RNAseq data of the YB-1 knockdown cell lines was analysed, and it suggests that OGG1 was not a direct target of YB-1 regulation. Though 8-oxoguanine levels are regulated by OGG1 and YB-1, in the parental untreated HD-MB03 cells still measurable levels of 8-oxoguanine are present indicating that despite these repair mechanisms being active there is still the presence of this lesion.

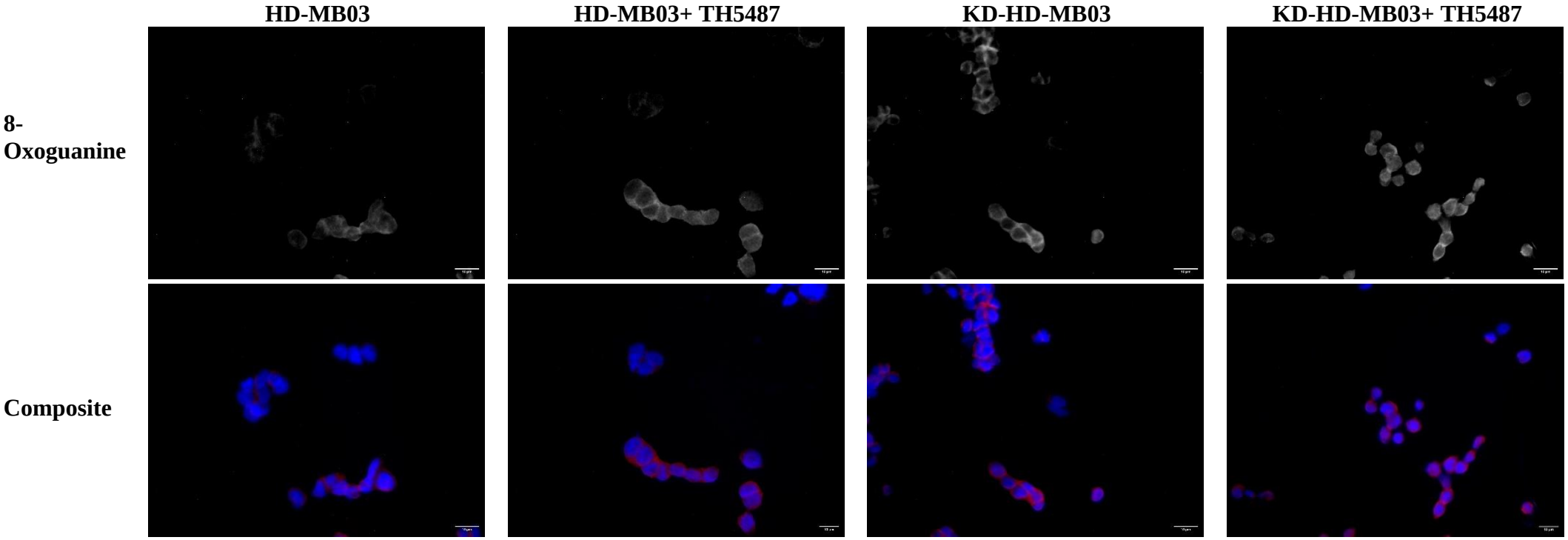

Figure 3.11 Analysis of 8-oxoguanine lesion in the absence of its repair mechanisms

Immunofluorescence was employed to determine the presence of 8-oxoguanine lesions in Group 3 MB cell lines. Cells were fixed and immunostained for 8-oxoguanine (red) with DAPI (blue) used to identify the cell nuclei. The level of 8-oxoguanine lesions increased in OGG1 inhibited cell lines and YB-1 knockdown cell lines. Representative images shown; n=3; all the scale bars represent 10µm

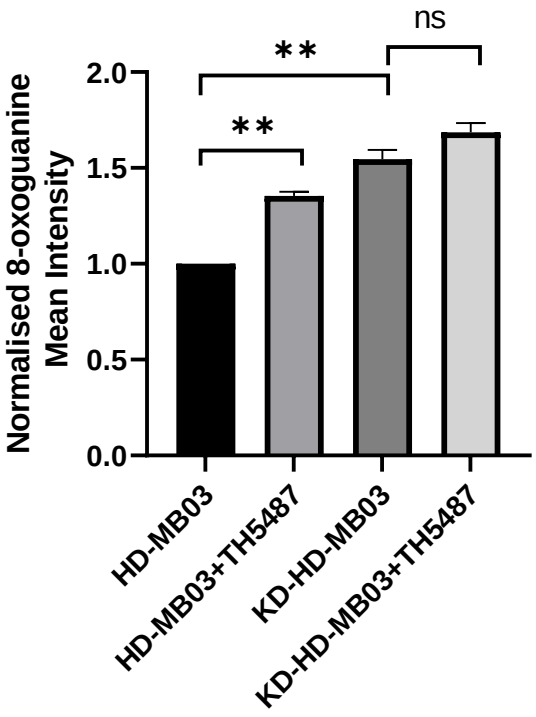

Figure 3.12 Automated analysis of 8-oxoguanine lesions

The immunostained cells were analysed automatically by using Fiji (ImageJ) software. The score of the individual cells was averaged and normalised with respect to HD-MB03. Mean ± SEM plotted; n=3; Overall P value is **P < 0.0001. Significance was assessed by ordinary one-way ANOVA analyses using Tukey's multiple comparisons test.

3.5 Determination of the role of YB-1 and 8-oxoguanine in metastasis

Taylor 2022 showed that knocking down YB-1in group 3 MB cell lines significantly reduced the cell's invasive ability in the modified Boyden chamber (Taylor 2022), similarly several studies have shown that YB-1 plays a role in the metastasis of various tumours. Lin *et al.,* in their study, showed 8-oxoG lesions to be associated with lymphatic metastasis of cervical carcinoma (Lin *et al.,* 2022). We, therefore, wanted to see if there was any difference in 8-oxoguanine and YB-1 expression and colocalization between matched pairs of cell lines arising from primary and corresponding metastatic tumours.

The colocalization of YB-1 and 8-oxoguanine between Group 3 MB's primary tumour cell line D425 and its corresponding metastatic cell line D458 (Table 2.2) was analysed by immunofluorescence dual staining (section 2.4.2). As shown in Figure 3.13 the green fluorescence of YB-1 and the red fluorescence of 8-oxoguanine were seen overlapping both in the primary tumour cell line (D425) as well as in its corresponding metastatic cell line (D458) suggesting the possibility of colocalization. Colocalization doesn't suggest direct interaction, in this case it could be supportive of the interaction because in section 3.4 we see that YB-1 has a role in regulating 8-oxoguanine. Quantification of this data reveals elevated chances of colocalization of YB-1 and 8-oxoguanine in the primary D425 cell line compared to the D458 metastatic cell line; this was in the absence of any difference in the relative levels of 8-oxoguanine and YB-1 individually between D425 and D458 cell lines. This suggests that YB-1 could be interacting with something else other than 8-oxoguanine in the D458's (Figure 3.14).

Though the data may suggest colocalization, but due to the limitations of using a low resolution, standard fluorescence microscope further experiments need to be conducted. Imaging using a super-resolution microscope can provide better evidence of colocalization or single-molecule Förster Resonance Energy Transfer (smFRET) can be employed to study the interaction between YB-1 and 8-oxoguanine. Additionally, the colocalization analysis was performed

here on a whole cell basis, an additional nuclear mask will be needed to differentiate between cytoplasmic and nuclear staining.

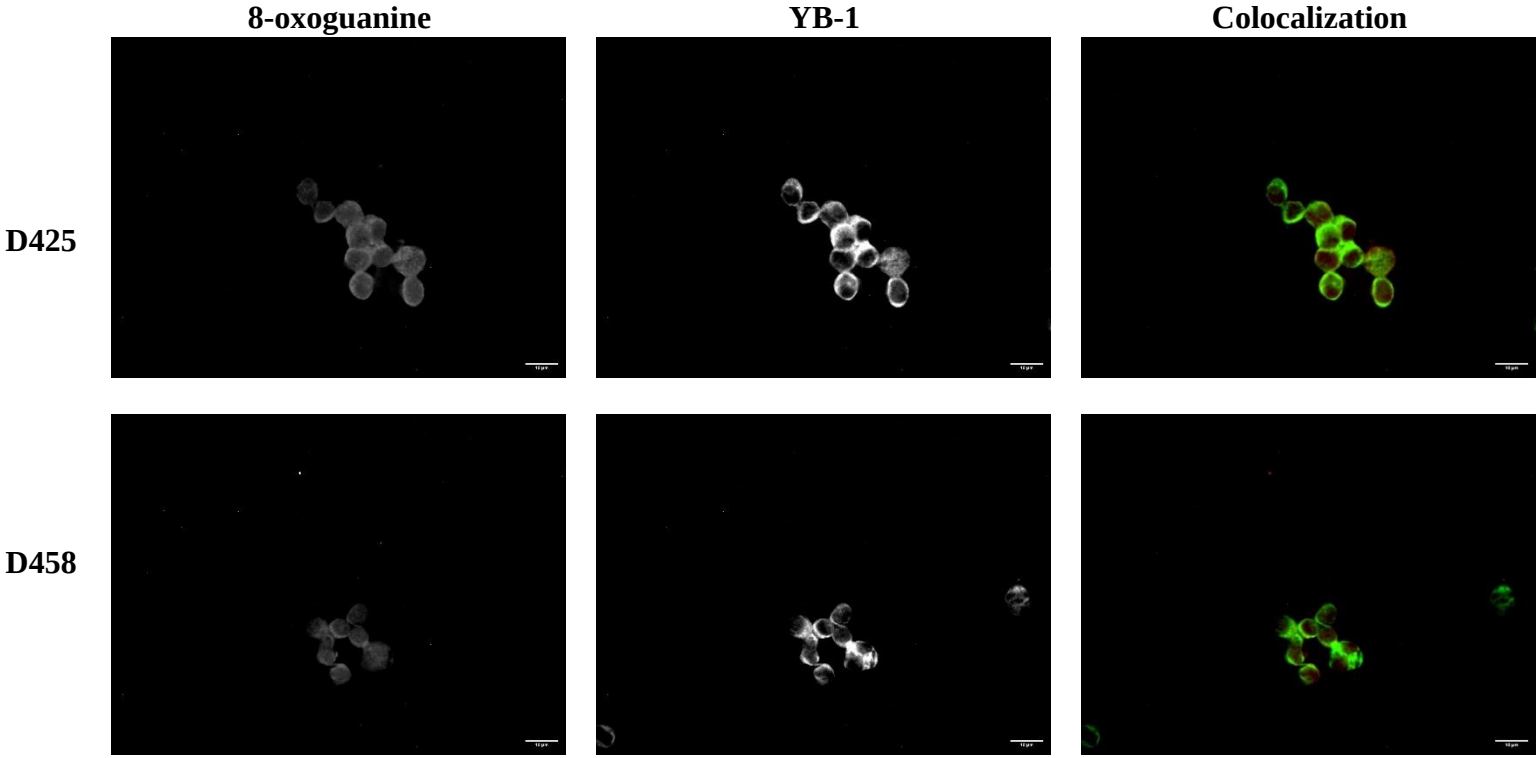

Figure 3.13 Colocalization of YB-1 and 8-oxoguanine in Group 3 MB primary tumour cell line D425 AND D458

Immunofluorescence was employed to determine the colocalization of 8-oxoguanine and YB-1 lesions in Group 3 MB primary tumour cell lines and their corresponding metastatic cell lines. Cells were fixed and immunostained for 8-oxoguanine (red) and YB-1 (green). Representative images shown; three independent passages (n=3); number of cells analysed in each experiment, for each cell line=20, so the total number of cells analysed for n=3 for each cell line=60 cells; all the scale bars represent 10µm.

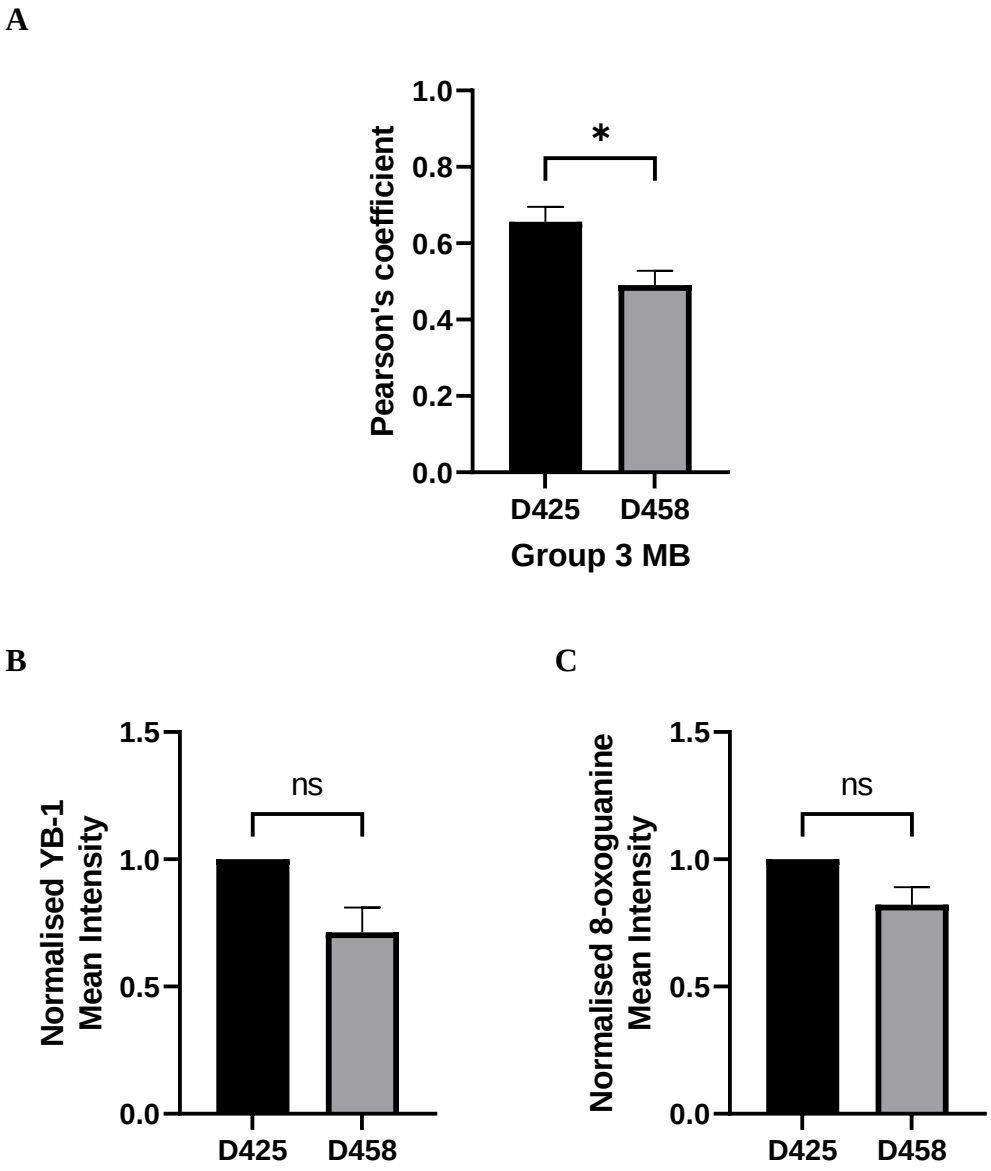

Figure 3.14 Automated analysis of YB-1 and 8-O-G colocalization in D425 and D458

The immunostained cells were analysed automatically by using Fiji (ImageJ) software. Total number of cells analysed for n=3 is 180, with 60 cells being analysed in each independent experiment. Pearson's coefficient of the cells was determined using the "coloc2" tool. Pearson's coefficient varies from +1 for perfect correlation to 0 for no correlation to -1 for perfect anti-correlation Mean ± SEM plotted; n=3. A) Average of the Pearson's coefficient of n=3 of D425 and D458. Mean ± SEM plotted; *P =0.0366. Significance was assessed by unpaired t-test. B) & C) The fluorescence intensity of the individual cells was averaged and normalised with respect to D425. No significant difference was seen in the levels of YB-1 and 8-oxoguanine in the D425 and D458 cell lines. Mean ± SEM plotted; n=3.

4. DISCUSSION

Taylor 2022 worked on characterising the role of multi-functional oncoprotein YB-1 in medulloblastomas. While trying to determine the transcriptional targets regulated by YB-1 under acute and chronic treatment of chemotherapeutic drugs cisplatin and vincristine in Group 3 MBs by performing ChIP Sequencing she got unexpected peak enrichment in her input samples caused by 8-oxoguanine. The aim of this work began with determining the cause of 8-oxoguanine lesions.

4.1 Summary of the results

8-oxoguanine is the most abundant oxidative lesion and 8-oxoguanine accumulation can cause mutations and is believed to be a major cause of cancer (Li *et al.,* 2022; Nakabeppu 2014). The 8-oxoguanine peaks in Taylor's work could have either occurred artefactually while preparing the samples for ChIP-sequencing (Costello *et al.,* 2013) or could have been naturally present in Group 3 medulloblastoma cell lines as the brain is more susceptible to oxidative stress due to its high oxygen consumption (Van den Boogaard *et al.,* 2020; Salim 2016). Thus, the first aim of the work was to determine if the 8-oxoguanine lesions detected during ChIP sequencing was natural or artefactual; by conducting immunofluorescence assays across Group 3 MB cell lines (HD-MB03) and its corresponding drug-tolerant and vehicle cell lines (DT-HD-MB03-CIS and DT-HD-MB03-DMF) I was able to demonstrate that 8-oxoguanine lesions are naturally occurring in Group 3 MB's, therefore the ChIP sequencing data was unlikely to be artefactual. The parental cell line HD-MB03 exhibited the highest 8-oxoguanine lesion compared to its corresponding drug-tolerant and vehicle cell lines.

These 8-oxoguanine lesions in the DNA are repaired through the base excision repair (BER) pathway where OGG1 excises the 8-oxoguanine paired with cytosine and MUTYH excises the adenine paired opposite 8-oxoguanine (Figure 1.7) and 8-oxoguanine lesions in the RNA are assumed to be repaired by YB-1 (section 1.4.3) and this thesis contributed evidence for YB-1 recognising and regulating 8-oxoguanine.

The expression levels of OGG1 and MUTYH were determined across HD-MB03, DT-HD-MB03-CIS and DT-HD-MB03-DMF cell lines to check if the difference in the 8-oxoguanine lesion levels between these three cell lines was caused by the difference in the expression of the repair mechanisms but there was no significant difference in the expression of OGG1 and MUTYH across the three cell lines. No significant differences in the expression levels of YB-1 across these three cell lines were seen in Taylor 2022's work. Though the cause for the drop in the 8-oxoguanine levels in the vehicle cell line remains unclear but a study conducted in 2018 by Zhao and Wen showed that DMF had the ability to inhibit oxidative stress by activating the Nrf2 signalling pathway suggesting that this could have been a contributing factor for the decrease in oxidative damage of the guanine base in the vehicle cell line (Zhao and Wen 2018)

With the group 3 parental cell line (HD-MB03) having the highest 8-oxoguanine lesion levels and also exhibiting YB-1 and OGG1 expression, the next step was to determine if YB-1 had played a role in regulating 8-oxoguanine levels in group 3 MB's if so could the reduction of YB-1 and inhibition of OGG1 have an influence on the 8-oxoguanine levels. Conducting immunofluorescence assays revealed that knocking down YB-1 (KD-HD-MB03) and inhibiting OGG1 (HD-MB03+TH5487) individually increased the 8-oxoguanine lesion levels significantly both in the cytoplasm and nucleus but in case of TH5487 (OGG1 inhibitor) treated YB-1 knockdown cell lines (KD-HD-MB03+TH5487) the combination of both has a moderate effect on 8-oxoguanine levels which is statistically insignificant when compared to the 8-oxoguanine levels of the untreated knockdown cell lines (KD-HD-MB03) suggesting that YB-1 and OGG1 could have a coordinated response but through Taylor 2022's RNASeq data of YB-1 knockdown cell lines we know that OGG1 is not a direct target of YB-1. Despite YB-1 and OGG1 regulating the 8-oxoguanine levels, detectable levels of 8-oxoguanine lesions are still present in the parental cell lines.

YB-1 and 8-oxoguanine have been individually reported to be involved in the metastasis of other cancers and with YB-1 regulating the expression levels of 8-oxoguanine, their colocalization in primary tumour and its corresponding

metastatic tumour analysis was attempted. Fluorescence of YB-1 and 8-oxoguanine were seen overlapping in Group 3 MB's primary tumour cell line and its corresponding metastatic cell line and their quantification suggest that there is a probability of colocalization of YB-1 and 8-oxoguanine. Imaging using a super-resolution microscope would provide better evidence of colocalization, similarly single-molecule Förster Resonance Energy Transfer (smFRET) can be employed to study the interaction between YB-1 and 8-oxoguanine. Determining the interaction of YB-1 and 8-oxoguanine in Group 3 MB's primary tumour cell line and its corresponding metastatic cell line could help determine if YB-1 and 8-oxoguanine have a combined role in initiating metastasis. 8-oxoguanine and YB-1's combined role is least explored in paediatric medulloblastoma. Conducting further experiments to determine their combined role in metastasis could open a new target for therapy (Figure 4.1).

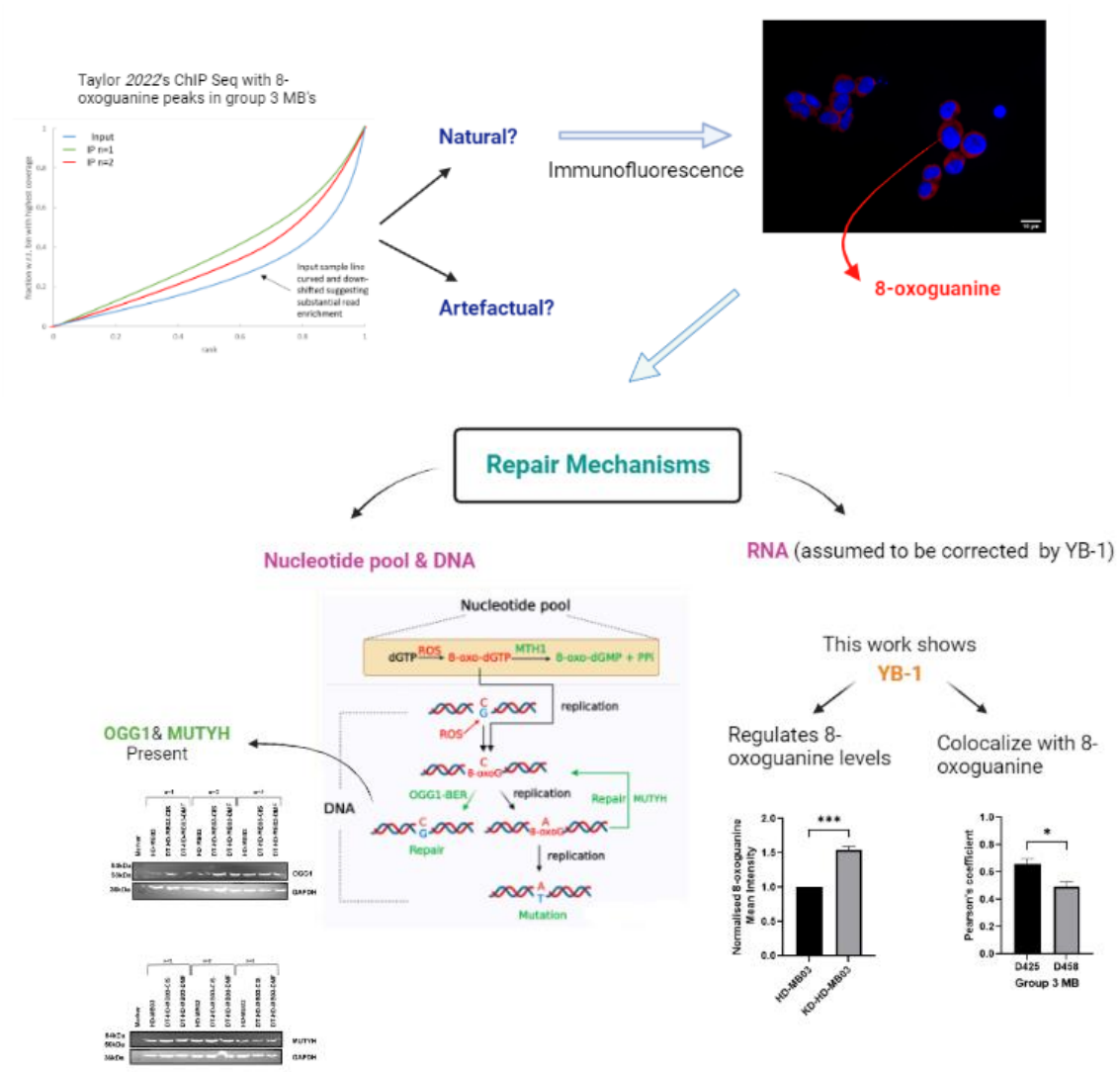

Figure 4.1 Graphical summary of this work

8-oxoguanine detection in group 3 MB's followed by analysing the expression levels of its repair mechanisms in the DNA and determining if YB-1 regulates 8-oxoguanine MB = medulloblastoma. Generated using Biorender (Taylor 2022; Li *et al* 2022).

4.2 Ideas for future work

Future Perspective

The role of 8-oxoguanine lesions, the most commonly oxidized base of the DNA, RNA and nucleotide pool as well as in the mitochondrial DNA least explored in the case of medulloblastomas (Li *et al.,* 2022; J.Y. Hahm et al., 2022; Torres-Gonzalez *et al., 2014*). This makes it a potential gold mine for research. Mitochondria consumes approximately 2% of the oxygen which is reduced to form superoxide, hence they are considered to be the main site of ROS production (Li *et al.,* 2022). Lack of protective histones makes mitochondrial DNA more susceptible to oxidative damage (Bodenstein *et al.,* 2019) The nucleotide pool and the RNA are also susceptible to oxidative stress and exploring them would help understand the involvement of 8-oxoguanine in medulloblastoma ((Li *et al.,* 2022; J.Y. Hahm et al., 2022). 8-oxoguanine and YB-1's could have a combined effective on the metastasis of medulloblastoma future works analysing 8-oxoguanine levels in the nucletotide pool, RNA and mitochondrial DNA along with YB-1 would open a potentially new target for therapy.

YB-1 and 8-oxoguanine

From section 3.4 in this work, we see that 8-oxoguanine lesion levels change with the presence and absence of YB-1 meaning YB-1 is likely involved in the regulation of 8-oxoguanine. Conducting further immunofluorescence assays on HD-MB03 (parental cell lines), and KD-HD-MB03 (YB-1 knockdown cell lines) under normal conditions, after inducing oxidative stress on the parental and knockdown cell lines using $KBrO_3$ (Visnes et al., 2018) and treating the parental and knockdown cell lines them with antioxidants and comparing the changes in the levels of 8-oxoguanine and YB-1 under different conditions will help understand better the involvement of YB-1 in the regulation of 8-oxoguanine. Further conducting smFRET assay would help us determine YB-1 and 8-oxoguanine interaction.

Section 3.5 in this work shows that though no significant difference in the individual levels of YB-1 and 8-oxoguanine was seen in the primary tumour

cell lines than its corresponding metastatic cell lines, the chances of colocalization of 8-oxoguanine and YB-1 is higher in the primary tumour cell lines than its corresponding metastatic cell lines. This could suggest that YB-1 being a multifunctional protein is interacting with something else other than 8-oxoguanine in the metastatic cell line. Analysing the colocalization and the levels of YB-1 and 8-oxoguanine in group 3 and group 4 primary tumour cell lines and their corresponding metastatic cell lines using super resolution microscope would help us understand this better.

To check if this colocalization has any role in initiating metastasis a modified Boyden chamber assay can be performed. Taylor 2022 conducted a modified Boyden chamber assay to determine if YB-1 was involved in the invasion of group 3 medulloblastoma using the parental cell line and the corresponding YB-1 knockdown cell line (Taylor 2022). In a similar fashion to check this hypothesis, a modified Boyden chamber assay can be performed using the parental cell lines (primary tumour cell line), YB-1 knockdown cell lines (knocking down YB-1 in primary tumour cell lines) under normal conditions, with the parental tumour and knockdown cell lines subjected to $KBrO_3$ (to induce oxidative stress) and antioxidant treated parental and knockdown cell lines. This would help us understand the combined and individual roles of YB-1 and 8-oxoguanine in metastasis.

NUDT Hydrolases and 8-oxoguanine

NUDT hydrolases or the *NUDIX hydrolases* are enzymes that carry out hydrolysis reactions and the human genome codes for at least 24 NUDT hydrolases. NUDT enzymes help clean the cell from deleterious metabolites, such as oxidized nucleotides in the nucleotide pool thereby preventing their incorporation into the DNA and ensuring proper cell homeostasis. Despite years of study, several members of the NUDT hydrolase family are completely uncharacterized (Carreras-Puigvert *et al.,* 2017; Wang *et al.,* 2017). Out of all the members of the NUDT family that have been studied so far, NUDT1, NUDT15 and NUDT18 are said to be involved in the hydrolysis of oxidized nucleoside triphosphates thereby preventing the mispairing during DNA

replication whereas NUDT5 hydrolases are to be involved in the hydrolysis of oxidized nucleoside diphosphates (https://www.genecards.org/).

As a prelude to experimental work on the NUDTs, the expression of *NUDT1, NUDT15* and *NUDT5* was shown to be significantly elevated across all the molecular subgroups of medulloblastoma whereas the expression levels of *NUDT18* were significantly lower in medulloblastoma when compared to normal cerebellum (Roth et al., 2006, Northcott et al., 2017) (Figure 4.2). The overall survival of medulloblastoma patients with higher expression of NUDT1 is worse (Figure 4.3).

Group 3 medulloblastomas have a poor prognosis amongst all the molecular subgroups of medulloblastoma. From section 3.1 we know that 8-oxoguanine lesions are naturally occurring in group 3 MB subgroup and from section 1.4.3 we know that NUDT1 is involved in the repair of 8-oxo-dGTP by converting them to 8-oxo-dGMP thereby preventing the incorporation of oxidized nucleoside triphosphates into the DNA. It has been proposed that tumorigenesis could be highly correlated with the accumulation of mutations and 8-oxoguanine accumulation may increase the risk of spontaneous mutagenesis, resulting in the malignant transformation of cells (Li *et al.*, 2022). Tsuzuki T*et al* showed that NUDT1 deficiency increased the spontaneous mutagenesis frequency by 2-fold in mice models compared to their wild type (Tsuzuki *et al*., 2001). NUDT1 is said to protect the brain from neurodegenerative diseases associated with oxidative stress (Li *et al.*, 2022) and any defect in the NUDT1 would increase the susceptibility of the brain to oxidative stress thereby it could lead to 8-oxo-dGTP accumulation.

Van den Boogard *et al.*, saw a high frequency of somatic cytosine > adenine (C > A) substitutions during the whole-genome sequencing of primary neuroblastoma tumours which was associated with poor survival. They showed that increased levels of C > A substitutions correlated with copy number loss (CNL) of OGG1 or MUTYH and this was established using tumour organoid models with CNL of OGG1 or MUTYH and by employing CRISPR-Cas9 genome editing to create knockout clones of MUTYH and OGG1 in neuroblastoma cells and performing whole-genome sequencing to determine

the C>A substitutions (Van den Boogaard *et al.*, 2020). A strategy similar to van den Boogard *et al.* can be employed to check if there is a defect in NUDT1 levels that led to the accumulation of 8-oxoguanine lesions in Group 3 medulloblastoma despite the other repair mechanisms being active, leading to C>A substitutions causing spontaneous mutagenesis thereby correlating to the poor prognosis of this subgroup.

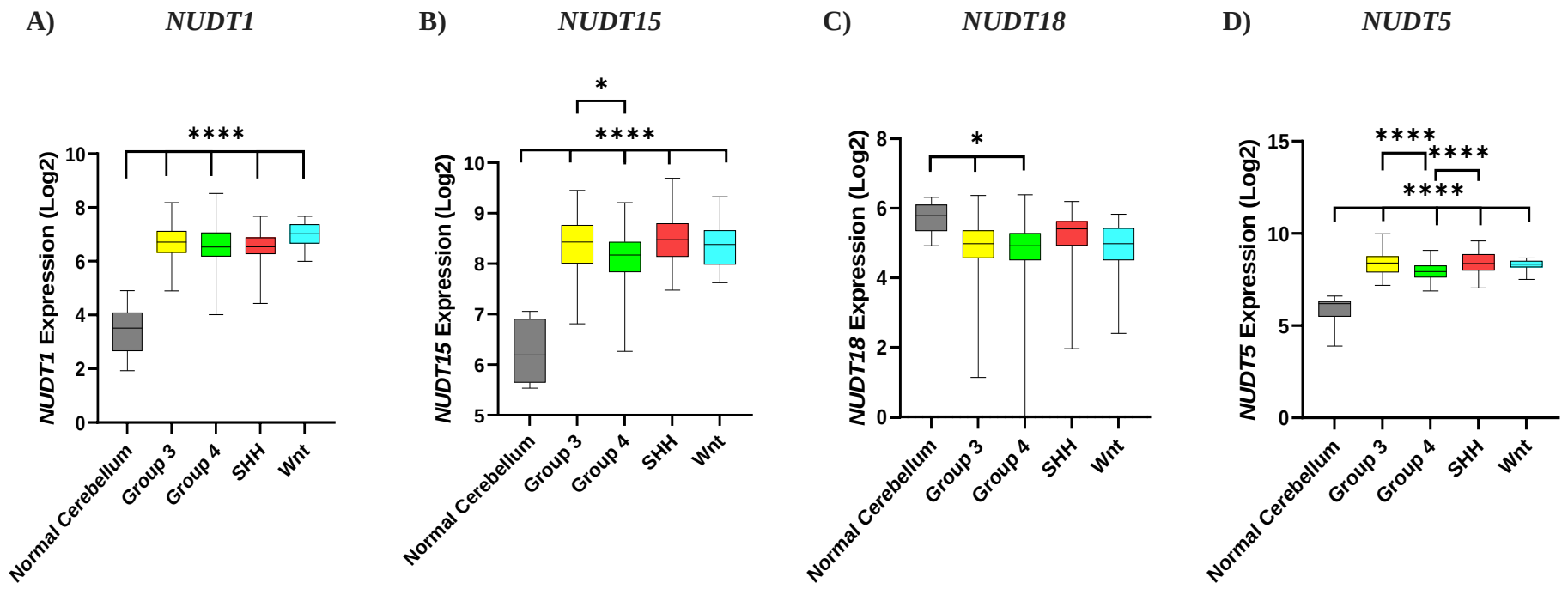

Figure 4.2 Expression levels of NUDT1, NUDT15, NUDT18 and NUDT5 between normal cerebellum and the molecular subgroups of medulloblastoma

R2 Genomic Analysis was utilised to analyse differences in *NUDT1, NUDT15, NUDT18* and *NUDT5* expression in medulloblastoma A) *NUDT1* expression levels are elevated in the molecular subgroups of medulloblastoma (Pfister dataset, n = 223) compared to the normal cerebellum (Roth dataset, n = 9) and the difference is significant ****P <0.0001. B) *NUDT15* expression is also elevated across all four medulloblastoma subgroups when compared to the normal cerebellum ****P < 0.0001. C) *NUDT18* expression is lower in all four medulloblastoma subgroups and is significantly different in Group 3 and Group 4 MB's compared to the normal cerebellum **P =0.0045. D) *NUDT5* expression is also elevated across all four medulloblastoma subgroups when compared to the normal cerebellum ****P < 0.0001. Normal cerebellum (Roth dataset) n=9; Group 3 n=56, Group 4 n=91, SHH n=59, WNT n=17 (Pfister dataset). Significance was assessed by one-way ANOVA with Tukey's multiple comparisons test.

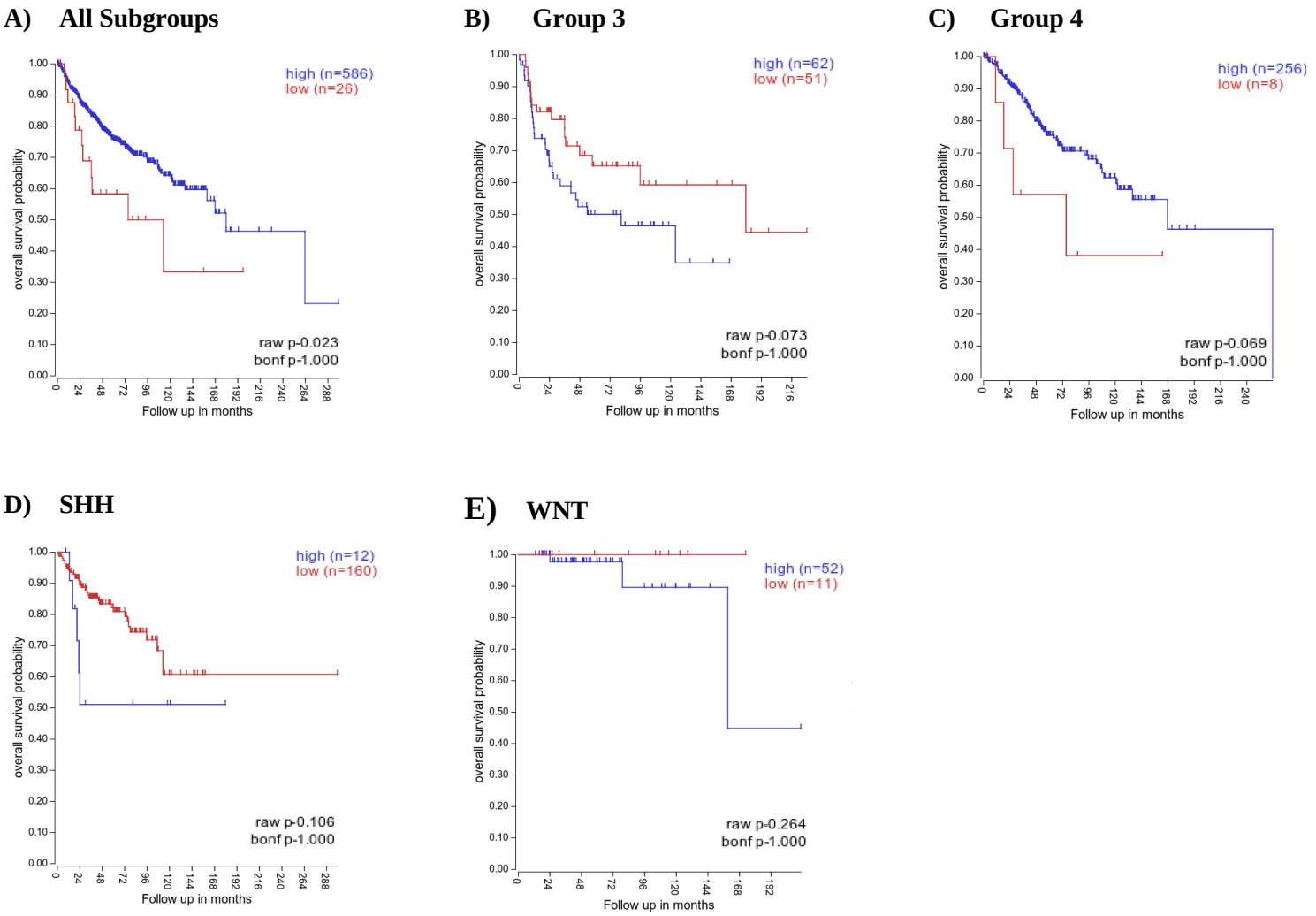

Figure 4.3 Kaplan Meier survival curves of the overall survival probability for high or low NUDT1 gene expression in medulloblastoma patients

Kaplan Meier survival curves of the overall survival probability over a 120-month follow-up period based on high or low *NUDT1* gene expression. Overall survival probability for all molecular subgroups A) All Subgroups B) Group 3 C) Group 4 D) SHH E) WNT were assessed using the Cavalli data.

4.3 Conclusion

In this work, we have determined that 8-oxoguanine lesions are found naturally occurring in Group 3 medulloblastoma cell lines and are likely regulated in the nucleus as well as the cytoplasm by YB-1. The ability of YB-1 to interact with 8-oxoguanine could have been the reason why 8-oxoguanine was picked up during the ChIP sequencing analysis for YB-1 in Taylor 2022's work. YB-1 and 8-oxoguanine were also seen colocalizing in Group 3 primary tumours and their corresponding metastatic tumours suggesting they could be involved in metastasis initiation. With future works, the relationship between YB-1 and 8-oxoguanine lesions and their role in paediatric brain tumours can be established.

References

Alkrekshi, A., Wang, W., Rana, P. S., Markovic, V. and Sossey-Alaoui, K. (2021) 'A comprehensive review of the functions of YB-1 in cancer stemness, metastasis and drug resistance', *CELLULAR SIGNALLING*, 85.

Anastasiadou, E., Jacob, L. S. and Slack, F. J. (2018) 'Non-coding RNA networks in cancer', *NATURE REVIEWS CANCER*, 18(1), pp. 5-18.

Bakhshinyan, D., Venugopal, C., Adile, A. A., Garg, N., Manoranjan, B., Hallett, R., Wang, X., Mahendram, S., Vora, P., Vijayakumar, T., *et al.*, (2019) 'BMI1 is a therapeutic target in recurrent medulloblastoma', *ONCOGENE*, 38(10), pp. 1702-1716.

Becker, A., Thakur, B. K., Weiss, J. M., Kim, H. S., Peinado, H., & Lyden, D. (2016) 'Extracellular Vesicles in Cancer: Cell-to-Cell Mediators of Metastasis', *CANCER CELL*, *30*(6), pp. 836–848.

Bergmann, S., Royer-Pokora, B., Fietze, E., Jurchott, K., Hildebrandt, B., Trost, D., Leenders, F., Claude, J. C., Theuring, F., Bargou, R., Dietel, M. and Royer, H. D. (2005) 'YB-1 provokes breast cancer through the induction of chromosomal instability that emerges from mitotic failure and centrosome amplification', *CANCER RESEARCH*, 65(10), pp. 4078-4087.

Bodenstein, D. F., Kim, H. K., Brown, N. C., Navaid, B., Young, L. T., & Andreazza, A. C. (2019) 'Mitochondrial DNA content and oxidation in bipolar disorder and its role across brain regions', *NPJ SCHIZOPHRENIA*, *5*(1), pp. 21.

Buss, M. C., Remke, M., Lee, J., Gandhi, K., Schniederjan, M. J., Kool, M., Northcott, P. A., Pfister, S. M., Taylor, M. D. and Castellino, R. C. (2015) 'The WIP1 oncogene promotes progression and invasion of aggressive medulloblastoma variants', *ONCOGENE*, 34(9), pp. 1126-1140.

Cancer Research UK. (2021). Children's cancer incidence statistics. Retrieved 06/07/2022 from https://www.cancerresearchuk.org/health-professional/cancer-statistics/childrens-cancers/incidence#heading-Three

Cancer Research UK. (2021). Children's cancers mortality statistics. Retrieved 06/07/2022 from https://www.cancerresearchuk.org/health-professional/cancer-statistics/childrens-cancers/mortality#heading-Three

Cancer Research UK. (2021). Different types of brain tumours in children. Retrieved 06/07/2022 from https://www.cancerresearchuk.org/about-cancer/childrens-cancer/brain-tumours/types/different-types

Cardall, A. (2021). 'Investigating the role of TWIST1 in medulloblastoma metastasis' PhD Thesis, University of Nottingham.

Carreras-Puigvert, J., Zitnik, M., Jemth, A. S., Carter, M., Unterlass, J. E., Hallstrom, B., Loseva, O., Karem, Z., Calderon-Montano, J. M., Lindskog, C., Edqvist, P. H., Matuszewski, D. J., Blal, H. A., Berntsson, R. P. A., Haggblad, M., Martens, U., Studham, M., Lundgren, B., Wahlby, C., Sonnhammer, E. L. L., Lundberg, E., Stenmark, P., Zupan, B. and Helleday, T. (2017) 'A comprehensive structural, biochemical and biological profiling of the human NUDIX hydrolase family', *NATURE COMMUNICATIONS*, 8.

Cassia, G. d. S. e., Alves, C. A. P. F., Taranath, A., López, N. S., Oztekin, O., Gonçalves, F. G. and Patay, Z. (2018) 'Childhood Medulloblastoma Revisited', *TOPICS IN MAGNETIC RESONANCE IMAGING*, 27(6), pp. 479-502.

Cavalli, F. M. G., Remke, M., Rampasek, L., Peacock, J., Shih, D. J. H., Luu, B., Garzia, L., Torchia, J., Nor, C., Morrissy, A. S., Agnihotri, S., Thompson, Y. Y., Kuzan-Fischer, C. M., Farooq, H., Isaev, K., Daniels, C., Cho, B. K., *et al.*, (2017) 'Intertumoral Heterogeneity within Medulloblastoma Subgroups', *CANCER CELL*, 31(6), pp. 737-+.

Costello, M., Pugh, T. J., Fennell, T. J., Stewart, C., Lichtenstein, L., Meldrim, J. C., Fostel, J. L., Friedrich, D. C., Perrin, D., Dionne, D., Kim, S., Gabriel, S. B., Lander, E. S., Fisher, S. and Getz, G. (2013) 'Discovery and characterization of artifactual mutations in deep coverage targeted capture sequencing data due to oxidative DNA damage during sample preparation', *NUCLEIC ACIDS RESEARCH*, 41(6).

Daenen, K., Andries, A., Mekahli, D., Van Schepdael, A., Jouret, F. and Bammens, B. (2019) 'Oxidative stress in chronic kidney disease', *PEDIATRIC NEPHROLOGY*, 34(6), pp. 975-991.

Doyle, L. M., & Wang, M. Z. (2019) 'Overview of Extracellular Vesicles, Their Origin, Composition, Purpose, and Methods for Exosome Isolation and Analysis', *CELLS*, *8*(7), pp.727.

DuBridge, R. B., Tang, P., Hsia, H. C., Leong, P. M., Miller, J. H. and Calos, M. P. (1987) 'Analysis of mutation in human cells by using an Epstein-Barr virus shuttle system', *MOLECULAR AND CELLULAR BIOLOGY*, 7(1), pp. 379-387.

Dziaman, T., Banaszkiewicz, Z., Roszkowski, K., Gackowski, D., Wisniewska, E., Rozalski, R., Foksinski, M., Siomek, A., Speina, E., Winczura, A., Marszalek, A., Tudek, B., & Olinski, R. (2014) '8-Oxo-7,8-dihydroguanine and uric acid as efficient predictors of survival in colon cancer patients', *INTERNATIONAL JOURNAL OF CANCER*, *134*(2), pp. 376–383.

Eliseeva, I. A., Kim, E. R., Guryanov, S. G., Ovchinnikov, L. P. and Lyabin, D. N. (2011) 'Y-box-binding protein 1 (YB-1) and its functions', *BIOCHEMISTRY-MOSCOW*, 76(13), pp. 1402-1433.

Evdokimova, V., Tognon, C., Ng, T., Ruzanov, P., Melnyk, N., Fink, D., Sorokin, A., Ovchinnikov, L. P., Davicioni, E., Triche, T. J. and Sorensen, P. H. B. (2009) 'Translational Activation of Snail1 and Other Developmentally Regulated Transcription Factors by YB-1 Promotes an Epithelial-Mesenchymal Transition', *CANCER CELL*, 15(5), pp. 402-415.

Fares, J., Fares, M. Y., Khachfe, H. H., Salhab, H. A. and Fares, Y. (2020) 'Molecular principles of metastasis: a hallmark of cancer revisited', *SIGNAL TRANSDUCTION AND TARGETED THERAPY*, 5(1).

Ferrucci, V., de Antonellis, P., Pennino, F. P., Asadzadeh, F., Virgilio, A., Montanaro, D., Galeone, A., Boffa, I., Pisano, I., Scognamiglio, I., Navas, L., *et al.*, (2018) 'Metastatic group 3 medulloblastoma is driven by PRUNE1 targeting NME1-TGF-β-OTX2-SNAIL via PTEN inhibition', *BRAIN (London, England : 1878)*, 141(5), pp. 1300-1319.

Finkbeiner, M. R., Astanehe, A., To, K., Fotovati, A., Davies, A. H., Zhao, Y., Jiang, H., Stratford, A. L., Shadeo, A., Boccaccio, C., Comoglio, P., Mertens, P. R., Eirew, P., Raouf, A., Eaves, C. J. and Dunn, S. E. (2009) 'Profiling YB-1 target genes uncovers a new mechanism for MET receptor regulation in normal and malignant human mammary cells', *ONCOGENE*, 28(11), pp. 1421-1431.

Fults, D. W., Taylor, M. D. and Garzia, L. (2019) 'Leptomeningeal dissemination: a sinister pattern of medulloblastoma growth', *JOURNAL OF NEUROSURGERY-PEDIATRICS*, 23(5), pp. 613-621.

Gao, Y., Fotovati, A., Lee, C., Wang, M., Cote, G., Guns, E., Toyota, B., Faury, D., Jabado, N. and Dunn, S. E. (2009) 'Inhibition of Y-box binding protein-1 slows the growth of glioblastoma multiforme and sensitizes to temozolomide independent O6-methylguanine-DNA methyltransferase', *MOLECULAR CANCER THERAPEUTICS*, 8(12), pp. 3276-3284.

Gene Cards (2023). Retrieved 17/03/2023 from https://www.genecards.org/

Gill, J. G., Piskounova, E. and Morrison, S. J. (2016) 'Cancer, oxidative stress, and metastasis', *COLD SPRING HARBOR SYMPOSIA ON QUANTITATIVE BIOLOGY,* 81(1), pp. 163-175.

Gonzalez-Avila, G., Sommer, B., Mendoza-Posada, D. A., Ramos, C., Garcia-Hernandez, A. A. and Falfan-Valencia, R. (2019) 'Matrix metalloproteinases participation in the metastatic process and their diagnostic and therapeutic applications in cancer', *CRITICAL REVIEWS IN ONCOLOGY HEMATOLOGY,* 137, pp. 57-83.

Guarino, A. M., Troiano, A., Pizzo, E., Bosso, A., Vivo, M., Pinto, G., Amoresano, A., Pollice, A., La Mantia, G. and Calabro, V. (2018) 'Oxidative Stress Causes Enhanced Secretion of YB-1 Protein that Restrains Proliferation of Receiving Cells', *GENES,* 9(10).

Guo, Y., Ji, X., Liu, J., Fan, D., Zhou, Q., Chen, C., Wang, W., Wang, G., Wang, H., Yuan, W., Ji, Z. and Sun, Z. (2019) 'Effects of exosomes on pre-metastatic niche formation in tumors', *MOLECULAR CANCER,* 18(1), pp. 39-39.

Gupta, G. P. and Massague, J. (2006) 'Cancer metastasis: Building a framework', *CELL,* 127(4), pp. 679-695.

Gupta, T., Sarkar, C., Rajshekhar, V., Chatterjee, S., Shirsat, N., Muzumdar, D., Pungavkar, S., Chinnaswamy, G. and Jalali, R. (2017) 'Indian Society of Neuro-Oncology consensus guidelines for the contemporary management of medulloblastoma', *NEUROLOGY INDIA,* 65(2), pp. 315-332.

Hahm, J. Y., Park, J., Jang, E. S. and Chi, S. W. (2022) '8-Oxoguanine: from oxidative damage to epigenetic and epitranscriptional modification', *EXPERIMENTAL AND MOLECULAR MEDICINE,* 54(10), pp. 1626-1642.

Hayakawa, H., Uchiumi, T., Fukuda, T., Ashizuka, M., Kohno, K., Kuwano, M. and Sekiguchi, M. (2002) 'Binding capacity of human YB-1 protein for RNA containing 8-oxoguanine', *BIOCHEMISTRY,* 41(42), pp. 12739-12744.

He, X. M., Wikstrand, C. J., Friedman, H. S., Bigner, S. H., Pleasure, S., Trojanowski, J. Q. and Bigner, D. D. (1991) 'differentiation characteristics of newly established medulloblastoma cell-lines (D384 MED, D425 MED, AND D458 MED) and their transplantable xenografts', *LABORATORY INVESTIGATION,* 64(6), pp. 833-843.

Hennika, T. and Gururangan, S. (2015) 'Childhood medulloblastoma: current and future treatment strategies', *EXPERT OPINION ON ORPHAN DRUGS*, 3(11), pp. 1299-1317.

Iida, T., Furuta, A., Kawashima, M., Nishida, J., Nakabeppu, Y. and Iwaki, T. (2001) 'Accumulation of 8-oxo-2 '-deoxyguanosine and increased expression of hMTH1 protein in brain tumors', *NEURO-ONCOLOGY*, 3(2), pp. 73-81.

Juraschka, K. and Taylor, M. D. (2019) 'Medulloblastoma in the age of molecular subgroups: a review', *JOURNAL OF NEUROSURGERY-PEDIATRICS*, 24(4), pp. 353-363.

Kalluri, R. and Weinberg, R. A. (2009) 'The basics of epithelial-mesenchymal transition', *JOURNAL OF CLINICAL INVESTIGATION*, 119(6), pp. 1420-1428.

Karihtala, P., Soini, Y., Vaskivuo, L., Bloigu, R., & Puistola, U. (2009) 'DNA adduct 8-hydroxydeoxyguanosine, a novel putative marker of prognostic significance in ovarian carcinoma', *INTERNATIONAL JOURNAL OF GYNECOLOGICAL CANCER : OFFICIAL JOURNAL OF THE INTERNATIONAL GYNECOLOGICAL CANCER SOCIETY*, *19*(6), pp.1047–1051.

Kelley, J. B. and Paschal, B. M. (2019) 'Fluorescence-based quantification of nucleocytoplasmic transport', *METHODS (SAN DIEGO, CALIF.)*, 157, pp. 106-114.

Kong, Q. M. and Lin, C. L. G. (2010) 'Oxidative damage to RNA: mechanisms, consequences, and diseases', *CELLULAR AND MOLECULAR LIFE SCIENCES*, 67(11), pp. 1817-1829.

Kuzan-Fischer, C. M., Juraschka, K. and Taylor, M. D. (2018) 'Medulloblastoma in the molecular era', *JOURNAL OF KOREAN NEUROSURGICAL SOCIETY*, 61(3), pp. 292-301.

Li, C. S., Xue, Y. Y., Ba, X. Q. and Wang, R. X. (2022) 'The Role of 8-oxoG Repair Systems in Tumorigenesis and Cancer Therapy', *CELLS*, 11(23).

Li, M., Deng, Y. H. and Zhang, W. M. (2021) 'Molecular Determinants of Medulloblastoma Metastasis and Leptomeningeal Dissemination', *MOLECULAR CANCER RESEARCH*, 19(5), pp. 743-752.

Li, S., Wang, X., Wu, Y., Zhang, H., Zhang, L., Wang, C., Zhang, R., & Guo, Z. (2012) ‘8-Hydroxy-2'-deoxyguanosine expression predicts hepatocellular carcinoma outcome’, *ONCOLOGY LETTERS*, *3*(2), pp. 338–342.

Lin, R.-R., Li, X.-Y., Weng, Q.-H., Zhou, X.-X., Zheng, F.-Y. and Cai, J.-P. (2022) 'A study on UHPLC-MS/MS analyses of DNA and RNA oxidative damage metabolites in patients with cervical carcinoma: 8-oxoG in urine as a potential biomarker of cervical carcinoma', *HELIYON*, 8(4), pp. e09321-e09321.

Louis, D. N., Ohgaki, H., Wiestler, O. D., Cavenee, W. K., Burger, P. C., Jouvet, A., Scheithauer, B. W. and Kleihues, P. (2007) 'The 2007 WHO classification of tumours of the central nervous system', *ACTA NEUROPATHOLOGICA*, 114(2), pp. 97-109.

Louis, D. N., Perry, A., Reifenberger, G., von Deimling, A., Figarella-Branger, D., Cavenee, W. K., Ohgaki, H., Wiestler, O. D., Kleihues, P. and Ellison, D. W. (2016) 'The 2016 World Health Organization Classification of Tumors of the Central Nervous System: a summary', *ACTA NEUROPATHOLOGICA*, 131(6), pp. 803-820.

Lu, R. Z., Nash, H. M. and Verdine, G. L. (1997) 'A mammalian DNA repair enzyme that excises oxidatively damaged guanines maps to a locus frequently lost in lung cancer', *CURRENT BIOLOGY*, 7(6), pp. 397-407.

Lyabin, D. N., Eliseeva, I. A. and Ovchinnikov, L. P. (2014) 'YB-1 protein: functions and regulation', *WILEY INTERDISCIPLINARY REVIEWS-RNA*, 5(1), pp. 95-110.

Majidpoor, J. and Mortezaee, K. (2021) 'Steps in metastasis: an updated review', *MEDICAL ONCOLOGY*, 38(1).

Menyhárt, O., Giangaspero, F. and Gyorffy, B. (2019) 'Molecular markers and potential therapeutic targets in non-WNT/non-SHH (group 3 and group 4) medulloblastomas', *JOURNAL OF HEMATOLOGY AND ONCOLOGY*, 12(1), pp. 29-29.

Merve, A., Dubuc, A. M., Zhang, X., Remke, M., Baxter, P. A., Li, X.-N., Taylor, M. D. and Marino, S. (2014) 'Polycomb group gene BMI1 controls invasion of medulloblastoma cells and inhibits BMP-regulated cell adhesion', *ACTA NEUROPATHOLOGICA COMMUNICATIONS*, 2(1), pp. 10-10.

Milde, T., Lodrini, M., Savelyeva, L., Korshunov, A., Kool, M., Brueckner, L. M., Antunes, A., Oehme, I., Pekrun, A., Pfister, S. M., Kulozik, A. E., Witt, O. and Deubzer, H. E. (2012) 'HD-MB03 is a novel Group 3 medulloblastoma model demonstrating sensitivity to histone deacetylase inhibitor treatment', *JOURNAL OF NEURO-ONCOLOGY,* 110(3), pp. 335-348.

Millard, N. E. and De Braganca, K. C. (2016) 'Medulloblastoma', *JOURNAL OF CHILD NEUROLOGY,* 31(12), pp. 1341-1353.

Mordovkina, D. A., Kim, E. R., Buldakov, I. A., Sorokin, A. V., Eliseeva, I. A., Lyabin, D. N. and Ovchinnikov, L. P. (2016) 'Transportin-1-dependent YB-1 nuclear import', *BIOCHEMICAL AND BIOPHYSICAL RESEARCH COMMUNICATIONS,* 480(4), pp. 629-634.

Nakabeppu, Y. (2014) 'Cellular Levels of 8-Oxoguanine in either DNA or the Nucleotide Pool Play Pivotal Roles in Carcinogenesis and Survival of Cancer Cells', *INTERNATIONAL JOURNAL OF MOLECULAR SCIENCES,* 15(7), pp. 12543-12557.

Northcott, P. A., Buchhalter, I., Morrissy, A. S., Hovestadt, V., Weischenfeldt, J., Ehrenberger, T., Grobner, S., Segura-Wang, M., Zichner, T., Rudneva, V. A., Warnatz, H. J., Sidiropoulos, N., Phillips, A. H., Schumacher, S., *et al.*, (2017) 'The whole-genome landscape of medulloblastoma subtypes', *NATURE,* 547(7663), pp. 311-+.

Northcott, P. A., Jones, D. T. W., Kool, M., Robinson, G. W., Gilbertson, R. J., Cho, Y. J., Pomeroy, S. L., Korshunov, A., Lichter, P., Taylor, M. D. and Pfister, S. M. (2012) 'Medulloblastomics: the end of the beginning', *NATURE REVIEWS CANCER,* 12(12), pp. 818-834.

Northcott, P. A., Robinson, G. W., Kratz, C. P., Mabbott, D. J., Pomeroy, S. L., Clifford, S. C., Rutkowski, S., Ellison, D. W., Malkin, D., Taylor, M. D., Gajjar, A. and Pfister, S. M. (2019) 'Medulloblastoma', *NATURE REVIEWS. DISEASE PRIMERS,* 5(1), pp. 11-11.

Ock, C. Y., Kim, E. H., Choi, D. J., Lee, H. J., Hahm, K. B. and Chung, M. H. (2012) '8-Hydroxydeoxyguanosine: Not mer biomarker for oxidative stress, but remedy for oxidative stress-implicated gastrointestinal diseases', *WORLD JOURNAL OF GASTROENTEROLOGY,* 18(4), pp. 302-308.

Orr, B. A. (2020) 'Pathology, diagnostics, and classification of medulloblastoma', *BRAIN PATHOLOGY,* 30(3), pp. 664-678.

Ostrom, Q. T., Gittleman, H., Liao, P., Rouse, C., Chen, Y. W., Dowling, J., Wolinsky, Y. L., Kruchko, C. and Barnholtz-Sloan, J. (2014) 'CBTRUS Statistical Report: Primary Brain and Central Nervous System Tumors Diagnosed in the United States in 2007-2011', *NEURO-ONCOLOGY,* 16, pp. 1-63.

Ostrom, Q. T., Gittleman, H., Truitt, G., Boscia, A., Kruchko, C. and Barnholtz-Sloan, J. S. (2018) 'CBTRUS Statistical Report: Primary Brain and Other Central Nervous System Tumors Diagnosed in the United States in 2011-2015', *NEURO-ONCOLOGY,* 20, pp. 1-86.

Polkinghorn, W. R. and Tarbell, N. J. (2007) 'Medulloblastoma: tumorigenesis, current clinical paradigm, and efforts to improve risk stratification', *NATURE CLINICAL PRACTICE ONCOLOGY,* 4(5), pp. 295-304.

Qing, X., Shi, D., Lv, X., Wang, B., Chen, S., & Shao, Z. (2019) 'Prognostic significance of 8-hydroxy-2'-deoxyguanosine in solid tumors: a meta-analysis', *BMC CANCER, 19*(1), pp. 997.

Radicella, J. P., Dherin, C., Desmaze, C., Fox, M. S. and Boiteux, S. (1997) 'Cloning and characterization of hOGG1, a human homolog of the OGG1 gene of Saccharomyces cerevisiae', *PROCEEDINGS OF THE NATIONAL ACADEMY OF SCIENCES OF THE UNITED STATES OF AMERICA,* 94(15), pp. 8010-8015.

Resovi, A., Pinessi, D., Chiorino, G. and Taraboletti, G. (2014) 'Current understanding of the thrombospondin-1 interactome', *MATRIX BIOLOGY,* 37, pp. 83-91.

Roth, R. B., Hevezi, P., Lee, J., Willhite, D., Lechner, S. M., Foster, A. C. and Zlotnik, A. (2006) 'Gene expression analyses reveal molecular relationships among 20 regions of the human CNS', *NEUROGENETICS,* 7(2), pp. 67-80.

Sakai, Y., Furuichi, M., Takahashi, M., Mishima, M., Iwai, S., Shirakawa, M. and Nakabeppu, Y. (2002) 'A molecular basis for the selective recognition of 2-hydroxy-dATP and 8-oxo-dGTP by human MTH1', *JOURNAL OF BIOLOGICAL CHEMISTRY,* 277(10), pp. 8579-8587.

Salim, S. (2017) 'Oxidative stress and the central nervous system', *THE JOURNAL OF PHARMACOLOGY AND EXPERIMENTAL THERAPEUTICS,* 360(1), pp. 201-205.

Schindelin, J., Arganda-Carreras, I., Frise, E., Kaynig, V., Longair, M., Pietzsch, T., Preibisch, S., Rueden, C., Saalfeld, S., Schmid, B., Tinevez, J. Y., White, D. J., Hartenstein, V., Eliceiri, K., Tomancak, P. and Cardona, A. (2012) 'Fiji: an open-source platform for biological-image analysis', *NATURE METHODS*, 9(7), pp. 676-682.

Schwalbe, E. C., Lindsey, J. C., Nakjang, S., Crosier, S., Smith, A. J., Hicks, D., Rafiee, G., Hill, R. M., Iliasova, A., Stone, T., Pizer, B., Michalski, A., Joshi, A., Wharton, S. B., Jacques, T. S., Bailey, S., Williamson, D. and Clifford, S. C. (2017) 'Novel molecular subgroups for clinical classification and outcome prediction in childhood medulloblastoma: a cohort study', *LANCET ONCOLOGY*, 18(7), pp. 958-971.

Slupska, M. M., Luther, W. M., Chiang, J. H., Yang, H. J. and Miller, J. H. (1999) 'Functional expression of hMYH, a human homolog of the Escherichia coli MutY protein', *JOURNAL OF BACTERIOLOGY*, 181(19), pp. 6210-6213.

Somasekharan, S. P., El-Naggar, A., Leprivier, G., Cheng, H., Hajee, S., Grunewald, T. G. P., Zhang, F., Ng, T., Delattre, O., Evdokimova, V., Wang, Y., Gleave, M. and Sorensen, P. H. (2015) 'YB-1 regulates stress granule formation and tumor progression by translationally activating G3BP1', *THE JOURNAL OF CELL BIOLOGY*, 208(7), pp. 913-929.

Taillandier, L., Blonski, M., Carrie, C., Bernier, V., Bonnetain, F., Bourdeaut, F., Thomas, I. C., Chastagner, P., Dhermain, F., Doz, F., Frappaz, D., Grill, J., Guillevin, R., Idbaih, A., Jouvet, A., Kerr, C., Donadey, F. L., Padovani, L., Pallud, J. and Sunyach, M. P. (2011) 'Les médulloblastomes : revue générale', *REVUE NEUROLOGIQUE*, 167(5), pp. 431-448.

Tamayo-Orrego, L. and Charron, F. (2019) 'Recent advances in SHH medulloblastoma progression: tumor suppressor mechanisms and the tumor microenvironment [version 1 peer review: 2 approved]', *F1000 RESEARCH*, 8, pp. 1823.

Tang, L., Wei, D., Xu, X. Y., Mao, X. L., Mo, D. P., Yan, L. P., Xu, W. G. and Yan, F. (2021) 'Long non-coding RNA MIR200CHG promotes breast cancer proliferation, invasion, and drug resistance by interacting with and stabilizing YB-1', *NPJ BREAST CANCER*, 7(1).

Taylor, L. 2022. Investigating the role of Y-box binding protein 1 in medulloblastoma tumour progression and drug resistance. PhD Thesis, University of Nottingham

Taylor, L., Kerr, I. D. and Coyle, B. (2021) 'Y-Box Binding Protein-1: A Neglected Target in Pediatric Brain Tumors?', *MOLECULAR CANCER RESEARCH*, 19(3), pp. 375-387.

Taylor, L., Wade, P. K., Johnson, J. E. C., Aldighieri, M., Morlando, S., Di Leva, G., Kerr, I. D. and Coyle, B. (2023) 'Drug Resistance in Medulloblastoma Is Driven by YB-1, ABCB1 and a Seven-Gene Drug Signature', *CANCERS*, 15(4).

Thomas, A. and Noel, G. (2019) 'Medulloblastoma: optimizing care with a multidisciplinary approach', *JOURNAL OF MULTIDISCIPLINARY HEALTHCARE*, 12, pp. 335-347.

Torres-Gonzalez, M., Gawlowski, T., Kocalis, H., Scott, B. T., & Dillmann, W. H. (2014) 'Mitochondrial 8-oxoguanine glycosylase decreases mitochondrial fragmentation and improves mitochondrial function in H9C2 cells under oxidative stress conditions', *AMERICAN JOURNAL OF PHYSIOLOGY. CELL PHYSIOLOGY*, *306*(3), pp. C221–C229.

Traenka, C., Remke, M., Korshunov, A., Bender, S., Hielscher, T., Northcott, P. A., Witt, H., Ryzhova, M., Felsberg, J., Benner, A., Riester, S., Scheurlen, W., Grunewald, T. G. P., von Deimling, A., Kulozik, A. E., Reifenberger, G., Taylor, M. D., Lichter, P., Butt, E. and Pfister, S. M. (2010) 'Role of LIM and SH3 Protein 1 (LASP1) in the Metastatic Dissemination of Medulloblastoma', *CANCER RESEARCH*, 70(20), pp. 8003-8014.

Tsuzuki, T., Egashira, A., Igarashi, H., Iwakuma, T., Nakatsuru, Y., Tominaga, Y., Kawate, H., Nakao, K., Nakamura, K., Ide, F., Kura, S., Nakabeppu, Y., Katsuki, M., Ishikawa, T. and Sekiguchi, M. (2001) 'Spontaneous Tumorigenesis in Mice Defective in the MTH1 Gene Encoding 8-Oxo-dGTPase', *PROCEEDINGS OF THE NATIONAL ACADEMY OF SCIENCES - PNAS*, 98(20), pp. 11456-11461.

Udaka, Y. T. and Packer, R. J. (2018) 'Pediatric Brain Tumors', *NEUROLOGIC CLINICS*, 36(3), pp. 533-+.

Valastyan, S. and Weinberg, R. A. (2011) 'Tumor Metastasis: Molecular Insights and Evolving Paradigms', *CELL*, 147(2), pp. 275-292.

van den Boogaard, M. L., Oka, R., Hakkert, A., Schild, L., Ebus, M. E., van Gerven, M. R., Zwijnenburg, D. A., Molenaar, P., Hoyng, L. L., Dolman, M. *et al.*, (2021) 'Defects in 8-oxo-guanine repair pathway cause high frequency of C > A substitutions in neuroblastoma', *PROCEEDINGS OF THE NATIONAL ACADEMY OF SCIENCES - PNAS*, 118(36), pp. 1.

Visnes, T., Cazares-Korner, A., Hao, W. J., Wallner, O., Masuyer, G., Loseva, O., Mortusewicz, O., Wiita, E., Sarno, A., Manoilov, A., Astorga-Wells, J., Jemth, A. S., Pan, L., Sanjiv, K., Karsten, S., Gokturk, C., Grube, M., Homan, *et al.*, (2018) 'Small-molecule inhibitor of OGG1 suppresses proinflammatory gene expression and inflammation', *SCIENCE*, 362(6416), pp. 834-+.

Wang, H., Sun, R. W., Gu, M., Li, S., Zhang, B., Chi, Z. F. and Hao, L. C. (2015) 'shRNA-Mediated Silencing of Y-Box Binding Protein-1 (YB-1) Suppresses Growth of Neuroblastoma Cell SH-SY5Y In Vitro and In Vivo', *PLOS ONE*, 10(5).Wang, Y., Wan, F. N., Chang, K., Lu, X. L., Dai, B. and Ye, D. W. (2017) 'NUDT expression is predictive of prognosis in patients with clear cell renal cell carcinoma', *ONCOLOGY LETTERS*, 14(5), pp. 6121-6128.

Wilne, S., Collier, J., Kennedy, C., Koller, K., Grundy, R. and Walker, D. (2007) 'Presentation of childhood CNS tumours: a systematic review 3 and meta-analysis', *LANCET ONCOLOGY*, 8(8), pp. 685-695.

Wu, S. L., Fu, X., Huang, J. Y., Jia, T. T., Zong, F. Y., Mu, S. R., Zhu, H., Yan, Y., Qiu, S. W., Wu, Q., Yan, W., Peng, Y., Chen, J. X. and Hui, J. Y. (2015) 'Genome-wide analysis of YB-1-RNA interactions reveals a novel role of YB-1 in miRNA processing in glioblastoma multiforme', *NUCLEIC ACIDS RESEARCH*, 43(17), pp. 8516-8528.

Xu, J. Y., Margol, A. S., Shukla, A., Ren, X. H., Finlay, J. L., Krieger, M. D., Gilles, F. H., Couch, F. J., Aziz, M., Fung, E. T., Asgharzadeh, S., Barrett, M. T. and Erdreich-Epstein, A. (2015) 'Disseminated medulloblastoma in a child with germline BRCA2 6174delT mutation and without Fanconi anemia', *FRONTIERS IN ONCOLOGY*, 5.

Yin, Q. Y., Zheng, M., Luo, Q. M., Jiang, D. W., Zhang, H. F. and Chen, C. S. (2022) 'YB-1 as an Oncoprotein: Functions, Regulation, Post-Translational Modifications, and Targeted Therapy', *CELLS*, 11(7).

Zapotocky, M., Mata-Mbemba, D., Sumerauer, D., Liby, P., Lassaletta, A., Zamecnik, J., Krskova, L., Kyncl, M., Stary, J., Laughlin, S., Arnoldo, A., Hawkins, C., Tabori, U., Taylor, M. D., Bouffet, E., Raybaud, C. and Ramaswamy, V. (2018) 'Differential patterns of metastatic dissemination across medulloblastoma subgroups', *JOURNAL OF NEUROSURGERY-PEDIATRICS*, 21(2), pp. 145-152.

Zhang, J. F., Fan, J. S., Li, S. L., Yang, Y. H., Sun, P., Zhu, Q. J., Wang, J. N., Jiang, B., Yang, D. W. and Liu, M. L. (2020) 'Structural basis of DNA binding to human YB-1 cold shock domain regulated by phosphorylation', *NUCLEIC ACIDS RESEARCH*, 48(16), pp. 9361-9371.

Zhao, K. and Wen, L. B. (2018) 'DMF attenuates cisplatin-induced kidney injury via activating Nrf2 signalling pathway and inhibiting NF-kB signalling pathway', *EUROPEAN REVIEW FOR MEDICAL AND PHARMACOLOGICAL SCIENCES*, 22(24), pp. 8924-8931.

Zhao, X., Zhao, Z., Xu, W., Liu, H., Chang, J., Xu, W., Li, S., Cao, S. and Hou, J. (2020) 'Circ-sar1a promotes renal cell carcinoma progression through mir-382/ybx1 axis', *CANCER MANAGEMENT AND RESEARCH*, 12, pp. 7353-7361.

Zhou, L. M., Picard, D., Ra, Y. S., Li, M. H., Northcott, P. A., Hu, Y. Q., Stearns, D., Hawkins, C., Taylor, M. D., Rutka, J., Der, S. D. and Huang, A. (2010) 'Silencing of Thrombospondin-1 Is Critical for Myc-Induced Metastatic Phenotypes in Medulloblastoma', *CANCER RESEARCH*, 70(20), pp. 8199-8210.